Imperial College London
Department of Electrical and Electronic Engineering

Methods and Devices for Chronically-Reliable Packaging of Implantable Neural Microsystems

Federico Mazza

Supervised by Dr. Timothy G. Constandinou

Submitted in part fulfilment of the requirements for the degree of
Doctor of Philosophy in Electrical and Electronic Engineering of Imperial College London
and the Diploma of Imperial College London
March 2020

Declaration of originality

I herewith certify that all material in this dissertation which is not my own work has been properly acknowledged.

Federico Mazza

Copyright declaration

The copyright of this thesis rests with the author. Unless otherwise indicated, its contents are licensed under a Creative Commons Attribution-Non Commercial-No Derivatives 4.0 International Licence (CC BY-NC-ND).
Under this licence, you may copy and redistribute the material in any medium or format on the condition that; you credit the author, do not use it for commercial purposes and do not distribute modified versions of the work.
When reusing or sharing this work, ensure you make the licence terms clear to others by naming the licence and linking to the licence text.
Please seek permission from the copyright holder for uses of this work that are not included in this licence or permitted under UK Copyright Law.



Abstract

The current landscape of neurotechnology is thriving with a wide variety of systems and devices to study the brain and treat diseases associated with the nervous system. However, many patients who live every day with a prosthetic limb or with the consequences of a spinal cord injury are still waiting for a solution that could restore their abilities to move freely. In this regard, no established clinical solution exists at the moment, and the majority of the systems proposed and developed by the scientific community fail to translate to commercial products, mainly due to the lack of consistent chronic performances.

The design of an implantable system that can reliably work over decades is still a great challenge. The objective of this thesis is to explore the issues that impede long term operation, and to provide possible methods and solutions in the aspects regarding packaging and encapsulation of chronic implantable devices for cortical recording.

With such goal in mind, the following work starts by presenting a review of neural implantable devices, with an emphasis on the challenges they face when dealing with chronic implantation. The original contributions presented in the subsequent technical chapters are summarized here:

- The identification of a method to assess the level of hermeticity of a micro-packaged implantable device. The proposed solution is the use of a custom designed relative humidity sensor, to detect the presence of water molecules inside the packaged device. The full design of the sensor is described in detail, from the mathematical modelling of the sensing element to the readout circuit architecture, with focus on reducing the circuit footprint, as required by the specific application. The use of a commercially available sensor is also explored for the realization of a bench top hermeticity testing platform, by measuring its ability to withstand the temperatures required in the sealing process of an implantable micro-package.

- The quantification of the damages due to corrosion that occur on a silicon-based device encapsulated with a polymer coating. This has been achieved by designing dedicated test structures, and observing their behaviour in accelerated life tests, that have demonstrated the reliability of silicon substrates for chronic implantable devices. The use of an industry standard CMOS process increases the significance of the results. The idea of equipping implantable devices with self-diagnostic capabilities has also been explored. Two instrumentation circuits are proposed to monitor in real time the diffusion of water molecules within an implanted integrated circuit.

- The development of an overall structure and fabrication method for the realization of a fully autonomous, wireless, millimetre-sized neural implant, focusing on the hermeticity of the embedded electronics and on the use of penetrating microwires for cortical recording of local field potentials. The mechanical structure of the implant is presented in detail, and a first prototype is realized, together with a dedicated platform to speed up the assembly of the probes.

This work proposes devices and methods for the realization of miniaturized neural implantable devices, stressing the importance of chronic reliability and emphasizing the need for a design approach that keeps in mind the clinical applications of future neural interfaces.

To my family

Those who believe in telekinetics,
raise my hand.

Kurt Vonnegut Jr.

Acknowledgements

I would like to take a little space in this thesis to express my gratitude for all the people that have made every day of these last four years more enjoyable, and that have given me their continuous help and encouragement during my time at Imperial College.

First I would like to thank my supervisor, *Dr. Timothy Constandinou*. Your competence and enthusiasm are admirable, and I am deeply grateful for the guidance and the often undeserved support you gave me throughout my research during both the highs and the lows of my PhD journey.

A massive thank you to *Iza*, for always being present and for your infinite patience in dealing with any issue. The lab would not be the same without your heartfelt care for all the people who work there.

I want to thank all my colleagues and friends working on the ENGINI project, and in particular *Kasia*, *Matthew*, *Michal*, and *Peilong*. It has been a pleasure to collaborate with all of you, and I owe you much of what I learned during my PhD.

I also want to thank all the people from the Centre for Bio-Inspired Technology. You made me feel welcomed from the very first day, and you continued to provide an amazing environment and sense of community that goes well beyond the walls of the lab. You were all a major inspiration to me and often the reason I would walk into the office in the morning with a smile. A personal thank you goes to *Nick* for his constant encouragement and optimism, *Yan* for always finding the time to help me, and *Fran* for listening to my rambles everyday and still wanting to seat in the same row.

A special thank you to *Dorian*, who never shies away from reminding me that friends are always there to help, and to *Alberto* and *Enrico* for being my Italian family abroad.

Finally I would like to thank my parents, that gave me the possibility to undertake this doctorate and always supported me in this choice, my siblings for their encouragement and hospitality, and finally *Francesca* that always brings sunshine even in the many gray British days.

Contents

1. Introduction **17**
1.1. Motivation . . . 18
1.2. Research objectives . . . 20
1.3. Outline of thesis . . . 21
Bibliography . . . 21

2. Neural Implantable Medical Devices: Current Solutions and Future Technological Challenges **24**
2.1. Merging body and technology . . . 24
2.2. Connecting to the nervous system: neuroprosthetics and brain-computer interfaces . . . 26
2.2.1. Sensing brain activity . . . 29
2.2.2. Neural implants for cortical recording . . . 33
2.2.3. Challenges of chronic cortical implants . . . 36
2.2.4. Millimetre-scale distributed cortical implants . . . 37
2.3. Summary . . . 41
Bibliography . . . 42

3. Humidity Sensing for Monitoring Micro-Package Integrity **49**
3.1. Test methods for micro-package hermeticity . . . 49
3.2. Humidity monitoring . . . 53
3.2.1. Devices for sensing humidity . . . 54
3.3. Sensor design . . . 57
3.3.1. IDC mathematical model . . . 58
3.3.2. Numerical simulations . . . 61
3.3.3. Circuit architecture . . . 63
3.3.4. Sensor testing . . . 66
3.4. Commercial humidity sensor for package integrity testing . . . 67
3.4.1. Optoelectronic hermeticity platform . . . 70
3.5. Conclusions . . . 72
Bibliography . . . 73

4. Chronic Stability of Implanted Silicon Devices **77**
4.1. Water penetration in coated silicon devices . . . 78
4.1.1. Moisture induced damages to implants . . . 79
4.2. Structures for accelerated tests on implant encapsulation . . . 81
4.2.1. Test structures design . . . 81
4.2.2. Experimental setup . . . 83
4.2.3. Results . . . 86
4.3. Integrated Devices for Micro-Package Integrity Monitoring . . . 88
4.3.1. Inter-layer infiltration . . . 90
4.3.2. Intra-layer diffusion . . . 92
4.4. Conclusions . . . 95
Bibliography . . . 95

5. Design of a Microwire-based Mm-scale Cortical Recording Implant **99**
5.1. Materials for implantable devices . . . 100
5.1.1. Microwire-based feedthrough connections . . . 101
5.2. First generation ENGINI probe design . . . 103
5.3. Second generation ENGINI probe design . . . 106
5.3.1. Hermetic micro-package . . . 106
5.3.2. Wire module . . . 107
5.3.3. Prototype fabrication . . . 107
5.3.4. Prototype assembly . . . 108
5.3.5. Design outcomes . . . 110
5.4. Conclusions . . . 111
Bibliography . . . 112

6. Conclusion **115**
6.1. Summary and original contributions . . . 115
6.2. Future work . . . 117
6.3. Final thoughts . . . 119

A. Publications **120**

List of Figures

2.1. Examples of different types of past and current implantable medical devices for therapeutical applications . . . 25
2.2. Overview of the human nervous system . . . 27
2.3. Main different electrophysiological brain signals and location of their respective recording sites . . . 30
2.4. Examples of different types of intracortical implantable interfaces for neural recording . . . 34
2.5. Examples of current strategies for the realization of next-generation cortical neural interfaces . . . 39
2.6. Concept illustration of the ENGINI system and its elements . . . 41

3.1. Diagrams of the two main configurations for integrated capacitive humidity sensors . . . 56
3.2. Tools for the analysis of an interdigitated structure . . . 58
3.3. Equivalent circuit of an IDC with six electrodes . . . 59
3.4. Partial capacitance method used to separate the contributions of different dielectric layers over an interdigitated capacitor . . . 60
3.5. Screenshot of the Matlab application for the optimization of the IDC geometrical parameters . . . 61
3.6. The COMSOL model of the $100 \times 100\,\mu m^2$ IDC structure shows the confinement of the electric field between the capacitor finger electrodes. . . . 62
3.7. Schematic of the switched capacitor capacitance-to-voltage converter used for each RH sensor . . . 64
3.8. Timing diagram of the RH sensor circuit . . . 65
3.9. Micro-photograph of the fabricated device . . . 66
3.10. Humidity sensor test results for each of the three IDC sizes, compared with the pre-fabrication simulations . . . 67
3.11. Sensirion SHTW2 temperature and humidity sensor . . . 68
3.12. Solderless PCB setup for Sensirion SHTW2 testing . . . 69
3.13. Temperature profile of the LPKF reflow oven to simulate a AuSn eutectic bonding process . . . 69
3.14. Testing of two Sensirion SHTW2 temperature and humidity sensors inside the environmental chamber . . . 70

3.15. Micro-picture of one of the Sensirion SHTW2 sensors that underwent back-grinding . . . 71
3.16. Diagram of the platform for hermeticity monitoring with optical power transfer and data transmission . . . 72

4.1. Focused Ion Beam (FIB) cross section of the UMC 180nm eNVM process . 78
4.2. Representation of the mechanism of implant failure caused by water accumulation inside the voids present in the encapsulation layer . . . 80
4.3. Diagrams of the test structures for accelerated life testing of polymer encapsulated electronics . . . 82
4.4. Photographs of the test structures fabricated in AMS 0.35 µm four metal technology . . . 84
4.5. Simplified schematic of one module of the test platform . . . 85
4.6. Set up and connection of individual samples within the platform for accelerated life testing . . . 86
4.7. Degradation of the silicone encapsulation during accelerated life tests . . . 87
4.8. Magnitude and phase plots of impedance measurement of samples aged at different temperatures . . . 88
4.9. Cross-section of a CMOS die showing the proposed structure to measure moisture penetration within the oxyde layers . . . 89
4.10. Proposed circuit for sensing moisture ingress along the interface between ILD layers . . . 91
4.11. Simulation results for the frequency response and noise profile of the leakage current sensing circuit . . . 92
4.12. Schematic of the circuit for sensing moisture diffusion in silicon dioxide by evaluating the impedance between metal tracks on different layers . . . 93

5.1. Illustration of the mm-sized ENGINI probes implanted in the motor cortex 99
5.2. Permeability to helium gas of different materials used for medical devices, as a function of thickness and time . . . 100
5.3. Examples of microwire-based implants for neural recording . . . 102
5.4. Concept and prototype of the passive section of the first version of ENGINI neural probe . . . 103
5.5. Detail of the microwire attachment to the silicon interposer using electroplating, with glass module to support the wire . . . 104
5.6. Passivation lift-off and excessive trace metallization during the electroplating process to attach the microwire to the silicon interposer in the first version of the neural probe . . . 105
5.7. Cross-section and exploded view rendering of the proposed neural implant design. Note the funcitonal separation between the hermetic package and the wire module . . . 107

5.8. Borosilicate glass sample of the interposer with TGVs, fabricated using a Rofin LFS laser workstation. 108
5.9. Prototypes of the three implant components manufactured form plastic resin using 3D printing: (a) interposer, (b) cap, (c) wire module 108
5.10. Assembly platform of the 3D printed probe prototype 109

List of Tables

2.1. Summary of the main characteristics of brain signals 32

3.1. Main hermeticity testing methods for small packages 51
3.2. Simulation results for the capacitance of a $100 \times 100\,\mu m^2$ IDC with and without Si_3N_4 passivation layer. 62
3.3. Results of the numerical simulations for the three test IDC structures . . . 63
3.4. Measurement error between environmental chamber and test sensors, before and after putting the sensors through the eutectic cycle 71

4.1. Results of accelerated life tests on IDC structures under constant DC bias and at different ageing temperatures. 87
4.2. Specification table of the two-stage TIA circuit 92
4.3. Specification table of the comparator 94

List of Abbreviations

AH	Absolute Humidity
ALD	Atomic Layer Deposition
AP	Action Potential
BCI	Brain-Computer Interface
BMI	Brain-Machine Interface
CANDO	Controlling Abnormal Network Dynamics using Optogenetics
CDS	Correlated Double Sampling
CE	Counter Electrode
CHLD	Cumulative Helium Leak Detection
CNS	Central Nervous System
DBS	Deep Brain Stimulation
DRIE	Deep Reactive-Ion Etching
DUT	Device Under Test
ECoG	Electrocorticography
EEG	Electroencephalography
EIS	Electrochemical Impedance Spectroscopy
ENGINI	Empowering Next Generation Implantable Neural Interfaces
FBR	Foreign Body Response
FDA	U.S. Food and Drug Administration
FEM	Finite Element Method
FEOL	Front End Of Line
FIB	Focused Ion Beam
FRA	Frequency Response Analyzer
FTIR	Fourier Transmission Infrared Spectrometry
IC	Integrated Circuit
IDC	Inter-digitated Capacitor
ILD	Inter-Layer Dielectric
IMD	Implantable Medical Device
LFP	Local Field Potential
PBS	Phosphate Buffered Saline
PCB	Printed Circuit Board
PDMS	Polydimethylsiloxane
PEEK	Polyether Ether Ketone

PNS	Peripheral Nervous System
RDL	Redistribution Layer
RH	Relative Humidity
SNR	Signal-to-Noise Ration
SCI	Spinal Cord Injury
TGV	Through Glass Via
TIA	Trans-Impedance Amplifier
TSV	Through Silicon Via
UEA	Utah Electrode Array
WE	Working Electrode

1. Introduction

The history of our species is a strange and wonderful tale of exceptional ingenuity, discoveries, and inventions. As humans, we have explored and conquered the planet Earth, as well as explored beyond its boundaries and literally reached for the stars. But if we look at ourselves as individuals, the way our body is structured and the biological processes that govern it are very similar to most mammals, with which we share the majority of our DNA. The feature that really sets us apart is the prodigious development of the most incredible organ in our body, what UCSF neuroengineer Tim Hanson calls "*one of the most information-dense, structured, and self-structuring matter known*" [1]: the human brain.

The fascination for this elusive entity has fostered a tremendous amount of research, and incredible results have been achieved, especially in the last century: at the cellular level, we now know the mechanisms that regulate the behaviour of single neurons, while at the high level we have been able to map certain tasks and states to specific areas of the brain. However, all the functions that lie in between these two levels, the processes that regulate things such as memories, decision-making, or creativity, remain largely a mystery. Yet the current scientific era we are witnessing gives us hope: technological advancements and breakthrough scientific discoveries, paired with increasing multidisciplinary collaborations between natural sciences and engineering, seem to prove promising in pushing the boundaries of our understanding of the brain.

Nonetheless, we must be careful not to limit ourselves in viewing our brain only through the tools we currently have at disposal. The advent of electronics and computing, and most recently of artificial intelligence suggests a tempting parallel with our natural way of processing information, but it might as well be a limited interpretation, dictated by our state-of-the-art technology, similarly to what has happened in the past centuries, with hydraulic, mechanical, or electrical explanations for the human thinking process [2]. Besides, a full understanding of the brain might be just out of reach for us, as scientist Emerson Pugh observed: "*If the human brain were so simple that we could understand it, we would be so simple that we couldn't*" [3].

The only way to broaden our understanding of the brain is to continue encouraging research and innovation, promoting multidisciplinary cooperation, always keeping in mind the invaluable benefits that improvements in this field could bring to millions of people around the world suffering from neurological conditions or trauma.

1.1. Motivation

One of the most significant effects that scientific and technological progress has had, is the terrific impact on the average health of the world population. According to the World Health Organization (WHO), global life expectancy at birth has increased by 5 years between 2000 and 2015 [4]. Such breakthroughs give hope for an healthier future, but many challenges still remain to be faced, particularly regarding diseases of the brain and the nervous system. Neuro-psychiatric disorders currently take up five of the top ten causes of disability [5]. Moreover neurological diseases are usually chronically debilitating, and their long-term need for medical care and assistance has a large economical impact both for patients and for health care providers. Another study from the WHO estimates that nearly one billion people worldwide suffer from neurological disorders and mental illnesses, a figure destined to increase because of the overall ageing of the population, that will exacerbate the occurrence of pathologies such as Alzheimer, Parkinson's disease and various forms of dementia [6]. For example, epilepsy is ranked third within the most commonly diagnosed neurological disorders, and it affects more than 50 million people globally [7]. Traumatic injuries also play a significant role: as an example, an estimated 2.5 million people around the world suffer from paralysis caused by spinal cord injury (SCI) [8].

Together with affecting the everyday life of an extremely vast number of people, these conditions also create a considerable economical burden for society. In 2010, the overall European cost of brain disorders was estimated at about €800 billion [9]. In the US alone, the estimated lifetime cost for a patient with complete tetraplegia is about $3 million [8].

These astonishing figures have driven a tremendous effort in research specifically targeting the nervous system, its functional mechanisms, as well as targeted therapies for neurological conditions. Huge collaborative research efforts have been created, such as the European Human Brain Project, that aims at the creation of a computer simulation of the functions of a full human brain, or the BRAIN Initiative, a US project that involves collaborations between public and private institutions, such as the Allen Institute for Brain Science and the DARPA, launched in 2013 under the Obama administration. However, it is important to underline how these projects have largely focused on developing research tools rather than devices or techniques for clinical applications.

There is a general feel in the research community that the current generation of available technology might be approaching maturity, and that it might allow to close the gap between the research environment and the clinical applications. Supporting this assumption is the fact that in very recent years, large technological companies are venturing in the field of neurotechnology. Business investor and entrepreneur Elon Musk founded Neuralink in 2016, with the visionary long-term objective of creating complex brain-computer interfaces that might enhance human abilities. The company has attracted scientists and researchers from world renowned institution, and has released a first overview of its work

in 2019 [10]. Facebook founder Mark Zuckerberg confirmed in 2017 that his company is aiming at developing a brain-computer interface focused on decoding speech and language with the help of non-invasive devices, that will supposedly allow to type directly from the brain. Also Alphabet Inc., the parent company of Google, established in November 2016 Galvani Bioelectronics, in partnership with pharmaceutical giant GlaxoSmithKline, with the objective of developing implantable technology for targeted, personalized healthcare.

The continuous advancements in technology that allow for the creation of smaller, more efficient electronics, together with the advent of such big players and investments from both the research and the industry environment, seem to bring us closer to scenarios were the human brain can directly and effectively communicate with the external environment through the use of electronics and software. It is not hard to imagine the extraordinary applications that such technology would unlock, like the possibility to restore the complete motor capabilities of amputees, that would be able to control their prostheses in a natural way, and receive sensory feedback. Locked-in patients, who would be given a way to communicate with the outside world [11]. Even outside of the medical domain, it is possible to envision applications that augment the natural capabilities of the human body, such as brain-to-brain communication, learning enhancements, or the use of external devices controlled with the brain [12].

If there is literally no limit to the possible applications one can think of, it is important to have a realistic and critical vision, particularly in a domain where captivating headlines and prophetic announcements can be easily put up (and even more easily spread), and ask what are the missing pieces in current solutions. In particular, the main challenges associated with the use of invasive implantable systems still remain largely unsolved, although their resolution has proven critical for the success of such systems. Non-invasive solutions, while still showing promising results, currently lack spatial resolution and bandwidth required for seamless and natural operation [13]. Invasive methods, on the contrary, show extremely precise interfacing capabilities, down to the single cell, but pose critical issues, in particular regarding their chronic performances and the risks associated with cranial surgery.

Like with all medical devices, it is of utmost importance to ensure that the benefits for the patients outweigh the inherent risks, and that the degree of invasiveness is limited to the absolute necessary [14]. To be able to deliver a neural implantable device, capable of reliable operation over long periods of time with a minimal impact on the surrounding tissue would be a major breakthrough and could push further the study of our brain and its mechanisms, and allow new solutions to treat several conditions of the nervous system [15].

That is why the design of the next generation of implantable neural interfaces will have to adopt a broader approach, building on present results but at the same time without neglecting the essential aspects for a successful medical device: safety, long-term device reliability and signal stability, and system effectiveness.

1.2. Research objectives

The main objective of this research project is to address the issue of safe chronic operation and reliability of implantable neural devices, which importance has been highlighted in the previous section. In particular, it aims at establishing a method of assessing the long-term stability of millimetre-scale implantable micro-packages, and to investigate the design approaches necessary to deliver a subdural implant that presents a reliable encapsulation.

Achieving these objectives would contribute to the development of long lasting neural implants, thus reducing the need of multiple, very invasive surgical procedures, with all the associated risks, and greatly improving the patients' quality of life.

Based on these considerations, the following research objectives have been identified:

- Identify a reliable method to verify and monitor over time the hermeticity of mm-scale implantable micro-packages. This should be achieved in a way that can easily integrate with the implantable device, minimizing its impact in terms of required volume and power budget. This would allow for both bench top testing during implant prototype fabrication, as well as continuous monitoring over the device life time. Possible applications could be extended beyond the specific field of neural implants, as a general way of assessing the status of encapsulation of packaged devices in applications where chronic hermeticity is required.

- Investigate the resistance of silicon substrates to moisture penetration, to validate the feasibility of active implantable devices that adopt only polymer encapsulation, that might allow for the reduction of the overall size of the implants. Results in this area would produce valuable insights for the realization of sub-millimetre implants, as well as providing useful insights on the mechanism that regulate water penetration in active silicon stacks.

- Develop the design and the fabrication strategy for the manufacturing of a mm-scale, wireless neural implant for cortical recording, with focus on a suitable form-factor and materials choice to target chronic operation and minimal impact on the surrounding tissue.

1.3. Outline of thesis

This thesis is structured as follows:

- Chapter 1, "Introduction", has given a preface to the study of the brain and provided the motivation of the work, together with the main objectives of the research.
- Chapter 2, "Neural Implantable Medical Devices: Current Solutions and Future Technological Challenges", presents the relevant background regarding the field of implantable devices, with a focus on implantable neural interfaces. The need for invasive implants is discussed, followed by a review of current state-of-the-art devices for cortical recording. The challenges associated with chronic implantable devices are detailed, with emphasis on the necessity of implant miniaturization, and the main approaches currently explored in the research environment are presented.
- Chapter 3, "Humidity Sensing for Monitoring Micro-Package Integrity", identifies the challenge of moisture penetration in implantable devices, and reviews the current scientific literature regarding the methods to assess the hermeticity of micro-packages, with a focus on humidity monitoring. It then presents a review of current solutions for humidity sensing, to introduce the design of a custom capacity-based humidity sensor, from initial numerical simulations to circuit architecture and fabrication. The testing and use of a commercial humidity sensor is also described, as the initial off-the-shelf solution for the creating of a testing platform for hermeticity testing of micro-packages.
- Chapter 4, "Chronic Stability of Implanted Silicon Devices", investigates the chronic performances of silicon based implants when only polymer encapsulation is used. It presents the design of custom silicon test structures for accelerated life testing, together with the experimental setup and the obtained results. Two novel circuit topologies for the evaluation of water ingress in a CMOS stack are described and discussed.
- Chapter 5, "Design of a Microwire-based Mm-scale Cortical Recording Implant", presents the current trends for the fabrication of hermetic feedthroughs for neural applications and their associated challenges. It then discusses two iterations of a fabrication and assembly strategy for a microwire-based millimetre-scale neural implant.
- Chapter 6, "Conclusion", summarises the content of the thesis, and concludes by highlighting the original contributions and discussing future directions of the project.

Bibliography

[1] T. Urban, "Neuralink and the brain's magical future," *Wait But Why*, 2017. Available at `https://waitbutwhy.com/2017/04/neuralink.html`.

[2] R. Epstein, "The empty brain," *Aeon, May*, vol. 18.

[3] G. E. Pugh, *The biological origin of human values*. Basic Books, New York, 1977.

[4] World Health Organization, *World health statistics 2016: monitoring health for the SDGs sustainable development goals*. World Health Organization, 2016.

[5] A. D. Lopez and C. C. Murray, "The global burden of disease, 1990–2020," *Nature medicine*, vol. 4, no. 11, p. 1241, 1998.

[6] World Health Organization, *Neurological disorders: public health challenges*. World Health Organization, 2006.

[7] M. H. Kohrman, "What is epilepsy? clinical perspectives in the diagnosis and treatment," *Journal of Clinical Neurophysiology*, vol. 24, no. 2, pp. 87–95, 2007.

[8] A. Singh, L. Tetreault, S. Kalsi-Ryan, A. Nouri, and M. G. Fehlings, "Global prevalence and incidence of traumatic spinal cord injury," *Clinical epidemiology*, vol. 6, p. 309, 2014.

[9] M. DiLuca and J. Olesen, "The cost of brain diseases: a burden or a challenge?," *Neuron*, vol. 82, no. 6, pp. 1205–1208, 2014.

[10] E. Musk *et al.*, "An integrated brain-machine interface platform with thousands of channels," *Journal of medical Internet research*, vol. 21, no. 10, 2019.

[11] M. A. Lebedev and M. A. Nicolelis, "Brain–machine interfaces: past, present and future," *Trends in Neurosciences*, vol. 29, no. 9, pp. 536–546, 2006.

[12] C. I. Penaloza and S. Nishio, "BMI control of a third arm for multitasking," *Science Robotics*, vol. 3, no. 20, p. 1228, 2018.

[13] U. Chaudhary, N. Birbaumer, and A. Ramos-Murguialday, "Brain–computer interfaces for communication and rehabilitation," *Nature Reviews Neurology*, vol. 12, no. 9, p. 513, 2016.

[14] J. Wolpaw and E. W. Wolpaw, *Brain-computer interfaces: principles and practice.* OUP USA, 2012.

[15] V. Gilja, C. A. Chestek, I. Diester, J. M. Henderson, K. Deisseroth, and K. V. Shenoy, "Challenges and opportunities for next-generation intracortically based neural prostheses," *IEEE Transactions on Biomedical Engineering*, vol. 58, no. 7, pp. 1891–1899, 2011.

2. Neural Implantable Medical Devices: Current Solutions and Future Technological Challenges

During the course of history, we have always tried as humans to use our ingenuity when facing difficulties, and possibly no adversity is bigger of a danger that the ones threatening our own bodies, such as diseases and disabilities. The knowledge and tools available at any specific point in history were often put to use for healing sufferers and restoring body's capabilities. We have evidence of cosmetic foot prostheses from ancient Egypt dating as far back as the 28^{th} century BC, while the first devices that could be considered true rehabilitation aids were produced by the Greek and Roman civilizations [1].

The effectiveness of these solutions has always evolved together with the growing comprehension of the human body and the technological and manufacturing advancements. One of such major developments happened in the second half of the 18^{th} century, when Italian physician and physicist Luigi Galvani discovered the interaction between biological tissue and electrical stimuli, by observing the contraction of a dissected frog's limbs caused by a spark from a nearby electric machine [2]. His experiments pioneered the field of what he called at the time "medical electricity", and that we now know as electrophysiology. The impact of his results spread beyond the scientific community and went on to influence popular culture, most notably inspiring Mary Shelley's novel *Frankenstein*, that builds upon the idea of giving back life through artificial technology.

Continuous scientific discoveries and new technical solutions in the field of electricity, and in particular the advent of electronics at the beginning of the 20^{th} century, paved the way for major breakthroughs in the way technology interfaces with our bodies to provide medical treatments, and in particular for the development of implantable devices.

2.1. Merging body and technology

Medical devices can be defined as *implantable* when they are introduced, partly or totally, into the body with the intent to remain there after the procedure [3]. The earliest example is the implantable cardiac pacemaker, developed by Wilson Greatbatch in the mid-1950s and successfully implanted in a human in 1960 [4], replacing external pacemakers which were bulky and caused damages to the skin. This device was composed by a central unit implanted in the chest containing the electronics and the nickel-cadmium battery, from



(a) (b) (c)

Figure 2.1.: Examples of different types of past and current implantable medical devices for therapeutical applications: (a) Central unit of a Greatbatch cardiac pacemaker made by Medtronic (circa 1960). The diameter is approximately 55 mm (© Museum of Health Care, Kingston, CA); (b) Medtronic Advisa DR MRI™ SureScan™ cardiac pacemaker, compatible with full body MRI scans; (c) Flowonix Prometra® II drug delivery implantable pump.

which the stimulating electrodes departed (see Figure 2.1a). The housing was made of polymer-based epoxy resin, but this material experienced swelling over time, and dissolved into the body [5].

To resolve the issue, current implantable pacemakers use a laser welded titanium package, which is biocompatible, durable, and offers great mechanical and corrosion resistance. Ceramic-based connectors ensure a path for the electric signals in the leads while maintaining them electrically insulated from the metallic enclosure (Figure 2.1b). A similar type of devices, implantable defibrillators share an equivalent structure, and use the same type of enclosure as pacemakers. Devices like these have proven extremely successful and are currently implanted in millions of people worldwide.

Bone growth stimulators are devices that provide electrical stimulation to promote bone growth in fractures that are difficult to heal, most notably the spine. Titanium is again the material of choice for the packaging, and the leads are insulated with silicone (Figure 2.1c).

Another category of commercially available implantable medical devices (IMDs) are implantable drug delivery systems. An example is the Prometra® II pump, which delivers pain-relief medications to patients suffering with chronic pain. Titanium casing is still used to host the battery and the electronics, with a flexible catheter for drug delivery at the desired site.

These examples share some common design features regarding the casing, with titanium being the material of choice for the vast majority of them. This is often possible given the relatively large dimensions of these devices, but proves more challenging when shrinking the size of the implant to the millimetre scale, as will be discussed later in this chapter.

Another common feature is that from the advent of implantable devices until recently, the main function of these systems has been unidirectional, and particularly delivering stimuli, electrical or chemical, to the desired target region. More recently, thanks to the

continuous miniaturization in size and power consumption of electronic circuits, there have been many efforts towards closed loop systems, able to sense biological data in real time and react accordingly, processing the information within the body of the patient. This would be particular beneficial in our ageing society, where such technology could actively support patients at home and minimize hospital care [6].

All the devices mentioned above have been successfully applied as therapeutical devices for various parts of the human body, and they gave us an idea of the type of encapsulation and materials used for implantable devices; we now focus our attention on applications for the nervous system.

2.2. Connecting to the nervous system: neuroprosthetics and brain-computer interfaces

Before going into detail with regard to the various types of available neural implantable devices, we give a brief overview of the human nervous system (see Figure 2.2).

The nervous system can be divided in two main components, the central nervous system (CNS) and the peripheral nervous system (PNS). The CNS consists of the brain and the spinal cord, both of which are enclosed in three protective membranes called meninges: the dura mater on the outside, the arachnoid mater in the middle, and the pia mater on the inside, in contact with the neuronal tissue. The CNS is also protected from mechanical injuries by the skull and the vertebral column, and is chemically protected by the blood-brain barrier. The PNS is formed by the remaining nerves and ganglia, and mainly acts as a connection between the CNS and the other parts of the body.

Zooming in on the brain, it is possible to distinguish several regions, whose anatomy reflects the millennia of the brain's evolution. Starting from the junction between the brain and the spinal cord we encounter the medulla, pons, and cerebellum. Moving further up, there is the midbrain, the diencephalon, and finally the telencephalon, which constitutes the largest part of the brain and is split in the two cerebral hemispheres [7].

The outer layer of these hemispheres, called cortex, shows the characteristic folds which increase the surface area. Various areas of the cortex can be mapped based on the predominant functions that the neurons in that area are dedicated to (see top right in Figure 2.2).

Neurons are a very specific type of cell, and are the basic building block of the nervous system. There exist different types of neuron, each specialized for a specific task. For simplicity we take as an example a multipolar neuron (pictured bottom right in Figure 2.2). This neuron has a main cell body called soma that contains the nucleus and is surrounded by cellular ramifications called dendrites. A single, longer branch called axon, extends from the soma and has ramified ends. Neurons are connected to each other to form an extremely complex network. Signals are exchanged between neurons in an electrochemical way: the axon terminals of a neuron connect to the dendrites of multiple other neurons in what are called synapses. In a synapse, chemicals known as neurotransmitters are released

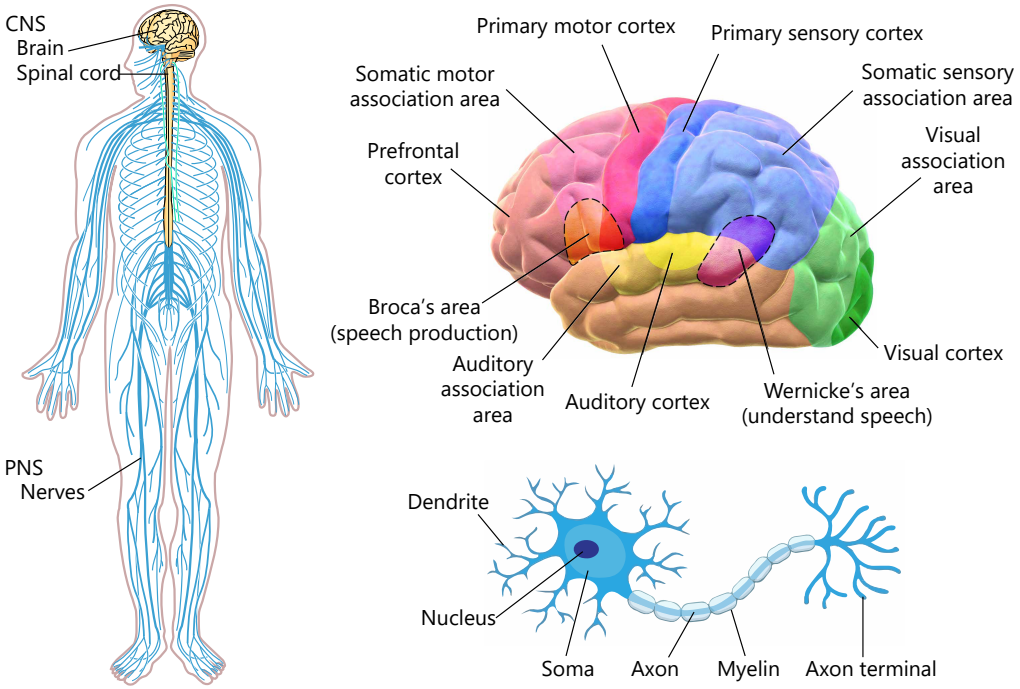


Figure 2.2.: Overview of the human nervous system: on the left a representation of CNS and PNS; on the top right, a diagram of the brain with highlighted the motor and sensory functional regions of the cortex (adapted from [8]); on the bottom right, a multipolar neuron.

from the axon terminal and sensed by the receptors on the dendrites of the target neuron. The neurotransmitters cause a raise in the membrane potential of the neuron (that usually rests at about $-70\,\mathrm{mV}$). When the concentration of neurotransmitters is high enough to cause this membrane potential to exceed a certain threshold value (in general around $-55\,\mathrm{mV}$), it causes a rapid positive spike that travels through the axon, and reaches the next synapse.

It is this electrical behaviour of the neurons that has opened the possibility of creating technology that can interface with the nervous system. The first example of such technology was created in 1924 by German psychiatrist Hans Berger, when for the first time and using rudimentary silver electrodes, he recorded electric signals from the scalp. To describe these signals he coined the name electroencephalogram (EEG) [9]. The discovery was the first seminal example of a Brain-Computer Interface (BCI), a term used for the first time in 1973 by University of California at Los Angeles professor Jacques Vidal in one of his publications [10]. This term and its equivalent Brain-Machine Interface (BMI) indicate those systems that measure activity of the nervous system and convert it into new, artificial outputs, different from the traditional hormonal or neuromuscular outputs of the CNS [9].

Not all kinds of neural interfaces that have been developed over the years fall into the above definition of BCI. As BCIs aim at providing new outputs from the CNS, other devices

deliver stimulation to target areas of the nervous system to restore function or replace lost tissue. This category of devices thus focuses on creating new inputs to the nervous system, as opposed to BCIs, and is usually referred to with the term *neuroprosthetics*.

The development of neuroprostheses has generated a number of successful applications over the last decades. Perhaps one of the major examples is the cochlear implant, a system designed to restore hearing capabilities in patients affected by profound deafness. It is composed of an external unit equipped with a microphone to pick up the sound from the environment, which is then processed and sent to an implanted device through a transcutaneous inductive link. The implant contains an array of electrodes inserted in the cochlea, inside the inner ear. The electrodes are able to directly stimulate the auditory nerve with the signal received from outside. Originally invented in 1957, the first successful multi channel devices were implanted in the 1970s. According to the US National Institutes on Deafness and Other Communication Disorders, as of 2017 more than 324,000 people across the world live with a cochlear implant [11].

Another successful example of neuroprosthetic device is the use of neurostimulators for deep brain stimulation (DBS). This device uses implanted electrodes that reach the internal areas of the brain and provide electrical stimulation to treat the symptoms of various conditions, like Parkinson's disease, essential tremor, and more recently certain forms of epilepsy [12]. The electrodes are connected to a generator implanted in the chest that hosts batteries and electronics, packaged in a way that is very similar to the IMDs presented in section 2.1.

Likewise, spinal cord stimulators have proven to be effective as pain relief devices by reducing the intensity and the duration of pain. Their electrodes interface with the nerve fibres in the spinal cord to provide electrical stimulation that attenuates the painful sensation [13].

Visual prostheses have also been an extremely active field of research. Their objective is to restore vision in blind patients by stimulating one of the neural areas of the visual pathway, from the retina to the visual cortex. Although several studies have reached human trials, many challenges are still present with this type of prostheses, and currently only few devices have been approved for medical use [14], like the Argus® II by Second Sight, a retinal stimulator for the treatment of *retinitis pigmentosa*.

In general, we can say that the development of neural interfaces has followed a similar development process as the other IMDs described in section 2.1: while the first successful examples were mainly stimulators that targeted the symptoms of specific conditions, current efforts are moving towards system that can sense the activity of the nervous system and respond accordingly in real time, by either actuating external technology, or acting back on the neural tissue. This blurs the lines between the definitions of BCIs and neuroprostheses, since inputs and outputs now operate in a closed feedback loop, but at the same time creates new opportunities for the development of novel systems that might improve the lives of millions of people around the world.

2.2.1. Sensing brain activity

To get a broader understanding of the way different BCIs operate, and to recognize the different technological challenges they pose, it is important to consider the various types of neural electrophysiological signals that they target (see Figure 2.3 for reference).

A general consideration valid for all the presented signals is that their quality is greatly influenced by multiple factors: from the amount of tissue damage during insertion and consequent immune response to the electrodes' material, impedance, separation, and placement. A significant amount of signal processing is required to enhance signal-to-noise ratio (SNR) and extract the desired features form the raw signals. Given the necessary amount of computational power and the consequent power dissipation, such processing is usually performed in a different site than the implant.

Electroencephalogram

Starting from the less invasive type of recording, the first kind of brain signal encountered is the already mentioned EEG. It is a low frequency electrical signal (<100 Hz), generated by the simultaneous activity of a very large population of neurons, which in turns generates a variable electrical potential across the surface of the brain that can be recorded from the scalp. Such activity can either be caused by specific events (such as a sensory stimulus or a performed action) or by the natural oscillation in neural potential. The practical use of EEG signals implies the establishment of an empirical correlation between the functions of the CNS and the recorded EEG patterns [15]. The signal spectrum can be separated in different bands, each associated with different states or activities of the recorded subject, and usually sensed in distinct locations.

EEG signals are recorded using electrodes placed on the surface of the scalp. Depending on the targeted functionality, different hardware configurations exist, with variable parameters, from the number of electrodes, to their placement, separation, and impedance. EEG systems are generally cost effective compared to other brain recording or imaging techniques, don't require any invasive procedure, and have no significant side effect. Thanks to these characteristics, they are commonly employed both in the diagnostic and research environment. More recently even the consumer sector is exploring their potential, especially in applications such as video games and virtual reality [16].

However, when compared to others more invasive solutions, EEG systems show a lower spatial resolution, and a poor SNR. This is mainly due to the considerable signal attenuation produced by the distance between the recording electrodes and the surface of the brain, as well as the susceptibility to artefacts caused by movement. Various signal processing and feature extraction techniques have been investigated to mitigate these drawbacks [17] but, as of today, EEG-based BCIs lack the resolution obtained using more invasive systems.

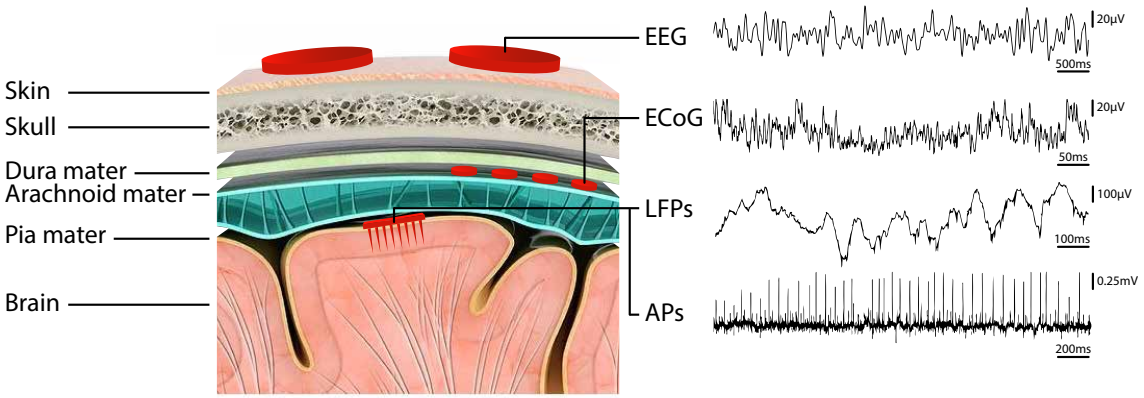


Figure 2.3.: Main different electrophysiological brain signals and location of their respective recording sites (adapted from [18]). The waveforms depicted here are illustrative, as each of these signals can present considerable variability due to factors such as type and placement of electrodes, or the data filtering and processing employed.

Electrocorticogram

By placing electrodes closer to the surface of the brain, it is possible to perform an electrocorticography (ECoG). The nature of the ECoG signal is the same of the EEG, but there are two main factors that differentiate these techniques: (i) being recorded directly from the surface of the brain, ECoG signals don't suffer from the attenuation due to the layers of bone and skin that affects the EEG. This results in a sharper activity and a larger signal amplitude; (ii) ECoG is recorded from an area of, at most, a few squared centimeters, making it a much more localized methodology for activity recording compared to EEG, which in turns records across the whole scalp. Therefore with ECoG the ability to sense large oscillatory patterns in brain activity is partly lost in exchange for a more accurate local resolution.

The ECoG devices generally consist of a one or two-dimensional array of metal electrodes embedded in a polymer substrate, with wires connecting to the outside of the skull. The array is usually placed below the dura, the ticker of the three meninges, but above the arachnoid mater, although in some case also the arachnoid is, at least partially, removed [19], and the ECoG electrodes are in contact with the pia mater. Being closer to the brain cortex, the spatial resolution of ECoG is significantly higher compared to EEG, but the obvious trade-off is the need for an invasive surgical procedure necessary to implant the electrode array.

Since its first applications in the 1950s, ECoG recording has been predominantly used to identify and monitor in the short term areas of the brain that require surgery. For example, in patients suffering from severe epilepsy, ECoG signals can be used to identify the areas of the brain from where seizures originate, and to monitor post-surgical brain activity [20]. ECoG arrays have also been used as stimulators to perform functional mapping of

the cortex. By using electrical stimuli to excite or inhibit specific areas of the brain, it is possible to map such areas to certain functions, and prevent unwanted damage during surgery [21].

More recently there has been increased interest in using ECoG recordings for BCIs applications [22]. Studies have demonstrated the use of high-density ECoG arrays for individual finger control [23], and the use of two wireless epidural recording implants to give a tetraplegic patient control over a robotic exoskeleton [24]. These results show the promising potential of ECoG-based BCIs, although currently they have yet to match the superior spatial resolution of intracortical solutions.

Local Field Potentials & Action Potentials

Using electrodes that penetrate the brain cortex, it is possible to get closer to neurons and record their activity with the highest spatial resolution. The firing activity of a single neuron can be observed by recording its action potential (AP), also referred to as *spike* due to its impulsive characteristic. As described in the previous overview of the nervous system, these spikes represent the sudden change in the electrical potential of the outer membrane of neuron cells, and their occurrence is a direct signal of neuron activity. Since the APs are generated by individual cells, it is necessary for the recording electrodes to be very close to the desired source in order to achieve good SNR. This implies sensing electrical activity in a radius of approximately 0.05 to 0.35 mm from the surface of the electrode. Moreover, in order to effectively record APs, a sufficiently high sampling rate is required, usually above 10 kHz [25].

APs provide a real-time measure of a single neuron being activated, and therefore by recording them it is possible to achieve the highest information granularity. However, it is particularly challenging to obtain consistent signal quality *in vivo* over time. The relative motion between the neurons and the electrodes makes it difficult to track the behavior of specific cells. Moreover, the glial encapsulation of the implant diminishes the sensitivity of the electrodes, as a consequence of foreign body reaction [26].

To overcome the challenges posed by the recording of APs, it is possible to shift the focus to another type of signal, known as local field potentials (LFPs). LFPs are electrical potentials generated by the simultaneous activity of clusters of nearby neurons. These signals are recorded in the extracellular space within the target tissue volume. Using a crowded room as a simplified analogy, where each person represents a neuron, we can compare the recording of APs with listening to single people speaking, while the recording of LFPs corresponds to get local averages of the loudness of the various conversation groups in the room. It is evident that, by using LFPs, the details in operation of single cells are lost. This reduction in spacial resolution is compensated by better chronic performances. In fact the larger recording area, around 0.5 to 3 mm from the electrode's tip, allows for a bigger margin for relative motion between implant and tissue, increasing the stability of the recording over longer periods of time. The requirements on the implant's electronics are

Table 2.1.: Summary of the main characteristics of brain signals

Signal	Size of recorded neuron population	Spacial resolution	Temporal resolution	Device size	Invasiveness of current recording devices
EEG	Billions of neurons	cm	100s of ms [29]	Full head coverage	Low (outside scalp)
ECoG	~500,000 neurons [30]	mm	ms [31]	Few cm^2	High (requires surgery but no brain penetration)
LFP	~100 to 10,000 neurons [32]	From 100s of µm to mm	ms [33]	From mm^2 to cm^2	Very high (brain penetration)
AP	Down to single neuron	µm	$\leq$ ms [34]	From mm^2 to cm^2	Very high (brain penetration)

also relaxed, since LFPs have lower frequencies than APs (up to a few tens of hertz), and are usually recorded with sampling frequencies of up to a few hundred hertz [25]. Despite containing less raw information than APs, it has been proposed that the information content of LFP signals might be sufficient for decoding brain activity related to motor skills [27]. This would allow for simpler, more reliable implants, by moving the engineering complexity to the off-site decoding of the brain signals. It is worth noting that at present, the types of micro-electrodes used to record LFPs and APs are in general similar, and the distinction between the two signals is often performed by the electronics and the necessary signal processing.

The main characteristics of the presented electrical signals are summarized in Table 2.1 (please note that the "Device size" column only indicates the dimensions of the recording elements, without considering the external hardware required for data processing). It is evident how a compromise needs to be made between invasiveness and resolution. On one hand, the development of medical devices has to keep the safety and well-being of the patient as the first priority, minimizing risks. The impact of a surgical operation, and in particular brain surgery, must not be underestimated. In fact, the main motivation behind many EEG studies derives from such considerations. On the other hand, invasive systems have shown superior spatial resolution, and have the potential for the development of high-bandwidth applications. Moreover, FDA-approved neural implantable stimulators like the previously mentioned systems for DBS, have been largely used in thousands of patients, showing a very low incidence of complications [28].

A number of different intracortical implants have been proposed and investigated, but they haven't proved to be mature enough to be employed outside the research environment. In fact, although they have demonstrated excellent performances in recording high-resolution brain signals, they still suffer from durability issues. The current state-of-the-art devices for intracortical recording will be further discussed in the next section.

2.2.2. Neural implants for cortical recording

In order to understand the challenges posed by chronic implantable interfaces, we examine the current state-of-the-art devices used for cortical recording of brain activity. The majority of these devices have proven to be very effective in the research environment. However, with just a few exceptions, they have not received FDA approval to be used as clinical tools.

Microwire-based implants

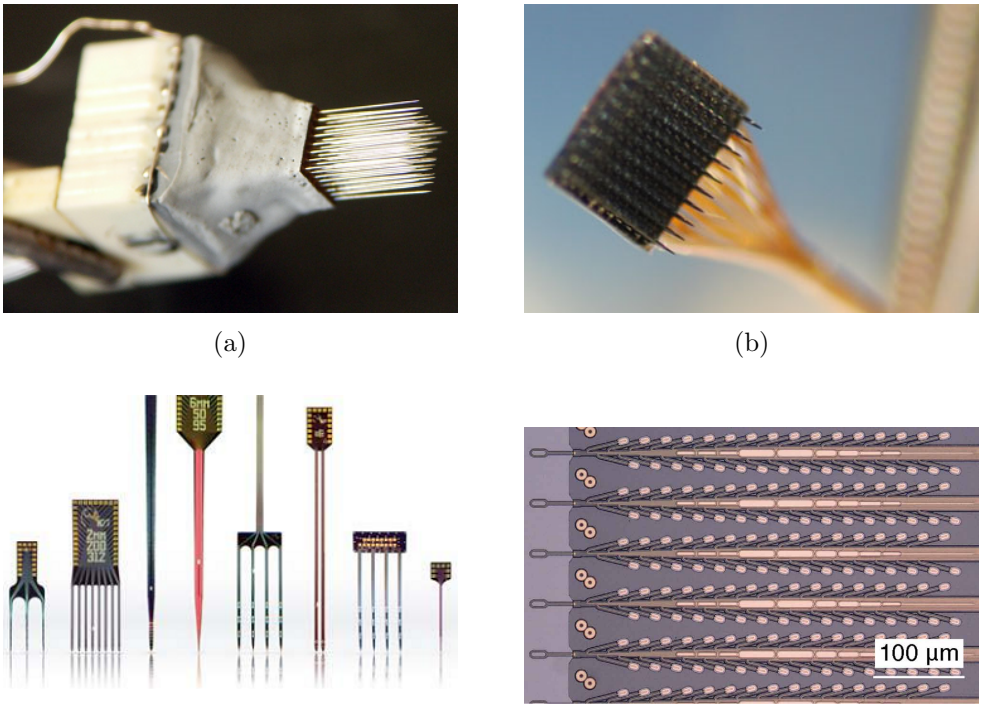
Microwires have been on of the earliest examples of implants to record neural signals. They consist of thin metal wires with a diameter of about 10 to 100 µm. Standard materials of choice are tungsten, platinum, or a platinum/iridium alloy. The wires are coated for insulation, except for the tip, which acts as the recording electrode [35]. Since every microwire only has a single recording site, multiple wires are usually combined together to form bundles or two-dimensional arrays, where the number of wires, together with their length and separation is custom designed to fit the desired application, and therefore the target area of the brain (see Figure 2.4a).

Microwire arrays allow for great design adaptability in the number and location of recording sites, as well as electrode's surface area and geometry. Also they have so far demonstrated remarkable chronic performances, reaching more than 5 years of cortical recordings from monkeys [36, 37]. However, microwire arrays still rely on bulky connectors for interfacing the wires with the required electronics for signal acquisition. Moreover, they generally require laborious manual assembly, and present challenges during insertion, given the flexible nature of microwires that move and spread inside the tissue, making it harder to target a specific recording area.

Utah electrode arrays

The Utah electrode array (UEA) (Figure 2.4b) is a silicon based microelectrode proposed in the 1990s by University of Utah professor Richard Normann [42], and is currently the most used recording implant for intracortical BCIs [9]. It is micro-machined from a single monocrystalline silicon substrate to produce a matrix of needles. The tips of these needles are then metallized, while the rest of the device is insulated with polymer deposition [43]. The usual configuration is a 10x10 array, with a total size of 4x4 mm and needle length that ranges between 1.5 and 2 mm. To this day, UEAs are the only cortical recording interfaces that have been approved for clinical use, as demonstrated by the BrainGate BCI, that allows the remote control of a prosthetic arm [44].

By exploiting fabrication methods typical of the microelectronics world, UEAs can be manufactured with high yield, and with a moderate degree of design variations in terms of dimensions and number of recording points. Although some wireless versions of UEAs have been proposed [45, 46], they remain mostly wired-based interfaces, that require con-



(a) (b)

(c) (d)

Figure 2.4.: Examples of different types of intracortical implantable interfaces for neural recording: (a) 64 channel platinum/iridium microwire array by Clunbury Scientific LLC [38]; (b) 4x4 mm Utah array, with recording electrodes configured in a 10x10 matrix [39]; (c) Various types of Michigan probes manufactured by NeuroNexus, showing the wide range of available geometries [40]; (d) Example of multi-channel polymer-based microelectrodes from Neuralink [41].

nectors mounted on the outside of the head, with wires piercing the skin, skull, and dura. Moreover, the implantation procedure requires a relatively high amount of force to push the needles in the cortex and avoid tissue dimpling, and it is generally carried out using a pneumatic insertion device [47]. This fact, together with the rigidity of UEA's needles, is one of the reasons why UEAs have shown significant tissue encapsulation when implanted for long periods of time, with associated degrading in recording quality [48].

Michigan probes

Michigan-style probes (Figure 2.4c) are also silicon based but, unlike UEAs, they are planar devices built in a way that more similar to standard electronic ICs. Michigan probes present one or multiple planar silicon shanks, on which the recording electrodes and metal traces are patterned through lithography. This allows for very high density of recording sites along the probe, with up to hundreds of channels, and a great freedom when designing the probe layout, from one-dimensional to stacked 3D arrays [49]. Thanks to the higher electrode density, Michigan probes are currently the implantable brain technology that allows for the highest spatial resolution when recording or stimulating neural tissue.

Moreover, while Utah arrays tend to have more standardized sizes and electrode arrangements, the design of Michigan probes can be customized to a much higher degree: all the design parameters, such as number and arrangement of recording sites, electrodes' dimension and separation, can be fine tuned for the desired application, depending on the animal and brain region to target, and the use of lithographic fabrication ensures good reliability. One major advantage over Utah arrays, which have a single recording site on the tip of each needle, is the possibility of interfacing with tissue at different depths. This allows to reach the different layers of the brain cortex, providing a very valuable investigation tool to scientists. Being fabricated on silicon substrates, Michigan probes are also more easily integrated with the required electronics for signal conditioning and processing. Thanks to these advantages and their high degree of customization, they have been widely adopted in the research community for *in vivo* acute studies and applications.

The drawbacks of Michigan-style probes mainly arise from their thicker and stiffer shank, in comparison to microwires, which causes a larger amount if tissue to be displaced and damaged during insertion. Attempts at thinning the substrate have to face the higher probability of probe fracture due to silicon rigidity [50]. They also tend to not sit flush with the surface of the brain, contrary to Utah arrays, and the upside of hosting tens to hundreds of electrodes is offset by the need for more wires and bulky connectors. This increases their overall fragility and complicates their use in chronic applications, where the dura and skull should be closed back after the implant insertion. These obstacles have so far prevented the use of Michigan probes in chronic applications, although they remain an extremely valuable research tool.

Polymer-based probes

Polymer-based cortical neural probes (Figure 2.4d) include a wide variety of designs, whose common denominator is the idea of using flexible polymers as passive substrate, replacing the silicon of previous examples. The main objective of such designs is to reduce the mechanical mismatch between the implanted device and the surrounding tissue. These benefits are balanced by additional challenges for the implantation, given the soft nature of polymer probes that requires the help of stiffeners to avoid curling of the implant, as well as a greater difficulty in targeting a specific area of the brain. Polymers also generally suffer from poor chronic performances due to higher water absorption rates, dissolution, and delamination [51]. Also the connection to the active electronics might present more difficulties, given the profoundly different fabrication strategies for both components.

The research community continues to develop and present new and improved implants, some of which are showing promising performances [52, 53], but the devices presented so far are the most widely used. This highlights the intense research activity in the field of BCIs, but also underlines the growing need for a reliable neural interface that could successfully aim at medical applications.

2.2.3. Challenges of chronic cortical implants

The implantation procedure of intracortical neural interfaces comes with all the risks associated with intracranial brain surgery. In order to avoid multiple interventions for replacing or remove the implantable devices, it is extremely important to design devices in a way to ensure a long lasting and safe operation, with minimal side effects. To achieve this, we first consider the major challenges faced by chronic implants. It is possible to identify three main categories of device failure: biological, material, and mechanical [48].

Biological failures are linked to the modalities in which the tissue responds to the trauma caused by the implant. This trauma provokes the foreign body response (FBR), an inflammatory reaction of the tissue to the presence of the implant. This triggers glial cells proliferation in proximity of the implant, at a distance of about 20 to 10 µm which, over time, can encapsulate the implanted device and displace it, as well as moving the neurons away from the electrodes, reducing the recording performances [54]. The rupture of blood vessels, and particularly the breach of the blood-brain barrier during implantation has proven to worsen the severity of FBR [55], and specific tool to avoid breaking the capillaries when inserting neural probes have been proposed [41]. The design parameters that have a major impact on these circumstances are the size and shape of the implant, together with its rigidity. Minimize the Young's modulus mismatch between implant and brain tissue has proven to have a great influence in reducing the symptoms of FBR. Using materials that conform to the neural tissue also help in diminishing relative motion of the implant with respect to the brain [56]. The implant materials in contact with the tissue also need to be bio-compatible and not present any toxicity that might cause infection. The presence of electronics embedded on the implant, or the use of wireless telemetry methods, must also ensure that the power dissipated in the tissue is limited, and does not cause a raise in tissue temperature higher than the consensus safety margin of 1 °C [57]. In the case of wired devices, other than the infection risks in proximity of the implant, it is also essential to consider possible sources of infection from wires piercing the meninges and the scalp. Finally, as stated previously, the insertion method plays an important role and must be devised to cause minimal tissue damage.

Material failures include the deterioration in the materials of the implant, from the metallization of the recording electrode, to cracks or delamination in the insulating encapsulation. Damage in the insulation close to the recording points usually leads to lower electrode impedance, which in turn translates into smaller signal amplitude [48]. An impermeable barrier is also required to prevent the fluids present in the body from entering the cavities of the device that host moisture sensitive elements that could suffer from corrosion. A breach in this barrier would not only cause implant deterioration, but also expose the tissue to possible contamination and outgassing from non-biocompatible materials used in the manufacturing of the implant.

Mechanical failures are associated to hardware damages that prevent data recording,

such as implant displacement, failure of cables, connectors or feedthroughs, or even device fracture. This factors are dependent once again from the materials and design of the implant, and on the way the various part of the implanted device are fixated in place [58].

These various modalities of failure show the vast amount of design aspects to be taken into account, and how each one of them impacts on the long term performances of an implanted neural interface. Of particular importance is the packaging aspect: in order to ensure a reliable operation, the choice of encapsulation materials and methods must be carried out concurrently with the functional design of the implant, since design choices in both domains heavily influence each other [59].

To deliver a successful chronic cortical interface, the target requirements remain safety, stable and effective operation for years, suitable data telemetry and power management (either using wireless power transfer or long-lasting batteries), and employment of external elements that are robust and convenient [9].

2.2.4. Millimetre-scale distributed cortical implants

In the light of the issues presented in the previous section, the research community is very actively exploring different approaches for the realization of chronic neural interfaces. Since reduction in size has proven to be a fundamental aspect for better long-term performances, the designs that propose extreme miniaturization of the implants are of particular interest.

While the methods for shrinking down the size of the implants can tap into the current expertise of microfabrication processes, the miniaturization also causes new issues to arise. In order to maintain a high channel count and retain the required resolution, a distributed architecture is required: a neural interface composed of many identical small devices, each one independent in its own functionality. This also leads to a different approach for power delivery and data transmission to and from the implants: the presence of tens to hundreds of devices prevents the use of wired connections, and a wireless strategy to transmit data is required. Similarly, power must be provided to each separate implant, but at the same time the miniaturization of the devices makes it difficult to use batteries to store power on the individual implants. Therefore, power efficiency of the embedded electronics becomes a crucial requirement. Moreover, the established fabrication methods for the encapsulation layers and feedthroughs seen in section 2.1 become extremely challenging on a sub-millimetre scale, and new strategies have to be investigated.

There are also further considerations to be made regarding the practical aspects of handling and manipulating the devices in the surgical context. These aspects are too often overlooked during the engineering design phase, but can be just as crucial as the performance specifications of the implants for a successful clinical translation. Handling the devices becomes increasingly hard for the surgeon when device dimensions scale down to and below the millimetre scale, requiring the designers to develop *ad hoc* instrumentation to facilitate the implantation procedure. Moreover, some degree of automation or robotic assistance might be of great help given that the majority of the proposed distributed

interfaces relies on the use of tens to hundreds of devices, which would made a manual insertion procedure unfeasible.

Another aspect to consider is the possibility of explantation: what happens if there is the need to remove part of the neural interface, or even all the implants? This operation might prove challenging when in presence of a very high number of implants, scattered on the surface of the brain. Currently proposed architectures have not provided specific solutions for this problem. However, they all tackle long-term, chronically debilitating conditions, and therefore should not be subject to frequent removal or replacement of the implants. Moreover, a common objective across the various proposed types of distributed interfaces, is to design the individual miniaturized implants to be non harmful to the body even in case of functional failure. In such cases, the neural interface should be able to determine which implants have lost functionality, and might therefore misbehave, and then act accordingly, for example by halting the power delivery to those specific implants.

So far there has not been a definite solution to such issues, and various research groups are experimenting with different architectures, both at device and at system level, to deliver a scalable, chronic neural interface. We report here a few examples, to show the current trends in the design of such systems (Figure 2.5). It is important to remind that, in contrast with the devices presented in subsection 2.2.2 that are mostly well established solutions in the research environment, these are experimental devices, currently under research and development, and in most cases still at a *proof of concept* stage.

A first example of a distributed neural interface that employs a multitude of identical, miniaturized implants is the concept called *neural dust*, developed by Prof. Michel Maharbiz and Prof. Jose Carmena's team at UC Berkeley (Figure 2.5a). The system is composed of tens to hundreds of grain-sized sensors, each having a recording and a reference electrode. These sensors also host an ASIC for data acquisition and conditioning, and a piezoelectric element, to allow for ultrasonic data transmission and power delivery to and from a sub-dural transceiver [60]. The use of ultrasound is motivated by the fact that it has considerably smaller losses in soft biological tissue compared to electromagnetic waves, and its lower propagation speed causes ultrasonic waves to have shorter wavelengths at low frequencies, which in turn allows for the miniaturization of piezoelectric components. On the downside, ultrasound has in general a lower short-range transfer efficiency compared to wireless electromagnetic solutions, and is greatly attenuated by rigid bone tissue. This last consideration explains why the first applications of neural dust are focusing on the recording from the PNS, where the neural tissue is not enclosed by the skull [63]. From the point of view of the encapsulation, the millimetre-sized implants rely only on a polymer layer, and long-term studies have not yet been reported.

Another approach can be found in the work carried out at Georgia Institute of Technology by Prof. Maysam Ghovanloo's team (Figure 2.5b). They propose a distributed intracortical interface, where each implant uses a tungsten microwire for brain activity

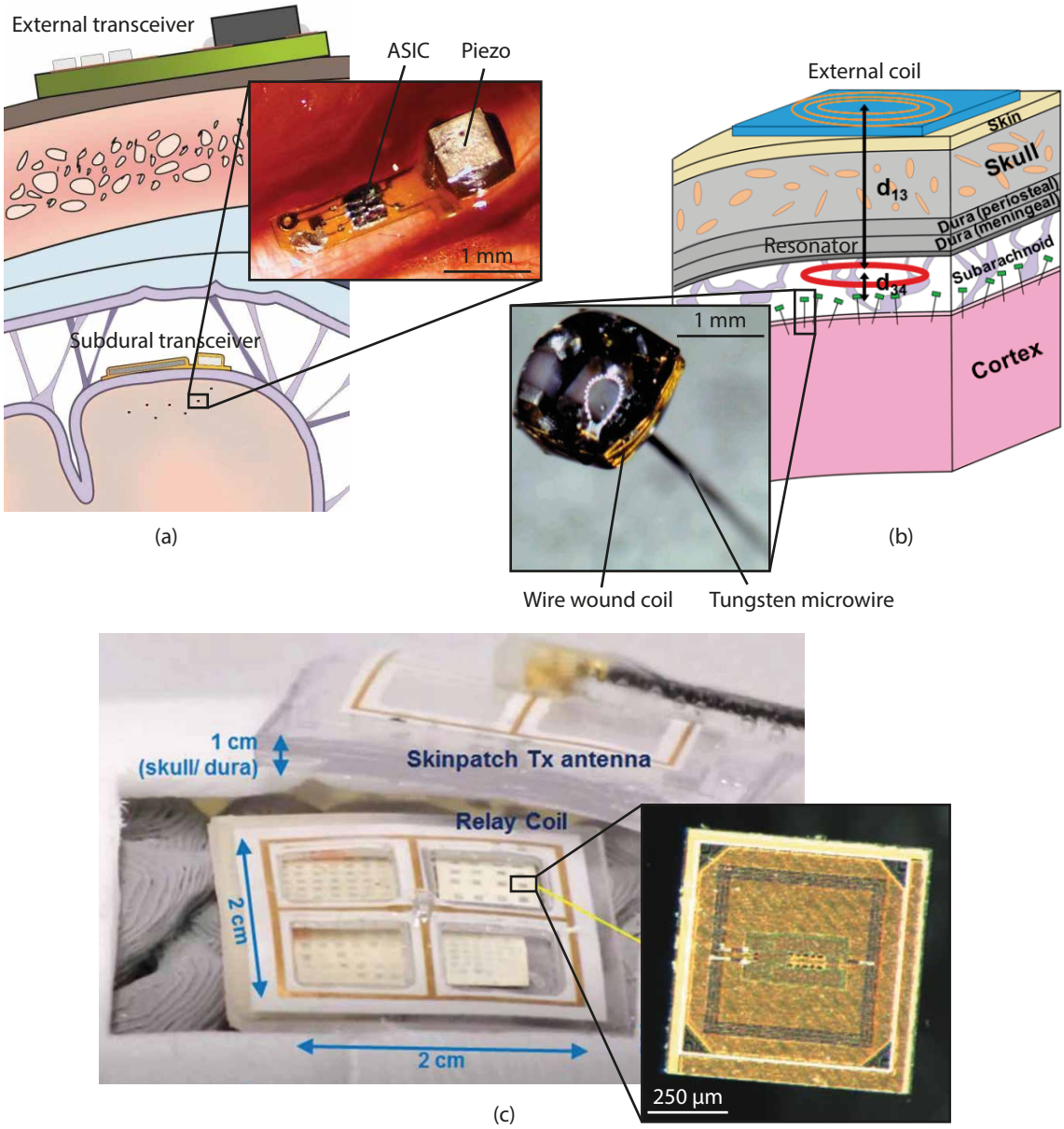


Figure 2.5.: Examples of current strategies for the realization of next-generation cortical neural interfaces: (a) Neural dust concept operating with ultrasonic power and data delivery (adapted from [60]); (b) GeorgiaTech architecture using microwire-based intracortical probes with wire wounded coils for telemetry and polymer encapsulation (adapted from [61]); (c) Array of neurograins with sub-millimetre on chip coils for RF data transfer and ALD encapsulation (adapted from [62]).

recording. The wire is bonded to a passive silicon die, and a copper coil is winded around the die to act as an antenna for data and power transfer. The encapsulation of the implant is made by coating the implant with a first layer of Parylene-C and an external layer of PDMS. The telemetry strategy employs a subdural resonator to act as middle element between the single implants and an external transceiver [61]. *In vitro* testing has proven

the robustness of the wireless link, but so far limited to the communication with a single recording device [64].

A further example is the one called *neurograins*, proposed by Prof. Arto Nurmikko's group at Brown University (Figure 2.5c). It too consists of a number of sub-millimetre implants placed on the brain cortex, with both recording and micro stimulation capabilities [65]. The implants are composed of single CMOS dies, sealed using multiple atomic layer deposition (ALD) coatings that provide hermeticity while keeping the overall volume to a minimum [62]. Data communication and power transfer is achieved using RF telemetry, with each implant having an on-chip micro-coil coupled to an external skin patch antenna, with the link being enhanced by an intermediate relay coil. This system architecture has been validated in bench top experiments, but so far has not been demonstrated in a *in vivo* setting.

The ENGINI concept

The research work presented in this thesis has been carried out as part of the EPSRC funded ENGINI project (Empowering Next Generation Implantable Neural Interfaces). Building upon the current trends for implantable interfaces, it proposes a new concept for chronic intracortical recording systems. The architecture of the system, reported in Figure 2.6a, is based on the following concepts:

- The use of a scalable, distributed interface, composed of tens to hundreds independent millimetre-sized, freely floating implants (Figure 2.6b). Each implant is equipped with microwire electrodes for recording from multiple intracortical sites, as well as a custom ASIC to perform on-board data conditioning and processing, in order to optimize data transmission. The implants are independent from each other and can be individually addressed and enabled, to allow maximum flexibility of the interface.

- A fully wireless design, necessary to avoid wired connections across the dura and across the skin, which are a main cause of infection. However, the use of full wireless transmission for both power and data poses a new set of design challenges. In particular, the communication between the individual implants and an external unit that lies on the patient's scalp has to overcome the considerable distance (at least at this scale) of a few centimeters of different tissues, including dura, bone, and skin. These tissues also absorb most of the power transmitted, thus decreasing considerably the efficiency of the inductive link. However, arbitrarily raising the power transmitted is not a viable solution, since strict safety limits on the amount of power that can be delivered through tissue have been established by regulatory bodies. The solution proposed within the ENGINI project is to split the inductive link from the outside device to the cortical implants into two, shorter links, by means of an intermediate stage. The result is the three-tier architecture shown in Figure 2.6a.

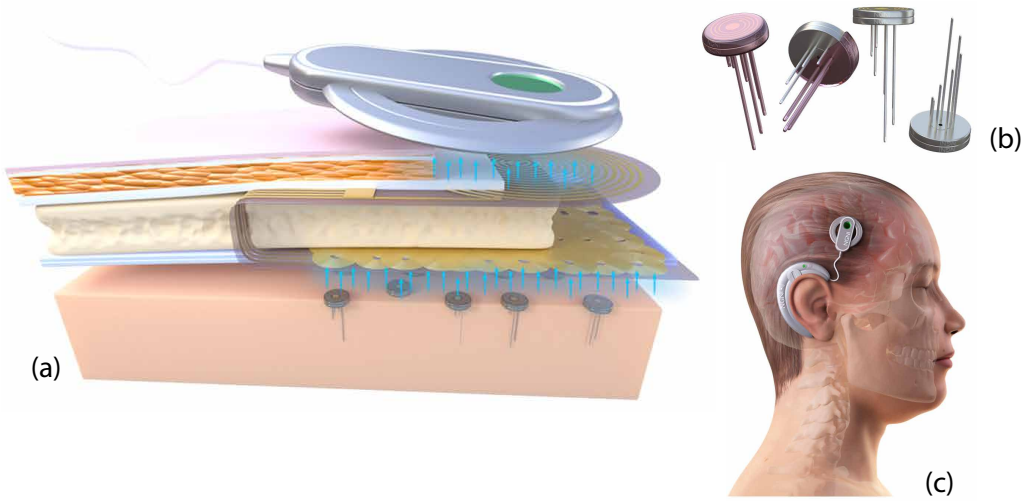


Figure 2.6.: Concept illustration of the ENGINI system and its elements: (a) The three-tier wireless network allows for data telemetry and power delivery while avoiding wired feedthroughs; (b) The independent, mm-sized implants, with microwires for intracortical recording and hermetic package. (c) The external unit that wirelessly couples with the implanted coil for power and data communication.

Power is delivered to each individual implant by an external, battery powered unit (Figure 2.6c) inductively coupled to an intra-cranial resonator coil, which allows for the addressing of single implants. The neural data recorded from the probes follows the reverse path, and is collected by the external unit for further application specific processing. The middle resonator helps by bridging the distance caused by the skull thickness, and could ideally be embedded into a custom manufactured portion of artificial bone, used during surgery to close the craniotomy.

- A strong emphasis on chronic clinical applications. In particular, the use of CMOS compatible micro-packaging techniques to achieve hermeticity for long-term reliability, while at the same time maintaining a high fabrication yield. The on-probe active circuitry is encapsulated in a hermetic cavity, which guarantees a higher level of protection when compared to the adoption of only polymer encapsulation.

The ENGINI system currently targets the recording of LFPs from the motor cortex, with applications for restoring movement in paralysed patients or to give control over artificial prostheses. Like the other solutions presented in this section, the concept is an ongoing research project, subject to modifications, and various design iterations are required in order to achieve the desired system.

2.3. Summary

This chapter has given an overview of implantable medical devices and their design challenges, from successful clinical solutions to the latest developments in brain implants.

It is clear how interfacing with the nervous system, and in particular the CNS, raises many challenging questions. In particular, given the characteristics of the various bio-electrical signals that can be recorded from the brain, a choice must be made between spatio-temporal resolution and invasiveness. For applications that require the extraction of detailed brain activity, down to single cell behavior, the only option at the moment is the use of invasive systems. While these solutions are currently adopted in the research environment, and have proven extremely useful in advancing our knowledge of the brain, they do not seem to easily translate into effective clinical tools.

In recent years, different research groups have proposed novel solutions, which share a common feature dictated by the need for chronic systems: the use of distributed interfaces, composed by many identical miniaturized implants to maintain a high spatial resolution while avoiding bulky, monolithic solutions. This paradigm promises to bridge the existing gap between research tools and clinical devices, but also faces new challenges, in particular on the aspect of fabrication, where the usual techniques for IMDs packaging can no longer be applied.

In the next chapter we will focus on the issue of hermeticity of millimetre-scale implants, and how to monitor the encapsulation status of micro-packages over time. A *in situ* sensor for relative humidity measuring is proposed, together with a testing platform for hermeticity monitoring.

Bibliography

[1] A. J. Thurston, "Paré and prosthetics: the early history of artificial limbs," *ANZ journal of surgery*, vol. 77, no. 12, pp. 1114–1119, 2007.

[2] M. Piccolino, "Animal electricity and the birth of electrophysiology: the legacy of luigi galvani," *Brain research bulletin*, vol. 46, no. 5, pp. 381–407, 1998.

[3] Y.-H. Joung, "Development of implantable medical devices: from an engineering perspective," *International neurourology journal*, vol. 17, no. 3, p. 98, 2013.

[4] W. Greatbatch and C. F. Holmes, "History of implantable devices," *IEEE Engineering in Medicine and Biology Magazine*, vol. 10, no. 3, pp. 38–41, 1991.

[5] J. Davies and H. Siddons, "Experience with implanted pacemakers: Technical considerations," *Thorax*, vol. 20, no. 2, p. 128, 1965.

[6] K. Bazaka and M. V. Jacob, "Implantable devices: issues and challenges," *Electronics*, vol. 2, no. 1, pp. 1–34, 2013.

[7] E. R. Kandel, J. H. Schwartz, T. M. Jessell, D. of Biochemistry, M. B. T. Jessell, S. Siegelbaum, and A. Hudspeth, *Principles of neural science*, vol. 4. McGraw-hill New York, 2000.

[8] B. Blausen, "Medical gallery of blausen medical 2014," *WikiJournal of Medicine*, vol. 1, no. 2, 2014.

[9] J. Wolpaw and E. W. Wolpaw, *Brain-computer interfaces: principles and practice*. OUP USA, 2012.

[10] J. J. Vidal, "Toward direct brain-computer communication," *Annual review of Biophysics and Bioengineering*, vol. 2, no. 1, pp. 157–180, 1973.

[11] N. I. of Health *et al.*, "NIDCD fact sheet - hearing and balance: Cochlear implants," 2017.

[12] P. L. Gildenberg, "Evolution of neuromodulation," *Stereotactic and functional neurosurgery*, vol. 83, no. 2-3, pp. 71–79, 2005.

[13] S. Kunnumpurath, R. Srinivasagopalan, and N. Vadivelu, "Spinal cord stimulation: principles of past, present and future practice: a review," *Journal of clinical monitoring and computing*, vol. 23, no. 5, pp. 333–339, 2009.

[14] R. K. Shepherd, M. N. Shivdasani, D. A. Nayagam, C. E. Williams, and P. J. Blamey, "Visual prostheses for the blind," *Trends in biotechnology*, vol. 31, no. 10, pp. 562–571, 2013.

[15] D. L. Schomer and F. L. Da Silva, *Niedermeyer's electroencephalography: basic principles, clinical applications, and related fields*. Lippincott Williams & Wilkins, 2012.

[16] L.-D. Liao, C.-Y. Chen, I.-J. Wang, S.-F. Chen, S.-Y. Li, B.-W. Chen, J.-Y. Chang, and C.-T. Lin, "Gaming control using a wearable and wireless eeg-based brain-computer interface device with novel dry foam-based sensors," *Journal of neuroengineering and rehabilitation*, vol. 9, no. 1, p. 5, 2012.

[17] S. Vaid, P. Singh, and C. Kaur, "Eeg signal analysis for bci interface: A review," in *2015 Fifth International Conference on Advanced Computing & Communication Technologies*, pp. 143–147, IEEE, 2015.

[18] P. Parmar, "Stroke: classification and diagnosis," *Prevention*, vol. 10, p. 00, 2019.

[19] T. Kaiju, M. Yokota, K. Watanabe, M. Inoue, H. Ando, K. Takahashi, F. Yoshida, M. Hirata, T. Suzuki, *et al.*, "High spatiotemporal resolution ecog recording of somatosensory evoked potentials with flexible micro-electrode arrays," *Frontiers in neural circuits*, vol. 11, p. 20, 2017.

[20] A. Palmini, "The concept of the epileptogenic zone: a modern look at Penfield and Jasper's views on the role of interictal spikes," *Epileptic disorders*, vol. 8, no. 2, pp. 10–15, 2006.

[21] P. E. Tarapore, M. C. Tate, A. M. Findlay, S. M. Honma, D. Mizuiri, M. S. Berger, and S. S. Nagarajan, "Preoperative multimodal motor mapping: a comparison of magnetoencephalography imaging, navigated transcranial magnetic stimulation, and direct cortical stimulation," *Journal of neurosurgery*, vol. 117, no. 2, pp. 354–362, 2012.

[22] G. Schalk and E. C. Leuthardt, "Brain-computer interfaces using electrocorticographic signals," *IEEE reviews in biomedical engineering*, vol. 4, pp. 140–154, 2011.

[23] G. Hotson, D. P. McMullen, M. S. Fifer, M. S. Johannes, K. D. Katyal, M. P. Para, R. Armiger, W. S. Anderson, N. V. Thakor, B. A. Wester, *et al.*, "Individual finger control of a modular prosthetic limb using high-density electrocorticography in a human subject," *Journal of neural engineering*, vol. 13, no. 2, p. 026017, 2016.

[24] A. L. Benabid, T. Costecalde, A. Eliseyev, G. Charvet, A. Verney, S. Karakas, M. Foerster, A. Lambert, B. Morinière, N. Abroug, *et al.*, "An exoskeleton controlled by an epidural wireless brain-machine interface in a tetraplegic patient: a proof-of-concept demonstration," *The Lancet Neurology*, vol. 18, no. 12, pp. 1112–1122, 2019.

[25] F.-S. Jaw, "Optimal sampling of electrophysiological signals," *Neuroscience Research Communications*, vol. 28, no. 2, pp. 75–84, 2001.

[26] J. W. Salatino, K. A. Ludwig, T. D. Kozai, and E. K. Purcell, "Glial responses to implanted electrodes in the brain," *Nature biomedical engineering*, vol. 1, no. 11, pp. 862–877, 2017.

[27] A. Jackson and T. M. Hall, "Decoding local field potentials for neural interfaces," *IEEE Transactions on Neural Systems and Rehabilitation Engineering*, vol. 25, no. 10, pp. 1705–1714, 2016.

[28] J. P. Donoghue, "Bridging the brain to the world: a perspective on neural interface systems," *Neuron*, vol. 60, no. 3, pp. 511–521, 2008.

[29] B. Burle, L. Spieser, C. Roger, L. Casini, T. Hasbroucq, and F. Vidal, "Spatial and temporal resolutions of eeg: Is it really black and white? a scalp current density view," *International Journal of Psychophysiology*, vol. 97, no. 3, pp. 210–220, 2015.

[30] G. A. Ojemann, N. F. Ramsey, and J. Ojemann, "Relation between functional magnetic resonance imaging (fmri) and single neuron, local field potential (lfp) and electrocorticography (ecog) activity in human cortex," *Frontiers in human neuroscience*, vol. 7, p. 34, 2013.

[31] N. J. Hill, D. Gupta, P. Brunner, A. Gunduz, M. A. Adamo, A. Ritaccio, and G. Schalk, "Recording human electrocorticographic (ecog) signals for neuroscientific research and real-time functional cortical mapping," *JoVE (Journal of Visualized Experiments)*, no. 64, p. e3993, 2012.

[32] G. Buzsáki, C. A. Anastassiou, and C. Koch, "The origin of extracellular fields and currents—eeg, ecog, lfp and spikes," *Nature reviews neuroscience*, vol. 13, no. 6, pp. 407–420, 2012.

[33] S. Ray, "Challenges in the quantification and interpretation of spike-lfp relationships," *Current opinion in neurobiology*, vol. 31, pp. 111–118, 2015.

[34] J. L. Schei, M. D. McCluskey, A. J. Foust, X.-C. Yao, and D. M. Rector, "Action potential propagation imaged with high temporal resolution near-infrared video microscopy and polarized light," *Neuroimage*, vol. 40, no. 3, pp. 1034–1043, 2008.

[35] G. Lehew and M. A. Nicolelis, "State-of-the-art microwire array design for chronic neural recordings in behaving animals," *Methods for neural ensemble recordings*, vol. 2, pp. 361–371, 2008.

[36] J. Krüger, F. Caruana, G. Rizzolatti, *et al.*, "Seven years of recording from monkey cortex with a chronically implanted multiple microelectrode," *Frontiers in neuroengineering*, vol. 3, p. 6, 2010.

[37] D. A. Schwarz, M. A. Lebedev, T. L. Hanson, D. F. Dimitrov, G. Lehew, J. Meloy, S. Rajangam, V. Subramanian, P. J. Ifft, Z. Li, *et al.*, "Chronic, wireless recordings of large-scale brain activity in freely moving rhesus monkeys," *Nature methods*, vol. 11, no. 6, p. 670, 2014.

[38] "Clunbury Scientific LLC - Electrode Arrays," Dec. 2017. Available at `http://www.clunburyscientific.com/ElectrodeArrays.html`.

[39] "The utah electrode array: a platform for cutting-edge advances in bionics," Dec. 2017. Available at `http://www.tvc.utah.edu/2014annualreport/array.php`.

[40] "Neuronexus neural probes," Aug. 2017. Available at `https://neuronexus.com/products/neural-probes`.

[41] E. Musk *et al.*, "An integrated brain-machine interface platform with thousands of channels," *Journal of medical Internet research*, vol. 21, no. 10, 2019.

[42] E. M. Maynard, C. T. Nordhausen, and R. A. Normann, "The utah intracortical electrode array: a recording structure for potential brain-computer interfaces," *Electroencephalography and clinical neurophysiology*, vol. 102, no. 3, pp. 228–239, 1997.

[43] R. Bhandari, S. Negi, and F. Solzbacher, "Wafer-scale fabrication of penetrating neural microelectrode arrays," *Biomedical microdevices*, vol. 12, no. 5, pp. 797–807, 2010.

[44] L. R. Hochberg, M. D. Serruya, G. M. Friehs, J. A. Mukand, M. Saleh, A. H. Caplan, A. Branner, D. Chen, R. D. Penn, and J. P. Donoghue, "Neuronal ensemble control of prosthetic devices by a human with tetraplegia," *Nature*, vol. 442, no. 7099, p. 164, 2006.

[45] S. Kim, R. Bhandari, M. Klein, S. Negi, L. Rieth, P. Tathireddy, M. Toepper, H. Oppermann, and F. Solzbacher, "Integrated wireless neural interface based on the utah electrode array," *Biomedical microdevices*, vol. 11, no. 2, pp. 453–466, 2009.

[46] D. A. Borton, M. Yin, J. Aceros, and A. Nurmikko, "An implantable wireless neural interface for recording cortical circuit dynamics in moving primates," *Journal of neural engineering*, vol. 10, no. 2, p. 026010, 2013.

[47] P. A. House, J. D. MacDonald, P. A. Tresco, and R. A. Normann, "Acute microelectrode array implantation into human neocortex: preliminary technique and histological considerations," *Neurosurgical focus*, vol. 20, no. 5, pp. 1–4, 2006.

[48] J. C. Barrese, N. Rao, K. Paroo, C. Triebwasser, C. Vargas-Irwin, L. Franquemont, and J. P. Donoghue, "Failure mode analysis of silicon-based intracortical microelectrode arrays in non-human primates," *Journal of neural engineering*, vol. 10, no. 6, p. 066014, 2013.

[49] T. Kozai, "The history and horizons of microscale neural interfaces," *Micromachines*, vol. 9, no. 9, p. 445, 2018.

[50] B. Ghane-Motlagh and M. Sawan, "Design and implementation challenges of microelectrode arrays: a review," *Materials Sciences and Applications*, vol. 4, no. 08, p. 483, 2013.

[51] K. M. Szostak, L. Grand, and T. G. Constandinou, "Neural interfaces for intracortical recording: Requirements, fabrication methods, and characteristics," *Frontiers in Neuroscience*, vol. 11, p. 665, 2017.

[52] R. Chen, A. Canales, and P. Anikeeva, "Neural recording and modulation technologies," *Nature Reviews Materials*, vol. 2, no. 2, p. 16093, 2017.

[53] G. Hong, X. Yang, T. Zhou, and C. M. Lieber, "Mesh electronics: a new paradigm for tissue-like brain probes," *Current opinion in neurobiology*, vol. 50, pp. 33–41, 2018.

[54] A. Campbell and C. Wu, "Chronically implanted intracranial electrodes: tissue reaction and electrical changes," *Micromachines*, vol. 9, no. 9, p. 430, 2018.

[55] T. D. Kozai, A. S. Jaquins-Gerstl, A. L. Vazquez, A. C. Michael, and X. T. Cui, "Brain tissue responses to neural implants impact signal sensitivity and intervention strategies," *ACS chemical neuroscience*, vol. 6, no. 1, pp. 48–67, 2015.

[56] S. P. Lacour, G. Courtine, and J. Guck, "Materials and technologies for soft implantable neuroprostheses," *Nature Reviews Materials*, vol. 1, no. 10, p. 16063, 2016.

[57] R. R. Harrison, "The design of integrated circuits to observe brain activity," *Proceedings of the IEEE*, vol. 96, no. 7, pp. 1203–1216, 2008.

[58] D. Prodanov and J. Delbeke, "Mechanical and biological interactions of implants with the brain and their impact on implant design," *Frontiers in neuroscience*, vol. 10, p. 11, 2016.

[59] R. K. Shepherd, *Neurobionics: The Biomedical Engineering of Neural Prostheses*. John Wiley & Sons, 2016.

[60] D. Seo, J. M. Carmena, J. M. Rabaey, E. Alon, and M. M. Maharbiz, "Neural dust: An ultrasonic, low power solution for chronic brain-machine interfaces," *arXiv preprint arXiv:1307.2196*, 2013.

[61] P. Yeon, S. A. Mirbozorgi, B. Ash, H. Eckhardt, and M. Ghovanloo, "Fabrication and microassembly of a mm-sized floating probe for a distributed wireless neural interface," *Micromachines*, vol. 7, no. 9, p. 154, 2016.

[62] J. Jeong, F. Laiwalla, J. Lee, R. Ritasalo, M. Pudas, L. Larson, V. Leung, and A. Nurmikko, "Conformal hermetic sealing of wireless microelectronic implantable chiplets by multilayered atomic layer deposition (ald)," *Advanced Functional Materials*, vol. 29, no. 5, p. 1806440, 2019.

[63] D. Seo, R. M. Neely, K. Shen, U. Singhal, E. Alon, J. M. Rabaey, J. M. Carmena, and M. M. Maharbiz, "Wireless recording in the peripheral nervous system with ultrasonic neural dust," *Neuron*, vol. 91, no. 3, pp. 529–539, 2016.

[64] S. A. Mirbozorgi, P. Yeon, and M. Ghovanloo, "Robust wireless power transmission to mm-sized free-floating distributed implants," *IEEE transactions on biomedical circuits and systems*, vol. 11, no. 3, pp. 692–702, 2017.

[65] V. W. Leung, J. Lee, S. Li, S. Yu, C. Kilfovle, L. Larson, A. Nurmikko, and F. Laiwalla, "A cmos distributed sensor system for high-density wireless neural implants for brain-machine interfaces," in *ESSCIRC 2018-IEEE 44th European Solid State Circuits Conference (ESSCIRC)*, pp. 230–233, IEEE, 2018.

3. Humidity Sensing for Monitoring Micro-Package Integrity

Among the various challenges associated with the design and fabrication of chronic implantable devices outlined in the previous chapter, the issue of long-term reliability of the implants is of major importance. In particular, for active implants that host electronic circuitry, it is essential to guarantee a barrier between the electronic components and the body environment, which is rich in water that can cause material corrosion, leading to device failure. Such humidity induced corrosion has proven to be a major factor in electronic failures [1].

In this chapter we present a brief review of test methods used to assess the hermeticity of micro-packages, with a particular focus on the method of humidity testing for the long-term monitoring of encapsulation. The design of a sub-millimetre custom humidity sensor is then proposed and discussed, together with the work towards the realization of a bench top wireless platform for package integrity testing.

3.1. Test methods for micro-package hermeticity

The possibility to produce hermetic packaging for electronic devices has proven to be critical in many applications, both in the medical field as well as for mass production consumer electronics. Many of the MEMS devices that are nowadays integrated in the devices we use everyday — such as accelerometers, gyroscopes, and pressure sensors — require an hermetic package in order to remain functional over time. However, the level of reliability required from these commercial devices does not generally compare with the extremely strict constraints imposed on devices targeted at medical applications, and more specifically implantable devices.

To meet such requirements, and to provide accurate ways to evaluate the hermeticity of micro-packages, many dedicated test procedures have been proposed. The most common reference for these procedures is the military standard MIL-STD-883, Method 1014.10, developed by the US Department of Defence, which details different methods to determine seal effectiveness in microcircuits [2]. The first of such methods, and most commonly employed across industry, is the helium fine leak test, which in its standard form is carried

The thinning of the Sensirion SHTW2 was carried out by Ms Rachael Savidis from Newcastle University. The work presented in subsection 3.4.1 has been the subject of two MSc students' theses and one BSc thesis.

out as follows: the packaged device to be tested is placed in a sealed chamber which is then filled with pressurized helium. In this way, if one or multiple cracks are present in the micro-package, helium will be able to infiltrate it and fill the cavity. After a specific amount of time, dependent on the size of the internal cavity of the device under test, the device is transferred to a leak detector, where a purposely calibrated mass spectrometer is used to measure the amount of helium particles that escape through the crack. The use of helium as a tracer gas is justified by the fact that it is able to rapidly penetrate into small gaps. Moreover, it is chemically inert, non-toxic, and only present in the atmosphere in small quantities (about 5ppm). There are different ways to define the leak rate, but generally it is expressed in terms of variation in the pressure of the device under test:

$$LR = -V\frac{dP}{dt}$$

where V is the internal volume of the tested device, P its internal pressure, and LR the leak rate. In the military standard mentioned above, the leak rates are expressed with the units $\mathrm{atm\,cm^3/s}$. The limit of detection for the fine helium leak test is usually around $10^{-10}\,\mathrm{atm\,cm^3/s}$, and therefore not suitable for cavities with a volume smaller than tens of $\mathrm{mm^3}$ [3].

A variation of the fine leak test is the cumulative helium leak detection (CHLD). By combining mass spectrometry with the use of cryogenic ultra-high vacuum to evacuate the chamber where the device under test is being measured, this method can allegedly decrease the detection limit down to $3 \times 10^{-13}\,\mathrm{atm\,cm^3/s}$ [4], but still not sufficiently stringent for small volume applications.

There exist variations of the leak test based on the use of different tracer gases other than helium, which all share a similar working principle. For example the radioisotope fine leak test, which uses a radioactive tracer gas to enhance the detection capabilities. However, the use of such substance can lead to safety risk, especially if used for medical devices [5].

Another category of hermeticity tests is composed of optical leak tests. These experiments rely on physical deformations of the micro-package when it is placed in a chamber with a pressure significantly different from the one inside the cavity of the device. The deflection can then be measured with an optical interferometer, and its variation over time gives an indication of the leak magnitude. This test is very dependent on the size of the device, and the thickness and stiffness of its materials, but, as an advantage, can be performed at wafer level [6].

Optical spectrometry methods such as Fourier Transmission Infrared Spectrometry (FTIR) and Raman spectroscopy tests rely on the optical absorption properties of gases to measure concentrations. The devices under test are packaged in a specific atmosphere (for example N_2O, SF_6, HCl), and a spectrometer measures over time the amount of gas still present inside the cavity. Note that in order to apply these tests the micro-package

Table 3.1.: Main hermeticity testing methods for small packages

Method	**Min. measurable leak rate** ($\mathrm{atm\,cm^3/s}$)	**Advantages**	**Limitations**
Helium fine leak	1×10^{-10}	• Standardized test • Non-destructive	• Not suitable for glass and polymers (helium diffuses through these materials) • Sensitivity issues for small volumes • No outgassing measurement
CHLD	3×10^{-13}	• Standardized test • Non-destructive • Full leak range measurable	• Sensitivity issues for small volumes and vacuum applications • No outgassing measurement • Bomb required, potentially undetectable one-way leak
Radioisotope fine leak	1×10^{-12}	• Standardized test	• Can be destructive for small structures • Sensitivity issues for small volumes and vacuum applications • No outgassing measurement
Optical leak	1×10^{-10}	• Standardized test • Non-destructive • No bombing required	• Need flexible lid • Sensitivity issues for most applications • No outgassing measurement
FTIR	1×10^{-12}	• Non-destructive • No issues with surface sorption	• Not standardized • IR transparent lid required • No outgassing measurement
Raman spectroscopy	Under study	• Non-destructive • No issues with surface sorption • No bombing required	• Not standardized • Transparent cap and reflective surface required

Table 3.1: Main hermeticity testing methods for small packages (continued)

Method	**Min. measurable leak rate** ($\mathrm{atm\,cm^3/s}$)	**Advantages**	**Limitations**
Copper test structures	5×10^{-16}	• Non-destructive • No issues with surface sorption • Not volume dependent	• Transparent lid required • One-time test • Long test duration • Only oxidation measurement
Q-factor sensors	1×10^{-14}	• Non-destructive • No issues with surface sorption • Not volume dependent • Long-term monitoring	• Free standing internal structure required
In situ pressure or humidity sensors	1×10^{-15}	• Non-destructive • No issues with surface sorption • Not volume dependent • Long-term monitoring • Electrical measurement	• Addition internal structure required

(Data presented in the table reported from [4])

must be transparent to the specific wavelengths used by each technique.

A different approach is the one followed by *in situ* tests, which use specific structures built inside the micro-package to monitor hermeticity. For example, copper test structures that oxidise in presence of moisture can be placed inside the cavity, providing a one-off test for the quality of the hermetic seal. Also free standing structures such as resonators or cantilevers can indicate an alteration of the pressure inside the cavity by mean of a shift in their Q-factor. Another alternative is the use of built-in sensors to monitor quantities such as pressure or humidity, and infer the hermeticity status of the device under test from their readings. Such sensors have reported leak rates as low as $10^{-15}\,\mathrm{atm\,cm^3/s}$ [4].

The various leak test methods just discussed are reported in Table 3.1, with a summary of their major advantages and drawbacks. It is worth noting that the majority of the above mentioned hermeticity tests provide one-off measurements and can not be executed once the device is in place for use, with a few of them even being destructive. Moreover, with the shrinking in device dimensions, many of them do not offer the sufficient resolution

for sub-millimetre cavities [7]. *In situ* methods have proven to have the highest sensitivity for the detection of leaks as well as the presence of out-gassing products from within the device [8]. They also allow to monitor the quality of encapsulation during device operation, and can be indicators of device failure throughout its lifetime, which can be crucial in critical applications such as neural implantable devices. However, being embedded inside the implant, the design of such *in situ* solutions is also severely constrained by the available volume. Humidity sensors have been investigated for this purpose [9], but at the moment no proposed implementation has been successfully integrated in a micro-package for integrity monitoring.

3.2. Humidity monitoring

Before describing the current available solutions for testing humidity, it is necessary to define what humidity is and what units are used to measure it. Humidity is defined as the amount of water vapour in a gas, usually air. Therefore, it is intrinsically a measurement of particle concentration. The most direct way to count these molecules is to define the absolute humidity (AH) in term of the amount of water molecules per given volume considered:

$$AH = \frac{m_{H_2O}}{V}$$

where m_{H_2O} is the total mass of water vapour molecules. The measured value of AH however also depends from temperature and pressure, and therefore it is usually unsuitable for calculations in phenomena that experience changes in these quantities.

To solve this issue, relative humidity (RH) is introduced. Instead of directly measuring the quantity of water vapour present in the air, RH expresses the amount of water vapour relative to the maximum amount of water vapour that the considered volume can contain. It is defined according to the following formula:

$$RH = \frac{p_{H_2O}}{p^*_{H_2O}}$$

where two elements of the fraction are respectively:

- p_{H_2O} is the partial pressure of water vapour, which is the pressure that the water particles would have if the given volume would be occupied only by them;
- $p^*_{H_2O}$ is the equilibrium vapour pressure of water, which is the pressure of water vapour when in thermodynamic equilibrium with its condensed liquid phase at a given temperature in a closed system.

Following from the definition, relative humidity values are dimensionless, and are usually expressed as percentages. This quantity is widely used in the meteorological field as well as in climate control applications, for its close relation to how humans perceive temperature and heat.

3.2.1. Devices for sensing humidity

Humidity measurements have proven to be extremely useful in a wide variety of applications, from the industrial field to the medical one, as well as the consumer electronic market. To meet this need, many types of sensing devices have been developed, with different devices tailored to specific applications or environments. The recent trend for smart consumer appliances and connected IoT devices has pushed even more for the realization of low power and low cost sensors.

A device that measures humidity is referred to as an hygrometer. As mentioned in the previous section, RH measurements are usually preferred to AH ones, and therefore the majority of hygrometers that have been designed target RH. Also, measuring RH is in general simpler, and thus the sensors are easier to fabricate and more cost-effective. However, AH sensors are still used in certain applications, like high-temperature settings or applications that require high-precision, and as primary sensors for the calibration of RH ones [10].

In general, the operation of a humidity sensor is based on the interaction between the water vapour molecules present in the air and the transducer. Depending on the different ways in which such transducer reacts to the water molecules, we can identify different types of hygrometers. One example is the category of gravimetric sensors, devices that exploit the change in the mass of a resonating device caused by moisture absorption. These sensors usually show great sensitivity and short response time, but the advantages are counterbalanced by the complexity in the fabrication of such micro-structures [11]. Thermal conductivity sensors, a type of AH sensors which employ two matched thermistors, one sealed in an hermetic chamber and the other exposed to the air, to differentially sense the variation of thermal conductivity between dry and humid air. However, in order to do so, the temperature of the thermistors is increased by resistive heating (usually $\geq 250\,^{\circ}\mathrm{C}$), making them unsuitable for very low power applications [12]. Another class of sensors is the one of chilled mirror optical humidity sensors. They rely on the changes in the reflectance of a micro-mirror that occur when it is fogged by the accumulation of moisture on its surface. This change is then sensed with a photodetector. These sensors have proven to show very high accuracy, together with the ability to operate without suffering interference from other electronic devices, but again in exchange for a greater complexity and cost of fabrication [13].

The sensing devices cited so far can all achieve very high accuracy, usually within the $\pm 0.1\,\%$ RH margin [13]. However this accuracy is obtained with more complex and delicate structures, and cannot be easily and effectively integrated within an implantable device. For this specific application there is the significant need to minimize complexity, footprint, and power consumption, even at the expenses of resolution and sensitivity.

The most common types of integrated humidity sensors, for their simplicity and cost-effectiveness, are resistive and capacitive RH sensors (the latters approximately account

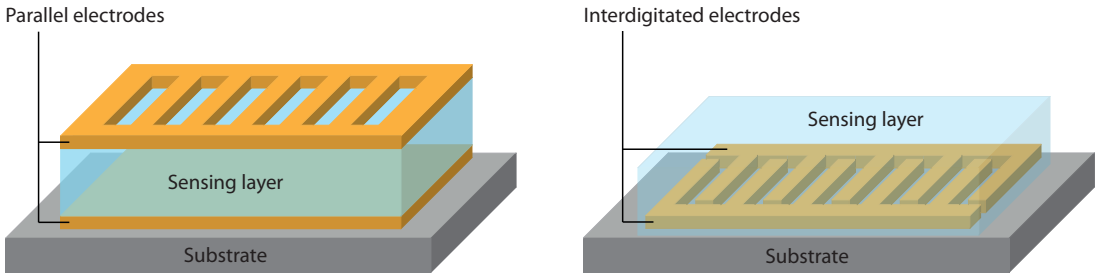
for 75% of commercially available humidity sensors [14]), which share a common structure: a moisture sensitive layer deposited between two metal electrodes. When exposed to the environment, the moisture present in the air accumulates and diffuses into the sensing layer, altering its physical properties. These modifications are translated into an electrical quantity that can be measured and conditioned according to the specific operation of the sensor. For resistive RH sensors, the change in electrical conductivity of the sensing layer is measured: the DC current flowing through the electrodes is proportional to such conductivity, and therefore to humidity. Capacitive RH sensors measure the change in the permittivity of the material of the sensing layer, which changes the total capacitance of the system. In general, capacitive RH sensors show a better accuracy and repeatability when compared to resistive sensors, as well as having a more linear response to changes in RH [15].

The accuracy of resistive and capacitive RH sensors can vary quite significantly depending on the hydrophilic properties of the material used as sensitive layer, but in general it is in the order of magnitude of $\pm 1\,\%$ RH (in the range from $10\,\%$ to $90\,\%$ RH), which is an acceptable value for the application of micro-packages hermeticity monitoring. Also, the use of a moisture sensitive layer allows for monitoring the presence of water in both liquid and vapour states, which is a relevant feature since the breakage of the micro-package could cause the presence of either one inside the cavity. Another further aspect to consider is the phenomenon of hysteresis, which is more present in these kinds of sensors, compared to the previously cited more accurate solutions, due to the rate at which the sensing layer absorbs and releases water molecules. However, for the desired application of hermeticity monitoring, it is not expected to have multiple cycles of absorption and desorption of water within the sensor, but a single ascending monotonic curve that starts in the presence of a leak in the encapsulation.

Integrated capacitive RH sensors

There exist mainly two types of established designs for integrated capacitive RH sensors. The first one (Figure 3.1a) is composed of two parallel metal electrodes, with the sensing layer sandwiched in between them acting as a dielectric. The top metal plate is slotted, and also often made of vapor-permeable thin metal films, to allow moisture to penetrate into the sensing layer [15]. This configuration allows for an easier evaluation of the values of capacitance, thanks to the parallel plate geometry, but requires a few extra post-processing steps compared to a standard CMOS fabrication. Also the presence of the top metal inhibits full absorption of moisture in from the sensing layer.

The second configuration, the most common one, is the interdigitated capacitor (IDC) layout: two co-planar comb-shaped electrodes face each other to form the capacitor, and the sensing layer is deposited on top of them (Figure 3.1b). Since the electrodes belong to the same metal layer, this topology only requires one extra deposition step for the sensing layer of choice to complete the fabrication process. The sensing layer is fully exposed to



(a) (b)

Figure 3.1.: Diagrams of the two main configurations for integrated capacitive humidity sensors: (a) Parallel plate configuration, with sensing layer between two planar metal electrodes; (b) Interdigitated configuration, where the sensing layer is deposited on top of two comb electrodes.

maximize moisture intake, however, given the same area, the overall value of capacitance is now smaller when compared to the parallel configuration. Also the analytical evaluation of the total capacitance becomes more challenging, as usual expressions for parallel plate capacitors cannot be used in the IDC case.

Thanks to their ease of fabrication, multiple designs of RH sensors based on interdigitated capacitors have been proposed [16, 17, 18]. When extreme miniaturization or performances are not required, their simple structure makes them also adapt for rapid and very low cost fabrication techniques, such as ink-jet printing [19]. Modifications of the classic IDC structure have also been explored, such as serpentine [20] or spiral designs [21], but they have not shown considerable improvements in sensor resolution or accuracy compared to the standard IDC topology.

In these types of integrated devices, it is evident how the choice of material used as sensing layer is of great importance for the overall performance of the sensor. Ideally, the sensitive layer should also respond linearly to changes in humidity, with minimal hysteresis when absorbing and desorbing moisture, as well as a high stability with minimal drift over time. For this reason, a large variety of materials have been tested to increase water absorption for an enhanced sensitivity.

A common category of materials for generic gas sensors are metal oxides, however their capillary condensation and high surface-to-volume ratio do not allow for fast desorption of moisture and can cause significant hysteresis [22]. Porous ceramic materials, such as Al_2O_3, TiO_2, and SiO_2, have also been successfully used. Blank et al. [23] give an extensive review on performance of numerous oxides, concluding that more progress is necessary in order to achieve sensors that might offer small manufacturing costs, low-power operation, and low maintenance. The use of carbon nanotubes has also been explored, producing very fast response time sensors, but again at the expense of a more complex fabrication method and high manufacturing costs [24].

Polymer-based solutions have been implemented for their numerous advantages: in general they show fast moisture absorption and desorption times, as well as a low hysteresis

when cycling between these two states. Also polymers (and in particular polyimides) can usually be easily integrated in electronic fabrication processes thanks to their compatibility with standard IC manufacturing techniques, and are very cost-effective compared to ceramics or other compound materials [25]. It is also possible to pattern polyimides to alter their surface characteristics to try to improve their moisture intake capabilities, for example by augmenting their surface to volume ratio [16].

Together with the type of transducer and the choice of sensing materials, an important part is also played by the readout circuit, which is responsible for converting the variable value of capacitance into an output signal. The two main categories of sensing circuits for capacitive sensors are charge-based and frequency-based topologies. Charge-based approaches operate by charging and discharging the sensing capacitor, and then measuring the amount of time required for the operation, or integrating the total amount of charge exchanged (using charge amplifiers) [26]. Frequency-based methods exploits the variation in the capacitance of the sensing element to modify the oscillation frequency of a resonant circuit, which is then measured and correlated to the value of humidity [27].

3.3. Sensor design

From the review of the current methods for hermeticity monitoring and the various types of humidity sensors exposed in the previous sections, it is possible to justify the need for a device for the detection of moisture ingress in neural implantable devices. The design of the proposed sensor has been carried out following these specific requirements:

- The sensor must be able to measure relative humidity in the range of 10 % to 90 % RH, with a desired accuracy of ±2 % RH. This value of accuracy is a reasonable objective, although it might be challenging to reach given the strict constraints on the size of the sensor.
- The overall area of the sensor must be minimized, in order to allow for the integration of the sensor inside the cavity of millimetre-sized implantable devices.
- The amount of total power available in such implants is very limited, and therefore sensor power consumption should be kept to a minimum, in order to leave the largest portion of the power budget for the processing and transmission of neural data.
- The fabrication of the sensor should be compatible with standard CMOS production methods, avoiding very high temperature processes, and require minimal post-processing, for an ease of integration within the implant and a high fabrication yield.

Following from these constraints, we decide to use a capacitive interdigitated polyimide based RH sensor, as it presents the following advantages: it has a small footprint, optimizing the area for such low-scale applications; it does not require a DC current to bias

the sensor, providing a low-power solution for humidity sensing; it is fully compatible with standard CMOS fabrication, and only requires the deposition of the polyimide sensing layer as an extra process step, simplifying the fabrication and reducing costs; capacitors are amongst the most reliable electronic components in current micro-technology fabrication processes.

For the design process of the sensor, numerical simulations have been carried out using MATLAB (The MathWorks, Inc., USA) and COMSOL Multiphysics (COMSOL AB, Sweden). The circuit layout of the sensor has been designed using the CADENCE Virtuoso development environment (Cadence Design Systems, Inc., USA), and a prototype has been fabricated in a four metal 0.35 µm CMOS process provided by Ams AG.

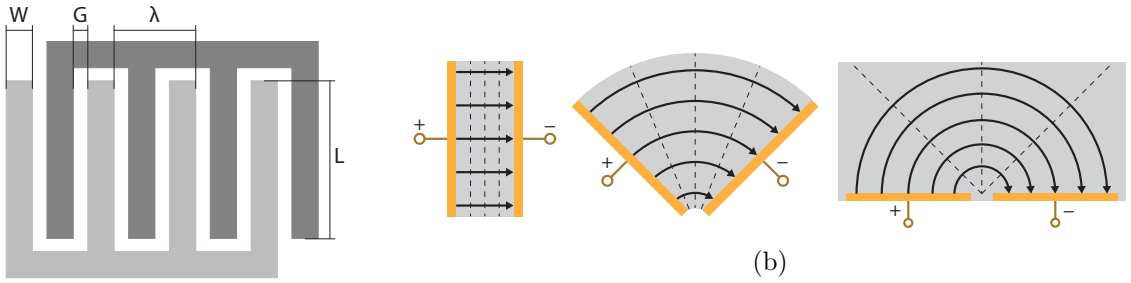
3.3.1. IDC mathematical model

In order to design a capacitive sensor based on an interdigitated structure, an analytical model is required. This would allow for the estimation of the value of capacitance, which is essential to optimize the geometrical parameters of the IDC structure, and to design a suitable readout circuit. Also, since one of the objectives is to minimize the area occupied by the sensor, the analytical results would indicate the lower dimensional limit at which the IDC can still be used to reliably measure RH, and validate the feasibility of a micro-sized sensor.

The main geometrical parameters to be determined when designing an IDC are shown in Figure 3.2a. They are the overlapping finger length L, the finger width W, the gap between the fingers G, and the total number of fingers N. It is also useful to define two additional parameters:

$$\lambda = 2 \cdot (W + G) \qquad \eta = \frac{W}{W + G} = \frac{2W}{\lambda}$$

where λ is called spatial wavelength, since it represents the periodicity of the IDC structure, and the adimensional parameter η is called metallization ratio, the equivalent of a *duty*



(a) (b)

Figure 3.2.: Tools for the analysis of an interdigitated structure: (a) The main geometrical design parameters of an IDC; (b) Graphical representation of the geometric transformation from parallel plate capacitor to IDC.

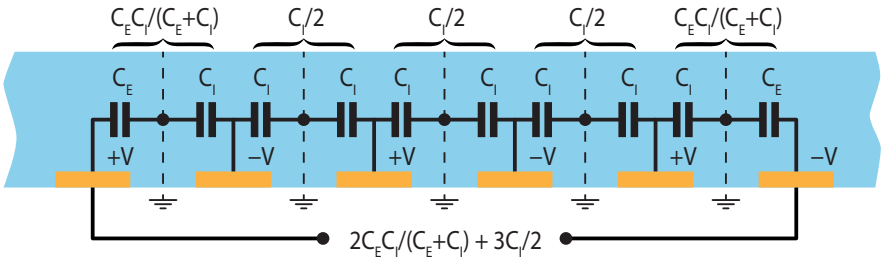


Figure 3.3.: Equivalent circuit of an IDC with six electrodes. The dotted lines represent the equipotential virtual ground planes (figure adapted from [28]).

cycle with respect to the alternation of metal fingers and gaps [28].

Unfortunately, there is no simple analytical expression to estimate the capacitance value of an IDC from these parameters. One way to tackle this problem is to use as a starting point the well known expression for the capacitance of a parallel plate capacitor:

$$C = \varepsilon \frac{A}{d}$$

where ε is the permittivity of the dielectric between the electrodes, A is the area of the capacitor, and d the distance between the metal plates. Using a specific geometrical transformation, it is possible to derive an expression for the case of a capacitor with two coplanar electrodes. This transformation, whose visual representation is shown in Figure 3.2b, takes advantage of the mathematical tools called conformal maps. These maps are functions typically used in complex analysis that allow to perform coordinate transformations while locally preserving angles. Such property is essential in this application, since it allows for the preservation of the electric field lines distribution [29].

Thanks to the periodicity of the IDC structure, the application of conformal maps can be extended to a capacitor with any number of fingers N. In fact, it is possible to approximate the total capacitance of the IDC as the sum of the individual contributions of contiguous fingers, as shown in Figure 3.3, obtaining the following result:

$$C_{IDC} = (N-3)\frac{C_I}{2} + 2\frac{C_I C_E}{C_I + C_E} \qquad \text{for } N > 3$$

where C_I is the capacitance between internal fingers and C_E represents the contribution of outer fingers [28]. The formula relies on the assumption that the electric field is uniformly distributed in the space between the electrodes. This means that the potential measured along the perpendicular planes lying between the fingers is zero, since it is exactly halfway between +V and −V. This is true in the case of an ideal structure that is infinitely periodic, but for a real finite IDC an error will be introduced, particularly on the edges of the capacitor. However, for the considered application this error can be neglected, since we expect most of the electric field to be confined in the inner region of the IDC.

There is one more factor to consider, other than the use of conformal maps, in order

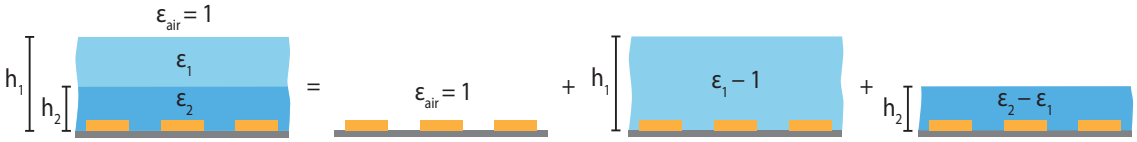


Figure 3.4.: Partial capacitance method used to separate the contributions of different dielectric layers over an interdigitated capacitor (figure adapted from [28]).

to obtain the expressions of C_I and C_E. Since the thickness of the polyimide sensitive layer is finite, part of the electric field generated by the charged IDC can extend beyond it and through the layer of air above, thus passing through two materials with different dielectric constants. To account for this circumstance, the partial capacitance method is used within the equations of the conformal mapping transformations. The concept behind this method, reported in Figure 3.4, is to split the various contributions of different dielectric layers stacked over the capacitive structure [28].

To summarize, the analytical derivation for the value of the IDC capacitance follows these principles:

- C_{IDC} is expressed as a function of the terms C_I and C_E by exploiting the periodicity of the IDC structure.
- The expressions for C_I and C_E as functions of the IDC geometrical parameters λ and η (and therefore W ang G) are calculated applying the conformal mapping transformations, using the formula for a parallel plate capacitor as a starting point.
- The formula for the partial capacitance method is embedded within the conformal mapping transformations, to account for the finite height of the polyimide sensing layer.

The full mathematical derivation, which is rather lengthy, is reported in [28]. This analytical model is then reproduced in Matlab, to create a software tool able to maximize the sensor capacitance by finding the optimal values for the geometrical design parameters of the IDC. A screenshot of the main window of the Matlab application is reported in Figure 3.5. Here it is possible to enter the technological constraints and parameters given by CMOS process of choice for the sensor fabrication, together with the outer dimensions (total width and total length) of the sensor. The application can then compute the values of λ and η that maximize the IDC capacitance. It can also produce a CADENCE compatible script to automatically generate the sensor geometry, to speed up the layout phase when doing the CMOS design of the sensor.

The results obtained using the Matlab application show that the value of IDC capacitance is maximum when the spatial wavelength λ is minimized, while at the same time a high metallization ratio η is maintained. This is in accordance with the findings from similar works based on the same mathematical model [28, 30]. Therefore, to achieve the

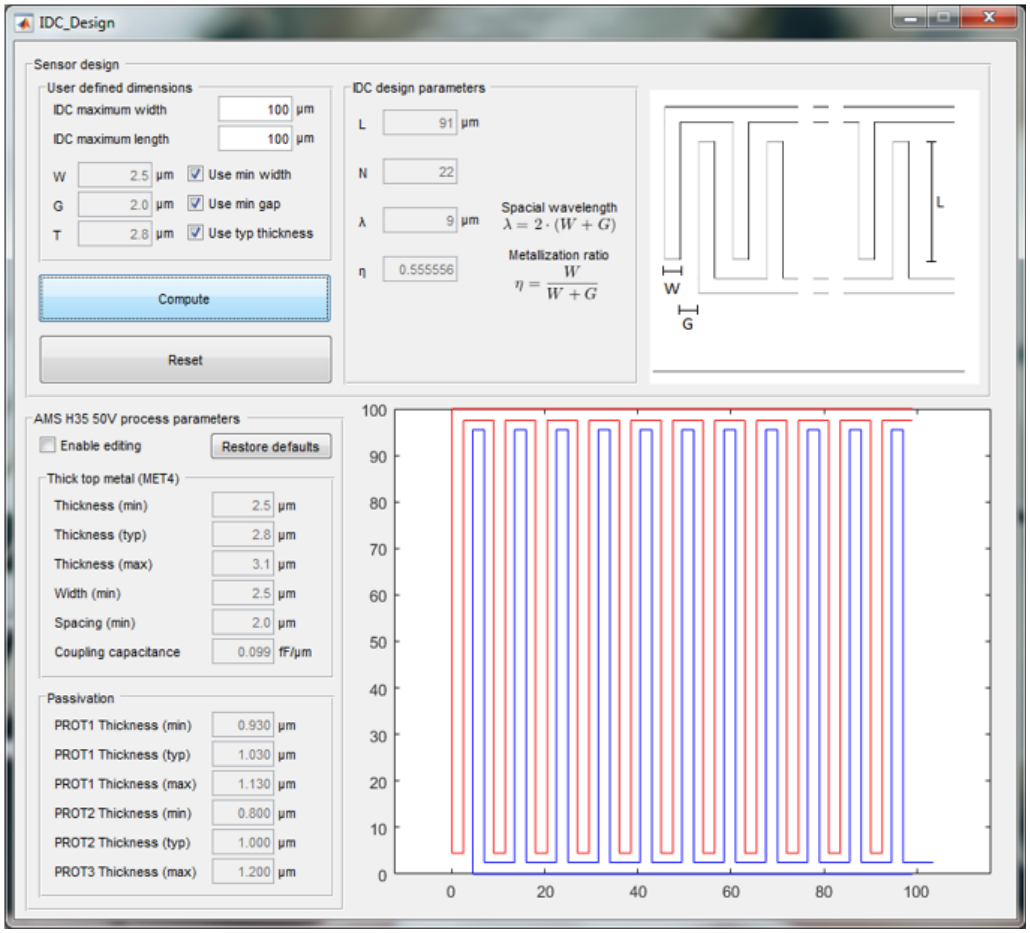


Figure 3.5.: Screenshot of the Matlab application for the optimization of the IDC geometrical parameters.

minimum λ, the values of W and G are selected as the minimum values allowed by the CMOS technology of choice. In our case, this gives $W = 2.5\,\mu m$ and $G = 2\,\mu m$ respectively. The thickness of the metal electrodes is fixed by the technology. In this case the CMOS process chosen offers a thick top metal layer, which has an average thickness of $2.8\,\mu m$. The total number of fingers N of the IDC is automatically determined once the overall sensor dimensions and the values of W and G are fixed.

Having established the various design parameters, and since we are interested in how small the IDC can be designed while maintaining good humidity sensing capabilities, we initially select three different IDC sizes to be fabricated (in accordance with the silicon area available for the project): $100 \times 100\,\mu m^2$, $300 \times 300\,\mu m^2$, and $1000 \times 1000\,\mu m^2$.

3.3.2. Numerical simulations

The analytical model has allowed us to fix the geometric parameters of the IDC. To confirm the results and obtain a numerical estimate of the capacitance of the IDCs of different sizes, we perform an analysis using finite element methods (FEM) on COMSOL Multiphysics.

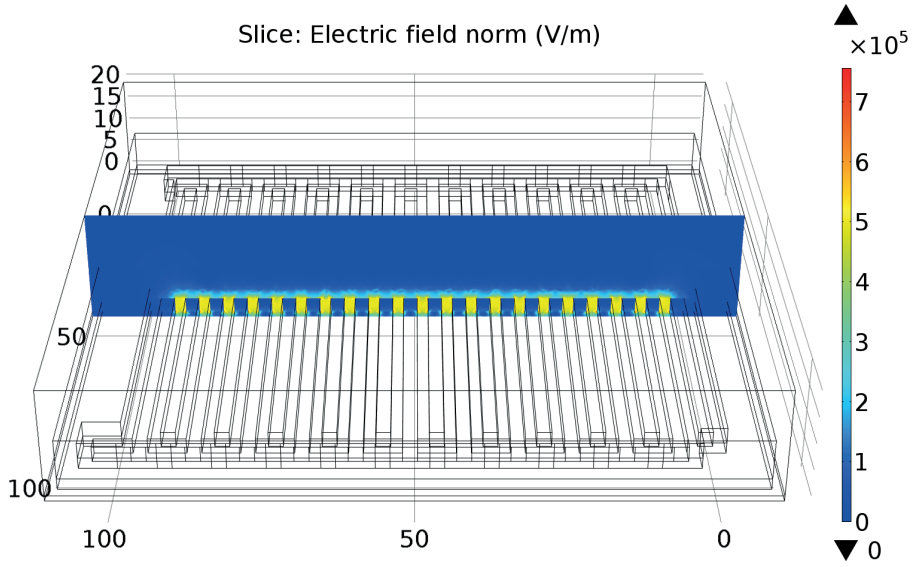


Figure 3.6.: The COMSOL model of the $100 \times 100\,\mu m^2$ IDC structure shows the confinement of the electric field between the capacitor finger electrodes.

Table 3.2.: Simulation results for the capacitance of a $100 \times 100\,\mu m^2$ IDC with and without Si_3N_4 passivation layer.

Passivation	W (µm)	G (µm)	λ	η	C_{dry} (fF)	C_{wet} (fF)	α
Yes	2.5	2	9	0.556	165.55	166.32	0.46 %
No	2.5	2	9	0.556	141.83	176.16	21.60 %

FEM has proven to be a reliable method to validate the mathematical models presented above [31].

The objective of these simulations is to evaluate the effect of the humidity on the change in value of the IDC's capacitance, which is represented by the change in the value of the polyimide's dielectric constant. To model the variation of the dielectric constant of the sensing layer due to water vapour absorption, the Looyenga equation has been used [32]:

$$\varepsilon_{wet} = \left(\gamma\left(\varepsilon_{water}^{1/3} - \varepsilon_{dry}^{1/3}\right) + \varepsilon_{dry}^{1/3}\right)^3$$

where ε_{dry} is the dielectric constants of dry polyimide, ε_{water} is the dielectric constant of water, and γ is the fractional volume of water absorbed by the polyimide layer. This is an empirical equation that has been widely used in the literature for such scope [14, 33]. The resulting values of the dielectric constant ($\varepsilon_{dry} = 3.35$ at 0 % RH and $\varepsilon_{wet} = 4.35$ at 100 % RH) have been used in the numerical simulations to estimate the changes in capacitance between a sensor exposed to 0 % RH and one exposed to 100 % RH.

The model (see Figure 3.6) is composed of a SiO_2 substrate, the two metal electrodes on top of it, the Si_3N_4 passivation layer that covers the electrodes, and the polyimide sensing layer. A volume of air around the structure is also used as simulation boundary.

Table 3.3.: Results of the numerical simulations for the three test IDC structures.

IDC dimensions (µm)	Number of electrode fingers	C_{dry} (pF)	C_{wet} (pF)	ΔC (pF)	α
304x300	68	1.3836	1.7202	0.3366	21.69 %
493x720	110	5.4640	6.7895	1.3255	21.63 %
925x930	206	13.155	16.348	3.1930	21.66 %

To evaluate the sensitivity of the sensors it is useful to introduce the full-scale deviation as a figure of merit:

$$\alpha = \frac{C_{wet} - C_{dry}}{C_M} \qquad \text{where} \qquad C_M = \frac{C_{wet} + C_{dry}}{2}$$

The simulation has been set up biasing the capacitor with a $1\,V$ voltage difference between the two electrodes, and the fringing capacitance through the underneath layer of oxide have also been considered. A first simulation showed an extremely low α (Table 3.2), due to the fact that the silicon nitride passivation layer occupies most of the space between the electrodes, where the majority of the electric field is concentrated, while leaving the sensing layer only on top. A second simulation has been then performed without the passivation, and the value of α was greatly increased.

It is then evident that the presence of the passivation compromises the function of the device. It is definitively much more desirable to have as much moisture sensitive material as possible between the electrodes of the capacitor. Therefore, during the circuit design phase, passivation openings will be defined on top of the sensitive areas, to avoid the deposition of silicon nitride from the manufacturer.

Another useful information can be obtained from the values of Table 3.2: even in the case where the passivation is absent, the total capacitance variation over the full range of humidity (0 % to 100 %) is about 34 fF, giving a sensitivity of 0.34 fF per 1 % increment in RH. Such capacitance values are very small to be reliably sensed. The $100 \times 100\,\mu m^2$ IDC design is therefore discarded. The three test designs have been updated with the following dimensions: $300 \times 300\,\mu m^2$, $600 \times 600\,\mu m^2$, and $1000 \times 1000\,\mu m^2$. However, for space constraints after the layout of the circuit, the real dimensions have been slightly adjusted. Their final dimensions, together with the simulated capacitance values, are reported in Table 3.3. The finger width and spacing are kept constant, and equal to the ones reported in Table 3.2.

3.3.3. Circuit architecture

Once the geometry of the IDCs is established, a suitable readout circuit is needed to complete the humidity sensor architecture. The chosen design is an analog switched capacitor based capacitance-to-voltage converter. This topology is fairly common as sensing circuit

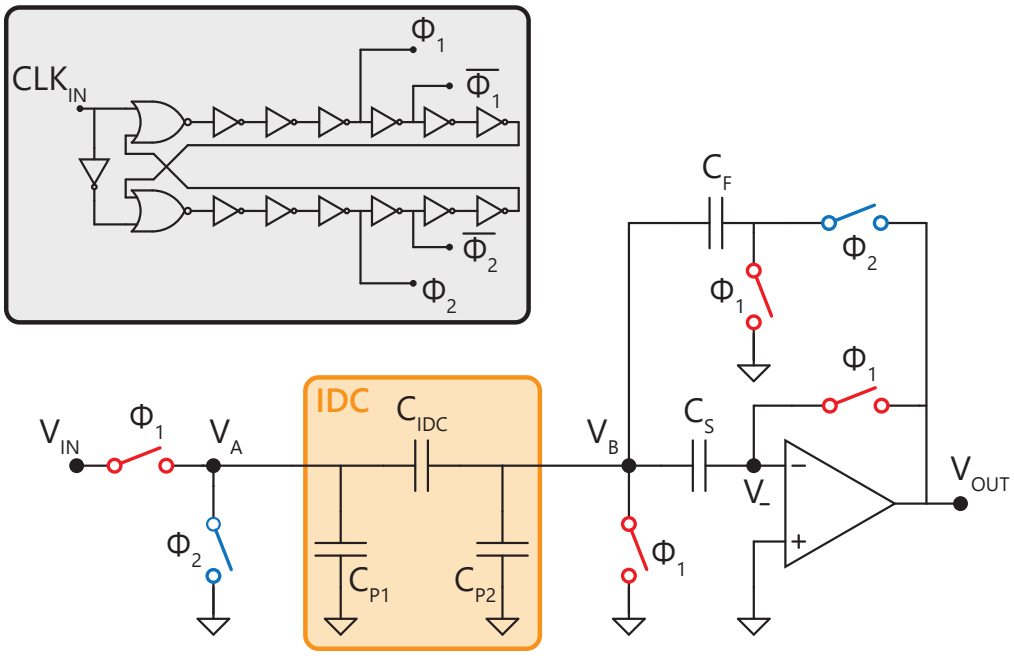


Figure 3.7.: Schematic of the switched capacitor capacitance-to-voltage converter used for the readout of each RH sensor. The area highlighted in orange represent the real IDC capacitance, composed of the ideal IDC together with the parasitic capacitances between the comb electrodes and the substrate. The SR-latch circuit used for generating the non-overlapping clock signals is shown in the grey box.

for capacitive sensors, and it is chosen here for its ability to minimize the contribution of parasitic capacitances [34]. In fact, since the IDC is composed of large metal surfaces that span over a broad area of the CMOS die, the amount of parasitic capacitance will be significant. If specific measures to reduce these parasitics are not taken, it becomes very challenging to achieve the required sensitivity which, according to the simulation results reported in subsection 3.3.2, is in the order of tens of fF. A further advantage of this configuration is the very low static power consumption, which is desired when used within a wirelessly powered micro-package.

The schematic of the sensing circuit is shown in Figure 3.7, and its timing diagram is reported in Figure 3.8. The operation of the circuit is the following:

- When ϕ_1 is active, C_{IDC} and C_{P1} are charged at a constant voltage of 3.3 V, with one terminal connected to V_{IN} and the other tied to ground. C_{P2} and C_F are fully discharged, with both terminals connected to ground, while C_S samples the offset voltage $V_{in,offset}$ between the input terminals of the operational amplifier.

- The signal ϕ_1 is then turned off, and ϕ_2 becomes active. The left terminal of the IDC is shortened to ground, while node V_B is a virtual ground minus V_{offset}, so the charge present in C_{IDC} is transferred to C_F, with the charge contribution due to

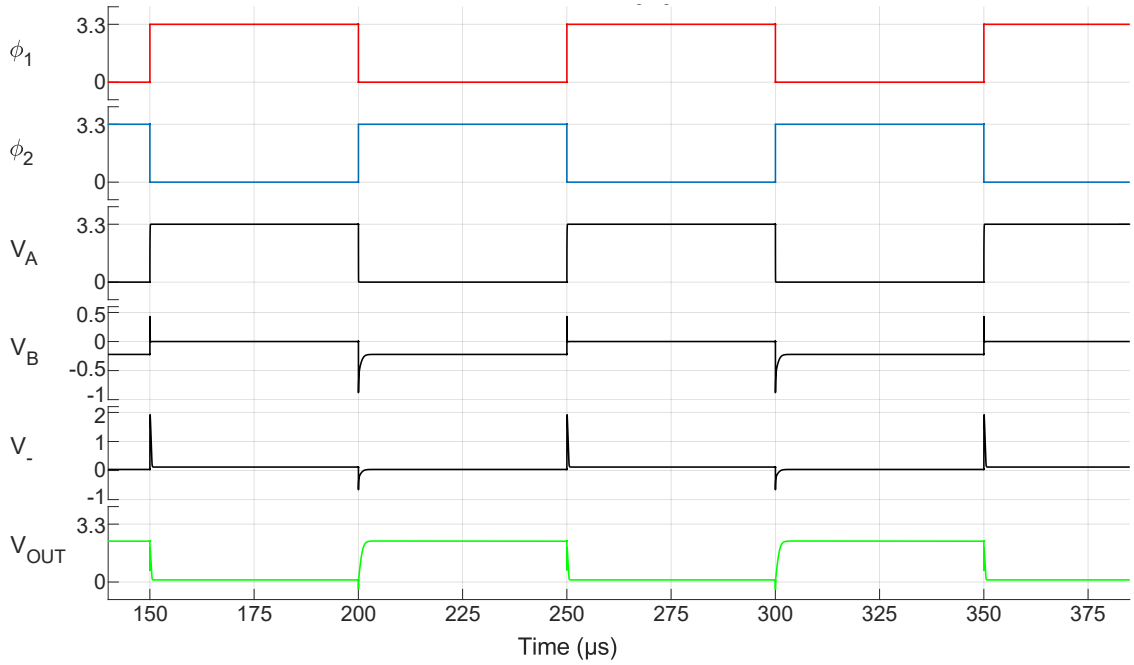


Figure 3.8.: Timing diagram of the RH sensor circuit (all vertical axes units are volts). For these simulations, the values of C_{P1} and C_{P2} have been estimated using Cadence's parasitic extraction feature.

C_S compensating for $V_{in,offset}$. This strategy of sampling $V_{in,offset}$ of the OpAmp during ϕ_1 to then subtract it during ϕ_2 is called Correlated Double Sampling (CDS), and it is very effective in eliminating the effect of $V_{in,offset}$ on the output reading of the sensor [35]. The output voltage V_{OUT} then settles to a value proportional to C_{IDC}/C_F.

For a proper operation of the circuit, ϕ_1 and ϕ_2 need to be non-overlapping clock signals. To produce such signals, the circuit highlighted in grey in Figure 3.7 is used. It is a NOR-based SR latch, with a series of inverter gates to set the desired commutation delay. Along with ϕ_1 and ϕ_2, their complementary signals $\overline{\phi_1}$ and $\overline{\phi_2}$ are also generated. This is necessary since the circuit employs transmission gates as switches, which need complementary signals for the correct driving of the nMOS-pMOS pair. The use of transmission gates allows for a reduction in charge injection: every time a MOS-based switch turns off, the charge present in its channel is free to leak into the circuit. By coupling an nMOS with a pMOS, the leaked charges partially cancel out, reducing the total amount of injected charges [36]. A further reduction in charge injection is achieved by using small area MOSFETs as switches, since the sensor does not need to work at high frequencies and would not benefit from the faster settling time of larger switches.

The choice of clock frequency relies on the following consideration: it should be low enough to reduce dynamic power consumption, but at the same time a higher clock frequency is desirable to increase the efficacy of CDS in reducing 1/f noise and to improve



Figure 3.9.: Micro-photograph of the fabricated device. The four interdigitated sensing areas are visible in a light blue colour (units in micrometers).

the overall noise performances of the system. Cadence simulations show 10 kHz is a good trade-off value for the correct operation of the sensor.

During the layout phase of the circuit, the option of having the output going through a unity gain voltage follower has been added, in order to reduce voltage spikes on V_{OUT} during clock commutations and to provide better impedance decoupling with laboratory measurement equipment.

3.3.4. Sensor testing

The circuit is fabricated in 0.35 µm, 4-metal CMOS technology by AMS. A micro-picture of the silicon die is reported in Figure 3.9. Four sensing elements are present, one for each of the three different sizes mentioned before, plus a replica of the 300x300 µm one. This has been added to evaluate if there are any noticeable effects in placing the readout circuit under or next to the sensing capacitor. Since it is important to minimize the silicon area required for the neural implant, it would be valuable to know if the space below the IDC can be used for other active circuitry without being too affected by parasitics.

To automate the testing process, a dedicated platform is designed in the form of a PCB shield that integrates with the Freescale FRDM-KL25Z development platform. In order to test the sensor, the polyimide sensing layer must be deposited on the surface of the die. The chosen material is the PI-2555 from HD MicroSystems, which is selected for its low viscosity, to allow for a uniform deposition even on high aspect ratio surfaces like that of the IDC. The use of the specific adhesion promoter VM-651 is also expected, to ensure a good bond between the polyimide and the die.

Unfortunately, severe delays were encountered when sourcing the polyimide, therefore it has not been possible test the sensors with the required sensing layer and under varying humidity conditions. However, the basic functional operation of the circuit is assessed, and the measured results are reported in Figure 3.10. For each of the three IDC sizes, the results of the measurements (taken at the output of the voltage follower) are shown with a solid black line, together with the output of Cadence simulations in both conditions of 0 % and 100 % RH. The fact that the measured V_{OUT} sits outside of the expected range is

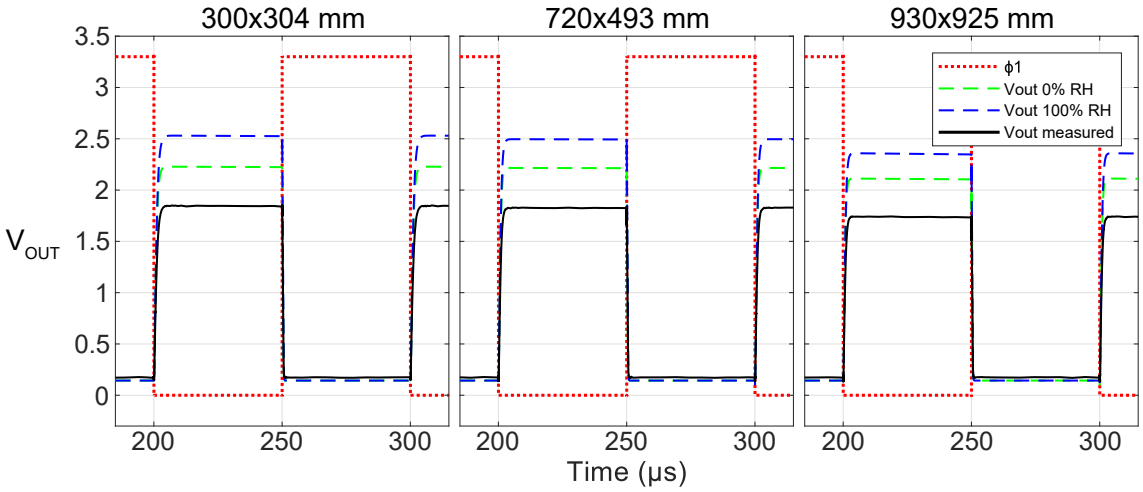


Figure 3.10.: Humidity sensor test results for each of the three IDC sizes, compared with the pre-fabrication simulations. The blue and green dashed lines represent simulation results at the extremes of the humidity range, while the black solid line is the direct measurement from the CMOS circuit.

expected, and it is due to the absence of the polyimide sensing layer. With no polyimide, the dielectric between the finger electrodes is simply air, whose lower permittivity reduces the capacitance of the IDC.

The measured results can only suggest a correct operation, and further testing is needed to fully characterize the sensor.

3.4. Commercial humidity sensor for package integrity testing

Alongside the development of the custom humidity sensor presented in the previous section, the use of a commercial sensor has been investigated, to allow for the development of a platform to test package integrity.

The choice for the commercial component is the Sensirion SHTW2 temperature and humidity sensor. This is a low power sensor that comes in a ultra-small flip chip form factor with no package, to keep dimensions to a minimum (see Figure 3.11). It measures $1.3 \times 0.7 \times 0.5\,\mathrm{mm}^3$. It has a supply voltage of 1.8 V and employs a digital I^2C communication interface, accessible through its four bottom contacts. The humidity sensing element is also placed on the bottom of the sensor, where an opening in the passivation is present to increase sensitivity.

Eutectic bonding compatibility

In the proposed initial design for the ENGINI neural implants, the strategy for the creation of an hermetic seal to protect the cavity that hosts the active electronics is to employ

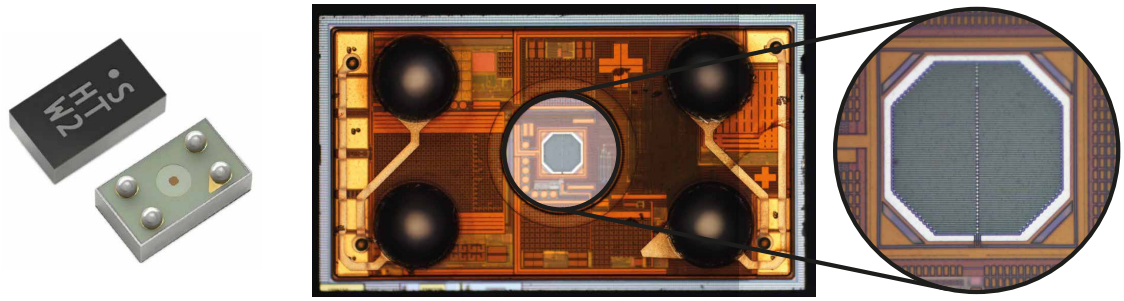
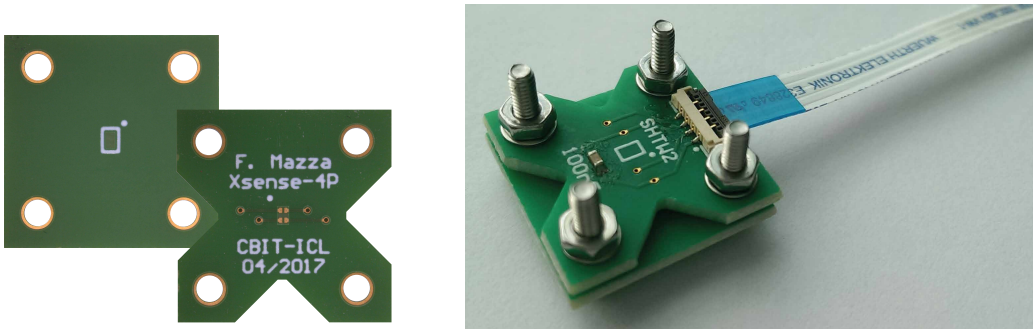


Figure 3.11.: Sensirion SHTW2 temperature and humidity sensor: on the left overall aspect of the sensor; in the centre and on the right a micro-photograph of the bottom side, with zoom on the sensing element.

eutectic bonding. This is a wafer bonding technique that uses a particular metal alloy as intermediate layer. Said metal alloy is in fact a eutectic system, which means it's composed by two substances that, when mixed together, have a melting temperature lower than the one of the individual substances. The value of this temperature, called eutectic temperature, is dependent on the mixing ratio of the two substances. In particular it is considered the use of a AuSn mix, that has demonstrated high bonding strength and is compatible with CMOS post-processing, having a eutectic temperature of 278 °C [37]. The process to create the eutectic bond requires a temperature cycle that goes up to 315 °C and is kept at that value for a minimum of 5 minutes. Therefore, it is necessary to ensure that the SHTW2 sensor can withstand such temperature, with no consequences on its calibration. According to its data sheet, the SHTW2 temperature operating range is −30 °C to 100 °C. It is also compatible with a reflow soldering profile with peak temperatures of 260 °C held for a maximum of 30 s. However, this figures are significantly lower, both in terms of temperature and time, of the values required by the eutectic process.

To test the SHTW2 through a simulated eutectic bonding process, a dedicated setup has been designed: the sensor's humidity response profile is first characterized using an Espec SH221 environmental test chamber. The sensor is then moved to a LPKF ProtoFlow reflow oven programmed to simulate the temperature cycle of a eutectic bonding process. Finally, a second humidity cycle in the environmental chamber is performed, to see if the sensor readout has been affected by the high temperature of the reflow oven. A possible issue is that the maximum eutectic bonding temperature is higher than the peak temperature of the sensor's reflow soldering profile. Therefore, there is the risk that the sensor might unsolder from the test PCB while in the reflow oven preventing it from going through the second humidity cycle. To solve this problem, a solderless approach is needed to connect to the sensor.

The proposed PCB design is composed of two separate boards that can be aligned and secured together to hold the SHTW2 sensor in between them. The electrical contacts with



(a) (b)

Figure 3.12.: Solderless PCB setup for Sensirion SHTW2 testing: (a) Picture of the two PCBs with alignment holes and solderless pads; (b) The assemlbed setup with the SHTW2 *sandwiched* in between the PCBs and connected to the testing equipment with a ribbon cable.

the sensor are formed by pressure only, without the need for soldering. The bottom PCB only hosts an aperture in the solder mask the same size of the sensor, to help keeping it aligned during assembly, while the top PCB includes the contact pads for the sensor, together with a bypass capacitor for power supply decoupling and the connector for the external ribbon cable (see Figure 3.12).

The testing procedure with the environmental chamber is automated thanks to the RS-485 serial communication capabilities of the instrument, through a Matlab script that sets the chamber parameters and records data from the sensors under test. The temperature profile of the reflow oven is reported in Figure 3.13, while the results from the test of two SHTW2 sensors in the environmental chamber, before and after the temperature cycle in the reflow oven, are detailed in Figure 3.14. The humidity inside the chamber is cycled through its whole swing, while the temperature is kept constant at 37 °C to mimic the body's internal temperature. The measurement errors between the value of relative

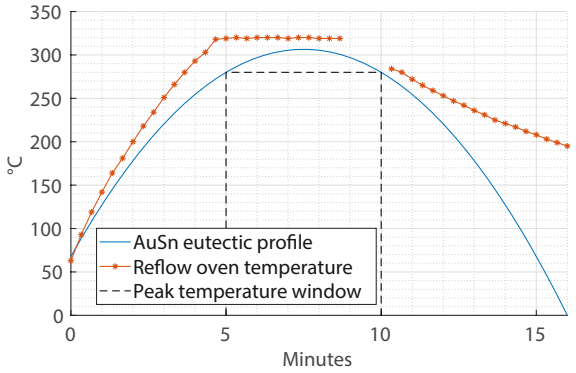


Figure 3.13.: Temperature profile of the LPKF reflow oven to simulate a AuSn eutectic bonding process: the interruption in the data is due to the instrument inability to show temperature values while switching off the temperature control.

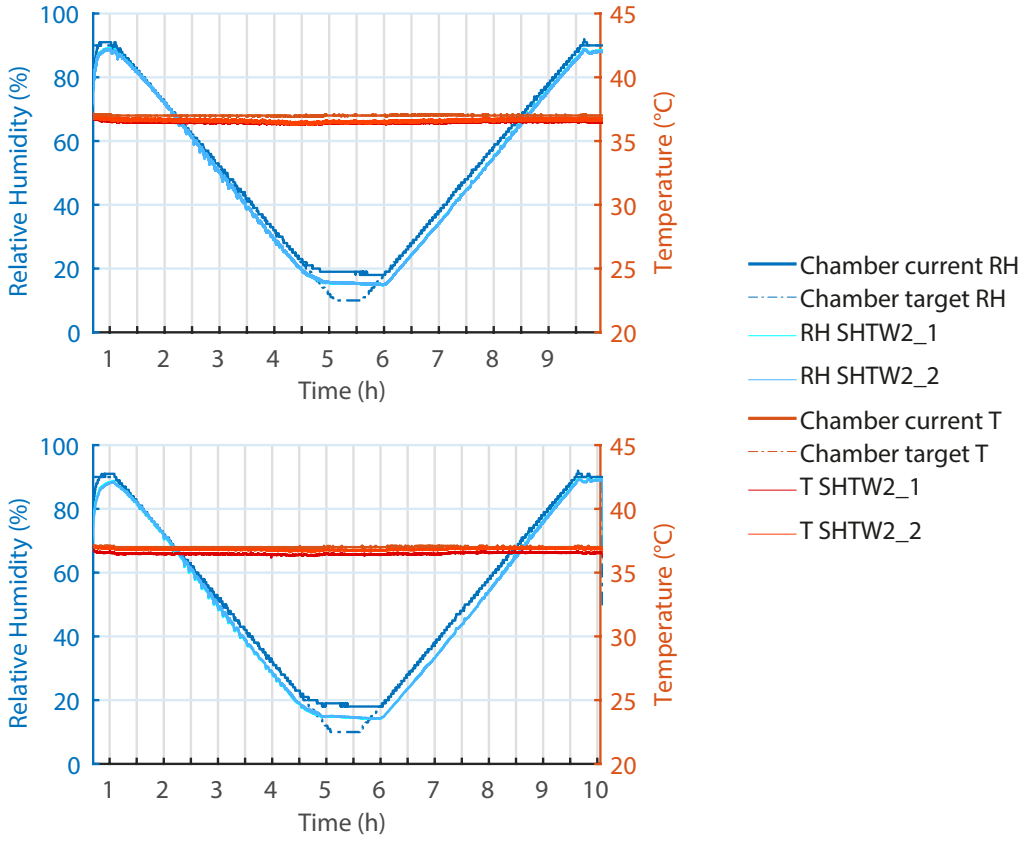


Figure 3.14.: Testing of two Sensirion SHTW2 temperature and humidity sensors inside the environmental chamber: on top the results before and at the bottom the results after the eutectic temperature cycle in the reflow oven.

humidity given by the environmental chamber and the reading of the two SHTW2 sensors under test are reported in Table 3.4. These errors, taken at regular time intervals, are measured before and after putting the two Sensirion sensors through the eutectic cycle simulation. As can be seen from both plots and error table, there is no evident difference between the performance of the sensors before and after the temperature cycle, as they are still able to reliably track the value of humidity inside the environmental chamber. This makes them good candidates for use in hermetic packages for encapsulation monitoring.

Despite their small footprint, the SHTW2 sensors are still relatively bulky for being integrated inside a micro-package. To address this issue, a thinning process was attempted. The thinning was performed by backgrinding the sensors' dies, however it proved to be very difficult to perform the operation at die level, and all of the five attempts resulted in non functioning sensors (see Figure 3.15).

3.4.1. Optoelectronic hermeticity platform

The Sensirion SHTW2 has proven to be a reliable sensor, able to withstand the temperature cycle of a eutectic bonding process, and therefore it can be used to monitor package

Table 3.4.: Measurement error between environmental chamber and test sensors, before and after putting the sensors through the eutectic cycle.

		Error (% RH)								
Elapsed time		1.5 h	2.5 h	3.5 h	4.5 h	5.5 h	6.5 h	7.5 h	8.5 h	9.5 h
Chamber % RH		80%	60%	40%	20%	20%	30%	50%	70%	90%
Sensor 1	Before	0.08	-0.95	-2.99	-2.92	-3.78	-3.72	-3.57	-2.26	-2.45
	After	0.11	-0.75	-2.95	-3.27	-3.62	-3.87	-4.49	-3.5	-2.24
Sensor 2	Before	0.05	-0.74	-2.7	-2.69	-3.63	-3.76	-3.7	-2.42	-2.59
	After	0.18	-0.53	-2.71	-3.06	-3.47	-3.88	-4.47	-3.43	-2.39

integrity. However, its dimensions do not allow for integration in sub-millimetre devices. Nevertheless, it can be integrated in larger assemblies to provide useful hermeticity information when testing packaged devices. There is however the issue of communication with the sensor when used in such a setting: if the package is required to be hermetic, we want to avoid feedthrough connections that might be cause of moisture ingress. A wireless strategy is therefore required to connect to the sensor and for data readout.

One possible way is the use of inductive coupling between the inside and the outside of the hermetic package [38]. This solution, however, has shown to be challenging, requires coils to be integrated in the system, and is susceptible to EM interference.

Another strategy is the use of an optoelectronic architecure, where power and data are transferred using two light source and photodetector pairs (see Figure 3.16). The work towards this platform has been carried out by the MSc student Noah Ng and the BSc student Yin Fang as their thesis project. The main challenge of this approach is to deliver a sufficient amount of power to the circuitry inside the sealed package. This also requires a careful selection of the wavelength, to achieve a sufficient power transfer while minimizing the absorption caused by the material of the package.

This project has led to the design of the optical transmitter and receiver circuit, together

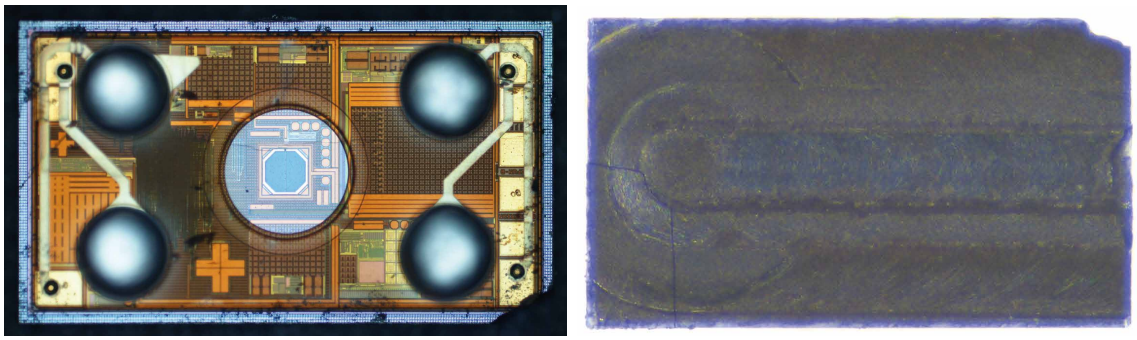


Figure 3.15.: Micro-picture of one of the Sensirion SHTW2 sensors that underwent back-grinding. Cracks are visible on both the front and the back surface of the sensor, together with the marks left by the milling machine.

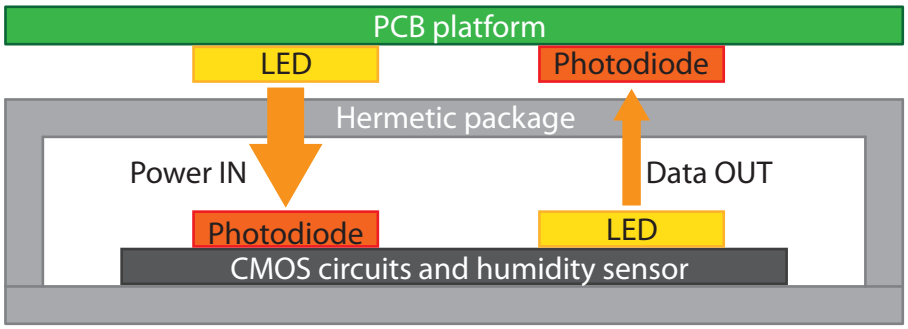


Figure 3.16.: Diagram of the platform for hermeticity monitoring with optical power transfer and data transmission.

with the selection of adequate photoelements for optimal power delivery, with promising results for the realization of a bench top testing platform for hermeticity of micro-packages.

3.5. Conclusions

In this chapter we have developed a custom sensor to measure humidity inside cavities with a sub-millimetre volume, with the scope of monitoring the hermeticity of implantable devices. The use of a commercial sensor has also been investigated. Based on the presented design process and test results, we draw the following conclusions:

- The Matlab tool based on the mathematical model for the calculation of an IDC capacitance proved accurate, and can be useful for the initial design choices and parameter optimization of similar structures.
- The total footprint of the readout circuit is smaller than the area required for the IDC. However, it could be reduced in a future iteration by adopting a different approach, maybe based on the humidity induced frequency shift of an oscillator.
- The sensor readout circuit could not be tested under different RH conditions. Nevertheless, the capacitance-to-voltage converter has proven functional for all three IDC dimensions.
- The sourcing of materials for conducting experiments was particularly challenging, compromising the testing of the sensor. A reminder of the importance of always planning for the worst when doing research.
- The performance of a thermally stressed Sensirion SHTW2 RH sensor has been evaluated, providing useful insight regarding the integration of this product in test platforms for package integrity.
- The obtained results are relevant to our specific application within the ENGINI project, and can be extended to the wider scientific community working on hermetic packaging in general, and on reliability of implantable devices in particular.

Bibliography

[1] A. Inmann and D. Hodgins, *Implantable sensor systems for medical applications*. Elsevier, 2013.

[2] U.S. Department of Defense, "Test Method Standard MIL-STD-883E - Microcircuits," December 1996.

[3] A. Vanhoestenberghe and N. Donaldson, "Corrosion of silicon integrated circuits and lifetime predictions in implantable electronic devices," *Journal of neural engineering*, vol. 10, no. 3, p. 031002, 2013.

[4] S. Costello, M. P. Desmulliez, and S. McCracken, "Review of test methods used for the measurement of hermeticity in packages containing small cavities," *IEEE Transactions on components, packaging and manufacturing technology*, vol. 2, no. 3, pp. 430–438, 2012.

[5] I. De Wolf, A. Jourdain, P. De Moor, H. Tilmans, and L. Marchand, "Hermeticity testing and failure analysis of mems packages," in *2007 14th International Symposium on the Physical and Failure Analysis of Integrated Circuits*, pp. 147–154, IEEE, 2007.

[6] G. Elger, L. Shiv, N. Nikac, F. Muller, R. Liebe, and M. Grigat, "Optical leak detection for wafer level hermeticity testing," in *IEEE/CPMT/SEMI 29th International Electronics Manufacturing Technology Symposium*, pp. 326–331, IEEE, 2004.

[7] A. Vanhoestenberghe and N. Donaldson, "The limits of hermeticity test methods for micropackages," *Artificial organs*, vol. 35, no. 3, pp. 242–244, 2011.

[8] S. Millar and M. Desmulliez, "Mems ultra low leak detection methods: a review," *Sensor Review*, vol. 29, no. 4, pp. 339–344, 2009.

[9] M. Dokmeci and K. Najafi, "A high-sensitivity polyimide capacitive relative humidity sensor for monitoring anodically bonded hermetic micropackages," *Journal of Microelectromechanical Systems*, vol. 10, no. 2, pp. 197–204, 2001.

[10] H. Farahani, R. Wagiran, and M. Hamidon, "Humidity sensors principle, mechanism, and fabrication technologies: a comprehensive review," *Sensors*, vol. 14, no. 5, pp. 7881–7939, 2014.

[11] Z. Rittersma, "Recent achievements in miniaturised humidity sensors—a review of transduction techniques," *Sensors and Actuators A: Physical*, vol. 96, no. 2-3, pp. 196–210, 2002.

[12] D. K. Roveti, "Choosing a humidity sensor: A review of three technologies this discussion of the operating principles of capacitive, resisitive, and thermal conductivity humidity sensors also addresses their advantages, disadvantages, and applications," *Sensors-the Journal of Applied Sensing Technology*, vol. 18, no. 7, pp. 54–58, 2001.

[13] J. Tao, L. Wang, H. Cai, T. Sun, J. Song, and Y. Gu, "A novel photonic dew-point hygrometer with ultra-high accuracy," in *2016 IEEE 29th International Conference on Micro Electro Mechanical Systems (MEMS)*, pp. 893–896, IEEE, 2016.

[14] D. Cirmirakis, A. Demosthenous, N. Saeidi, A. Vanhoest, and N. Donaldson, "An implantable humidity-to-frequency sensor in cmos technology," in *SENSORS, 2011 IEEE*, pp. 1511–1514, IEEE, 2011.

[15] Z. Chen and C. Lu, "Humidity sensors: a review of materials and mechanisms," *Sensor letters*, vol. 3, no. 4, pp. 274–295, 2005.

[16] N. Saeidi, J. Strutwolf, A. Maréchal, A. Demosthenous, and N. Donaldson, "A capacitive humidity sensor suitable for cmos integration," *IEEE Sensors Journal*, vol. 13, no. 11, pp. 4487–4495, 2013.

[17] Y. Wang, J.-N. Chen, D.-M. Ke, and J. Hu, "Modeling of a cmos capacitive relative humidity sensor," in *2009 First International Workshop on Education Technology and Computer Science*, vol. 3, pp. 209–212, IEEE, 2009.

[18] T.-Y. Yang, J.-J. Huang, C.-Y. Liu, and H.-Y. Wang, "A cmos-mems humidity sensor," in *Proceedings of the International Conference on Circuits, System and Simulation (ICCSS), Bangkk, Thailand*, vol. 2829, p. 212217, 2011.

[19] A. Rivadeneyra, J. Fernández-Salmeron, M. Agudo, J. A. López-Villanueva, L. F. Capitan-Vallvey, and A. J. Palma, "Design and characterization of a low thermal drift capacitive humidity sensor by inkjet-printing," *Sensors and Actuators B: Chemical*, vol. 195, pp. 123–131, 2014.

[20] A. Rivadeneyra, J. Fernández-Salmerón, J. Banqueri, J. A. Lopez-Villanueva, L. F. Capitan-Vallvey, and A. J. Palma, "A novel electrode structure compared with interdigitated electrodes as capacitive sensor," *Sensors and Actuators B: Chemical*, vol. 204, pp. 552–560, 2014.

[21] C.-L. Dai and D.-H. Lu, "Fabrication of a micro humidity sensor with polypyrrole using the cmos process," in *2010 IEEE 5th International Conference on Nano/Micro Engineered and Molecular Systems*, pp. 110–113, IEEE, 2010.

[22] C. Wang, L. Yin, L. Zhang, D. Xiang, and R. Gao, "Metal oxide gas sensors: sensitivity and influencing factors," *Sensors*, vol. 10, no. 3, pp. 2088–2106, 2010.

[23] T. Blank, L. Eksperiandova, and K. Belikov, "Recent trends of ceramic humidity sensors development: A review," *Sensors and Actuators B: Chemical*, vol. 228, pp. 416–442, 2016.

[24] M. J. Lee, H. P. Hong, K. H. Kwon, C. W. Park, and N. K. Min, "Fast-speed, high-sensitivity polyimide humidity sensors with superhydrophilic carbon nanotube network electrodes," *Sensors and Actuators B: Chemical*, vol. 185, pp. 97–104, 2013.

[25] Y. Qiu, C. Azeredo-Leme, L. Alcacer, and J. E. Franca, "Characterization of a cmos humidity sensor using different polyimides as sensing films," in *Electronics and Structures for MEMS II*, vol. 4591, pp. 310–315, International Society for Optics and Photonics, 2001.

[26] A. Hassanzadeh and R. G. Lindquist, "Capacitance measurement methods for integrated sensor applications," *ECE Department, The University of Alabama in Huntsville "unpublished*, 2013.

[27] C. Eder, V. Valente, N. Donaldson, and A. Demosthenous, "A cmos smart temperature and humidity sensor with combined readout," *Sensors*, vol. 14, no. 9, pp. 17192–17211, 2014.

[28] R. Igreja and C. Dias, "Analytical evaluation of the interdigital electrodes capacitance for a multi-layered structure," *Sensors and Actuators A: Physical*, vol. 112, no. 2-3, pp. 291–301, 2004.

[29] X. Hu and W. Yang, "Planar capacitive sensors–designs and applications," *Sensor Review*, vol. 30, no. 1, pp. 24–39, 2010.

[30] G. González, E. Kolosovas-Machuca, E. López-Luna, H. Hernández-Arriaga, and F. González, "Design and fabrication of interdigital nanocapacitors coated with hfo2," *Sensors*, vol. 15, no. 1, pp. 1998–2005, 2015.

[31] J. Oberländer, Z. Jildeh, P. Kirchner, L. Wendeler, A. Bromm, H. Iken, P. Wagner, M. Keusgen, and M. Schöning, "Study of interdigitated electrode arrays using experiments and finite element models for the evaluation of sterilization processes," *Sensors*, vol. 15, no. 10, pp. 26115–26127, 2015.

[32] H. Looyenga, "Dielectric constants of heterogeneous mixtures," *Physica*, vol. 31, no. 3, pp. 401–406, 1965.

[33] F. Deng, Y. He, C. Zhang, and W. Feng, "A CMOS humidity sensor for passive rfid sensing applications," *Sensors*, vol. 14, no. 5, pp. 8728–8739, 2014.

[34] W. Bracke, R. Puers, and C. Van Hoof, *Ultra low power capacitive sensor interfaces*. Springer Science & Business Media, 2007.

[35] C. C. Enz and G. C. Temes, "Circuit techniques for reducing the effects of op-amp imperfections: autozeroing, correlated double sampling, and chopper stabilization," *Proceedings of the IEEE*, vol. 84, no. 11, pp. 1584–1614, 1996.

[36] G. Wegmann, E. A. Vittoz, and F. Rahali, "Charge injection in analog mos switches," *IEEE Journal of Solid-State Circuits*, vol. 22, no. 6, pp. 1091–1097, 1987.

[37] K. M. Szostak and T. G. Constandinou, "Hermetic packaging for implantable microsystems: Effectiveness of sequentially electroplated ausn alloy," in *2018 40th Annual International Conference of the IEEE Engineering in Medicine and Biology Society (EMBC)*, pp. 3849–3853, IEEE, 2018.

[38] P. Feng, P. Yeon, Y. Cheng, M. Ghovanloo, and T. G. Constandinou, "Chip-scale coils for millimeter-sized bio-implants," *IEEE transactions on biomedical circuits and systems*, vol. 12, no. 5, pp. 1088–1099, 2018.

4. Chronic Stability of Implanted Silicon Devices

In the previous chapter, the importance of having *in situ* instrumentation to monitor over time the status of the encapsulation of implantable devices has been highlighted. This is particularly true when scaling down the implant dimensions to the millimetre or sub-millimetre domain. In fact, this downsizing often comes at the expenses of commonly employed safety precautions, such as extra layers of encapsulation or system redundancies.

Possibly, the only component of an implantable device that cannot be spared is the electronics core. With the use of silicon-based electronics it is possible to take advantage of the extreme miniaturization capabilities of IC manufacturing, and even to design entire implants integrated on a single silicon die, for example the Neurograins concept shown in chapter 2.

However, using only an active silicon substrate as implant poses numerous challenges from the point of view of biocompatibility and device longevity, due to the materials used and the fabrication process of a silicon die. To better understand these issues, it is important to review the main features of a typical CMOS process. As an example, Figure 4.1 shows the cross section of a 0.18 µm process. The fabrication steps are carried out from the bottom up: starting from the lower section of the image the FEOL (front end of line) is found. Here the transistors and most other devices (resistors and capacitors) are formed by patterning with photo-lithography the required wells and the gate, source, and drain modules. Moving upwards, the various metal layers are encountered. These layers provide the necessary interconnections between the devices, and are separated by the inter-layer dielectrics (ILDs), usually silicon dioxide (SiO_2). Finally, the top surface of the IC is covered by one or more passivation layers, whose goal is to protect the underlying structures from corrosion. Common materials for passivation are silicon dioxide, silicon nitride (SiN), and titanum nitride (TiN), but other compositions have been used for more specific purposes [3, 4]. The passivation is then removed only where necessary, like on bond pads for electrical connections or in the presence of surface sensors.

After the dicing process, which cuts the wafer into individual dies, commercial ICs are usually bonded and encapsulated in a thermoplastic or ceramic package, that protects the

A portion of the material presented in this chapter has been published in [1, 2]. The experimental setup described in subsection 4.2.2 has been developed by Prof. Nick Donaldson and his team in the Implanted Devices Group at University College London. Accelerated life testing has been carried out by Mr Callum Lamont and Mr Ahmad Shah Idil at UCL, and Mr Kambiz Nanbakhsh from TU Delf.

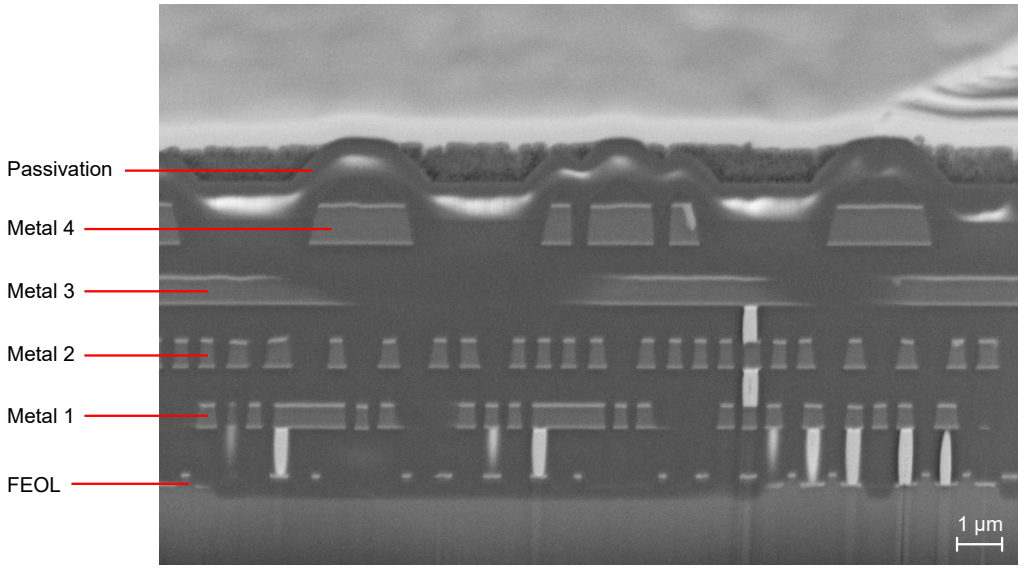


Figure 4.1.: Focused Ion Beam (FIB) cross section of the UMC 180nm eNVM process [5]. Starting from the bottom, there is the FEOL, which contains all the active devices, then the various metal layers for interconnections (in this case it is a four metal process), and finally the passivation layers.

die both mechanically and electrically from the environment, and provides the required electrical contacts. However, as previously stated, in order to scale down the dimensions of implantable devices to or below the millimetre domain, it might be preferable to avoid such packaging, and use only one or few layers of polymer encapsulation. While keeping dimensions to a minimum, these polymer layers help with the biocompatibility of the implant both from a point of view of materials and from a mechanical perspective. In fact, they act as a softer interface to the tissue, and cover the sharp edges of a silicon die.

The work present in this chapter aims at studying the long-term performances of polymer encapsulated silicon dies in the context of miniaturized implantable devices, in order to provide insights on the encapsulation requirements in the design process of such devices.

4.1. Water penetration in coated silicon devices

Many studies have been dedicated to the understanding of how water vapour affects the reliability of silicon devices, although the vast majority of them have mainly considered moisture diffusion mechanisms in the standard commercial packaging of CMOS devices [6]. The process of diffusion of water molecules in a multi-material device is not simple to study, given the many variables to be taken into account, from the environmental ones such as temperature, pressure, and humidity, to the materials employed, presence of impurities, or contact interfaces. To try and gain insight into such process, the scientific community has developed numerous numerical models of moisture absorption [7, 8].

Since water ingress is unquestionably one of the main concerns for devices inside the

human body, if we want to develop the next generation of miniaturized implantable devices it is of primary importance to study moisture absorption and chronic stability in the case of single silicon dies encapsulated only by polymer layers. There have been studies in such direction as well, most of which employ specifically designed test structures that are put under stress conditions, such as voltage and temperature, to accelerate the ageing of the devices [9]. However, given the extremely high degree of reliability needed for medical devices, the results from such tests are often very sparse and not easily translated into the real implants. Also, since the majority of the samples used in such experiments are test structures built in house, they might not reflect the behaviour of industry produced devices, which are the ones to be finally employed in clinical applications [2].

4.1.1. Moisture induced damages to implants

Silicone-based polymers have been successfully used as coating for implantable devices thanks to their advantageous properties, in particular when compared to the epoxy resins that were used in early implants: they are easy to mould to conform to the device and easily allow for the creation of custom implant shapes; their low modulus makes them able to relieve mechanical stresses; they have a very low content of ionic contaminants; they are transparent, facilitating the inspection of the encapsulation. As an example, polydimethylsiloxane (PDMS) has been employed as encapsulant for the cables and electrodes in pacemakers an neural stimulators [10].

On the other hand, the main drawback of polymers is their permeability. No polymer is able to offer total resistance to gas molecules, and therefore they can absorb water, and experience changes in their volume and elasticity as the result of hygroscopic swelling. Incorporating hydrophobic materials within the polymer has shown better chronic performances [11], but they still cannot provide the same level of protection as metals or ceramics. Moreover, in order to create an encapsulation that covers all sides of the implantable device, more than one processing step is usually required. This might enhance the formation of micro-cracks, bubbles or imperfections within the polymer.

Water molecules can be present inside the polymer's structure in two different states: *bound* molecules are chemically linked to the polymer chains by means of hydrogen bonds, while *unbound* or *free* molecules are trapped in nano-pores and free volumes and not chemically bound to the polymer molecules. The unbound water content present at the moment of fabrication is usually evaporated during a reflow phase, but more energy is generally needed to also release the bound molecules [12].

By looking at Figure 4.2 it is possible to understand how moisture trapped inside the encapsulation can be the cause of multiple ways of device failure. In this example, two voids are present within the encapsulant, one in the bulk of the material while the other is in contact with the active implant. As soon as the implant is placed in a fluid, the permeable polymer lets water molecules diffuse through it, until they reach a void and condense in it. If the void is in contact with the implant's surface, the water accumulated

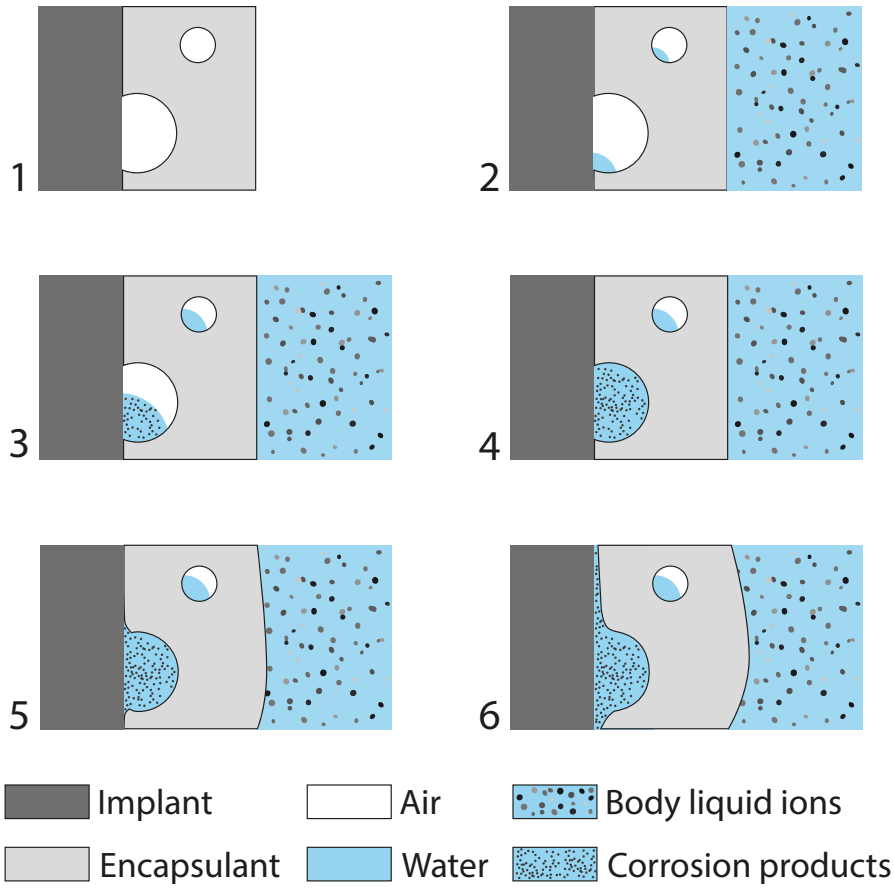


Figure 4.2.: Representation of the mechanism of implant failure caused by water accumulation inside the voids present in the encapsulation layer (adapted from [13]).

can start the process of corrosion of the implant. The result of such corrosion is the release in the condensed water of particles and ions of metal and metal oxide. Moreover, the concentration of ions generates a positive feedback effect that attracts more water molecules by modifying the osmotic gradient [13]. As the void is increasingly filled by condensed water and ions, its internal pressure rises, and might detach parts of the encapsulation from the implant, even reaching a complete separation between the two and delamination of the polymer layer.

Apart from corrosion, the presence of water accumulating at the interface between the polymer encapsulation and the implant can also cause problems of electrical nature: for example, it can promote electromigration and the formation of metal dendrites that could short together separated metal tracks [14]. If the void is formed between two conductors with a sufficient voltage difference, it can cause the hydrogen and the oxygen in the water molecules to dissociate, and the resulting gas can further expand the volume of the void. This might have a significant impact in miniaturized implants, where the scaling down in dimensions corresponds to locally higher electric fields. In case the bubbles inside the

encapsulation expand so much to cause the opening of a direct path from the implant to the body environment, leaching occurs: this is the diffusion in the biological tissue of the particles corroded from the implant, which are often toxic for the body [15].

Water ingress in implants is a major issue when designing devices that target chronic operation. It can cause multiple malfunctions and often leads to complete device failure. More in-depth testing is required, in particular regarding the performances of polymer encapsulation that is currently the main solution to achieve high implant miniaturization.

4.2. Structures for accelerated tests on implant encapsulation

The considerations exposed in the previous section regarding the damages caused by water penetration inside an implantable device highlight the need for meaningful tests to evaluate how silicon-based implants perform over long periods of time when protected with a polymer encapsulation. To better understand such phenomena, the use of custom designed test structures in silicon is explored, as it can provide more insight regarding the chemical interactions that occur in CMOS substrates when exposed to an environment such as the human body. Of particular interest is the resistance to corrosion of the functional parts of the CMOS device, such as the metal interconnections and the MOSFETs' junctions, as well as the importance of protection layers like passivation and polymer coatings in safeguarding the device. Each of the proposed test structures, detailed in the following section, is designed to investigate how these processes occur at different depths of the CMOS stack.

4.2.1. Test structures design

Three types of test structures have been designed and fabricated in the AMS 0.35 µm four metal CMOS process. In order to obtain consistent results, the technology is the same used for prototyping various neural recording circuits employed by both the ENGINI project an the CANDO (Controlling Abnormal Network Dynamics using Optogenetics) project. The latter is an EPSRC funded project that aims at delivering an implantable neural system for patients affected by focal epilepsy.

Interdigitated capacitor

The first test structure is an interdigitated capacitor, formed by two comb electrodes fabricated on the Metal 3 layer (see Figure 4.3a). IDCs hare the most common type of structure for encapsulant testing, as they allow the detection of leakage current between the electrodes or the change in insulation impedance [9]. The two electrodes that compose the capacitor are surrounded by a *Guard* electrode that acts as a shield, whose

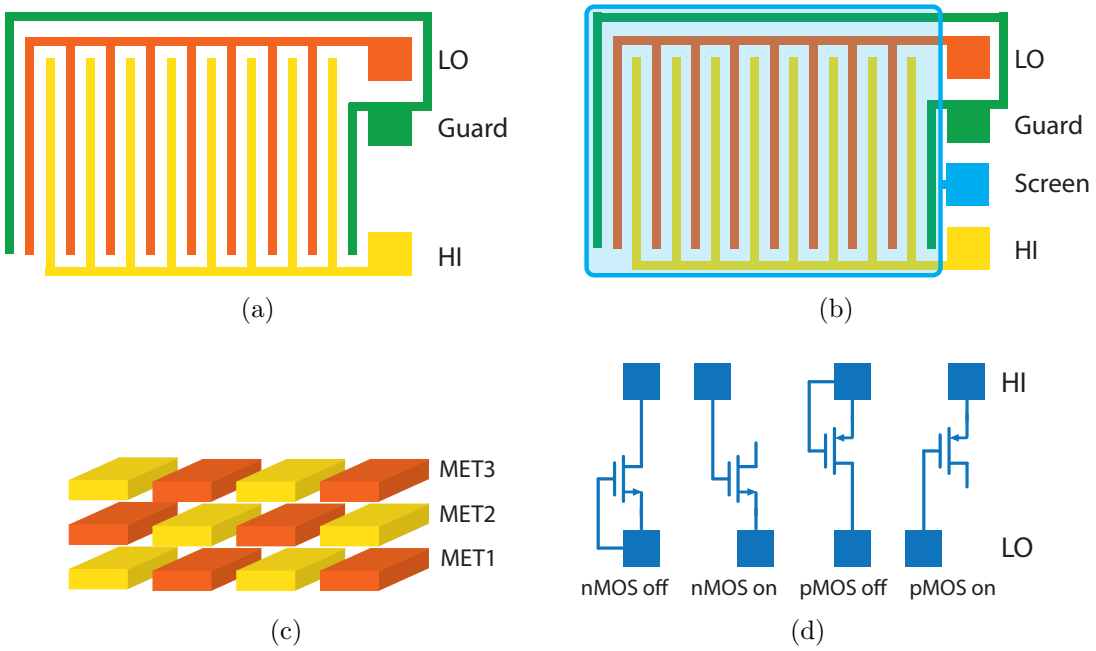


Figure 4.3.: Diagrams of the test structures for accelerated life testing of polymer encapsulated electronics: (a) IDC structure with *Guard* electrode to collect leaking charges; (b) Same IDC structure with an added screen on Metal 4 layer; (c) Vertical IDC with alternated electrodes on the bottom three metal layers; (d) Four different configurations of MOSFETs for testing gate-to-source and drain-to-source leakage.

function is to collect surface leakage charges. The total area of the IDC is approximately $1.15 \times 0.85\,\mathrm{mm}^2$, while the single electrodes have been designed with minimum finger width and gap (1 µm and 0.6 µm respectively) to maximize capacitance.

The IDC structure has also been replicated with the addition of a *Screen* pad, connected to a continuous planar surface on Metal 4, as a further protection (Figure 4.3b). This variation has been designed to assess if the implant's resistance to moisture penetration would benefit from the presence of such a continuous metal screen to shield the bottom layers. This would of course come at the expenses of having one less metal layer available for interconnections, thus setting a constraint on the complexity of the active circuits in the case of a real implant. In this case, the dimensions had to be readjusted to comply with the design rules, for a total IDC area of $0.97 \times 0.68\,\mathrm{mm}^2$. Of particular interest is the long term performance of the passivation layer, in this case composed by SiO_2 and SiN. As mentioned earlier in the chapter, the role of the passivation is to protect from corrosion and slow the oxidation process. However, the deposition of the passivation layers is the last step of fabrication, and no subsequent planarization is performed. This leaves the passivation with an irregular surface, also depending on the metal structures underneath, and makes it more prone to non-uniformities and cracks.

The IDC has also been redesigned, in its screened variation, in a following tape-out,

again using a AMS 0.35 µm process but with no thick top metal option. This was required to increase the impedance of the test structure. The new dimensions are $2.8 \times 1.5\,\mathrm{mm}^2$, which provide a measured capacitance of approximately 150 pF.

Vertical interdigitated capacitor

The second type of test structure is still an interdigitated capacitor, but in this case the comb electrodes are extended to the first three metal layers, in order to create a three dimensional, "chessboard"-like capacitive structure (see Figure 4.3c). Also in this case the screen on Metal 4 is used. This configuration aims at investigating the effect of ageing on the various metal layers of the CMOS process, other than only the top ones like the previously presented IDCs. The capacitor area is $0.82 \times 0.65\,\mathrm{mm}^2$, and minimum feature sizes have been used for the comb electrodes, like for the previous IDC.

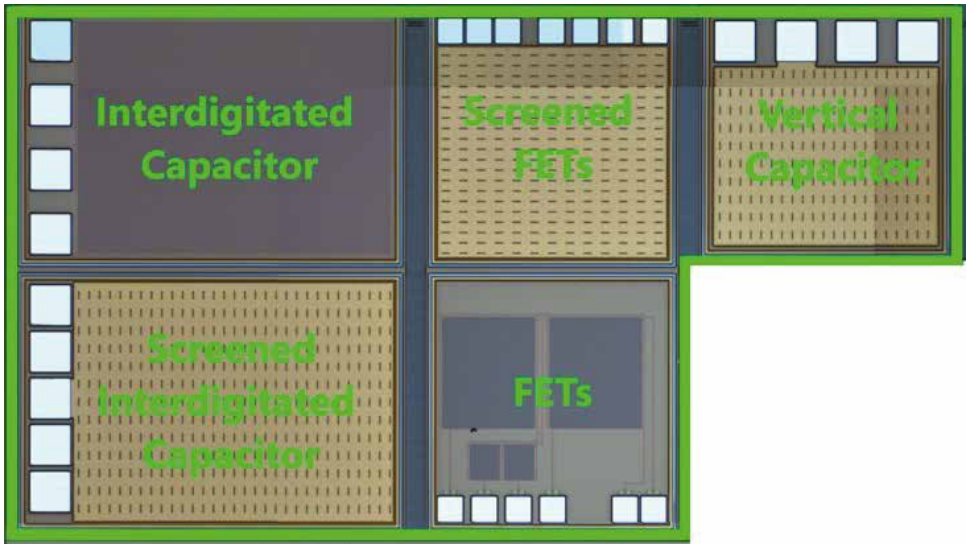
MOSFETs

The last kind of test structure is composed by four different MOSFETs (see Figure 4.3d). There are two couples of nMOS and pMOS, and for each couple one transistor is in a *off* configuration, with the gate contact shorted with the source terminal, while the other is in a *on* configuration, with no terminals shorted together. The aim of these transistor-based test structures is to study the chronic performances of the aged silicon die, but with a focus on the FEOL and the substrate. In particular, the *off* FETs target the drain-to-source leakage, while the *on* FETs the gate-to-source leakage. To increase the magnitude of possible leakage currents, the transistors have been designed with an interdigitated geometry for source and drain contacts. The MOSFETs have been replicated in two versions, with and without the Metal 4 screen, similarly to the IDCs.

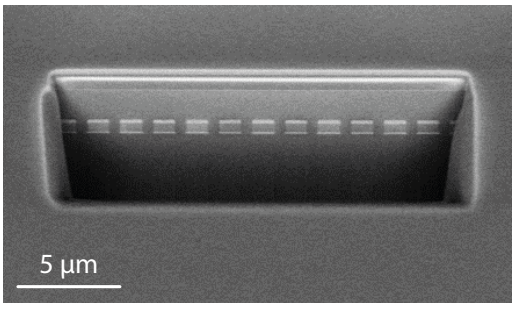
A micropicture of the fabricated test structures is reported in Figure 4.4a, together with two FIB cross sections of the unscreened IDC and the screened vertical capacitor (Figure 4.4b and Figure 4.4c respectively).

4.2.2. Experimental setup

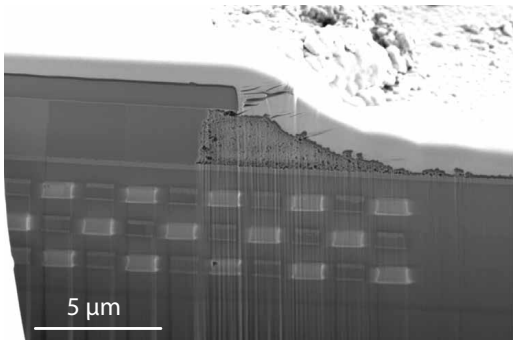
In order to conduct the accelerated life tests, a dedicated platform that allows for the parallel testing of multiple samples is required, in order to obtain statistically significant results. As mentioned earlier in this chapter, the test platform has been designed by Prof. Nick Donaldson and his collaborators at UCL, and refined over the years [16], in order to control and reduce all possible sources of interference that play a significant role in these kind of measurements. In fact, for a correct interpretation of the tests' results, the contributions of the measuring apparatus need to be distinguished from the ones of the device under test (DUT).



(a)



(b)



(c)

Figure 4.4.: Photographs of the test structures fabricated in AMS 0.35 µm four metal technology: (a) Micropicture of the full die containing all five of the designs. The narrow slots seen on the Metal 4 screens are openings required by the process' design rules to respect the maximum metal coverage of the layer; (b) FIB cross section of the unscreened IDC. Note how the aluminium fingers of the comb electrodes are covered on top and bottom by a protective layer, possibly TiN (image courtesy of Prof. Nick Donaldson); (c) FIB cross section of the vertical IDC. This sample was aged without encapsulation in PBS at 67 °C and biased at 15 V DC for one month. The thick Metal 4 layer presents clear signs of corrosion (image courtesy of Mr Callum Lamont).

The operation of the test platform is based on electrochemical impedance spectroscopy (EIS): this means that the samples are evaluated by mean of an AC stimulus with a frequency sweep, in order to obtain the frequency response of the DUT. The deviation of the resulting spectrum from the characteristic of an ideal capacitor may indicate the presence of a shunt impedance due to leakage. For this purpose a frequency response analyzer (FRA) is used, in conjunction with a femtoammeter for current detection.

To simulate the environment of the human body, the DUTs are immersed in phosphate-

buffered saline (PBS). This solution is the most widely used for biological *in vitro* experiments and cell cultures: being a buffered solution, it keeps its pH value almost constant even in presence of small changes in the concentration of acids or bases, at a value of approximately 7.4, which matches the pH of the human body. Moreover, its ion content (mainly sodium and potassium) and concentration correspond to the one inside the body, and is non-toxic to tissues. The ion composition of the solution can also be modified accordingly to meet specific requirements. Also for the particular case of *in vitro* testing of neural implants, the use of PBS has been largely documented [17, 18].

The working principle and the main components of the test platform are reported in the diagram in Figure 4.5. Given the necessity to perform tests at very low frequencies (down to 10^{-2} Hz) while at the same time needing many identical DUTs to collect significant data, the system is modular and it is designed to automatically cycle between the different DUTs. In the example of Figure 4.5 there are seven separate but identical silicon dies with the IDC test structures (the ones presented in the previous section) that act as DUTs. Each DUT is aged in a glass test tube filled with PBS (see Figure 4.6a). The tube is sealed by a bung made of polyether ether ketone (PEEK) fitted with a silicone O-ring. This prevents the PBS solution to evaporate over time. The level of PBS inside the tube is also monitored using a two-wire level detector. Using silicone, the CMOS die is bonded to an alumina (Al_2O_3) substrate where PtAu metal tracks have been patterned to allow for electrical connection. These tracks are insulated using a glass sealing layer. Finally the whole structure is then encapsulated in moulded silicone (MED-6015) (see Figure 4.6b).

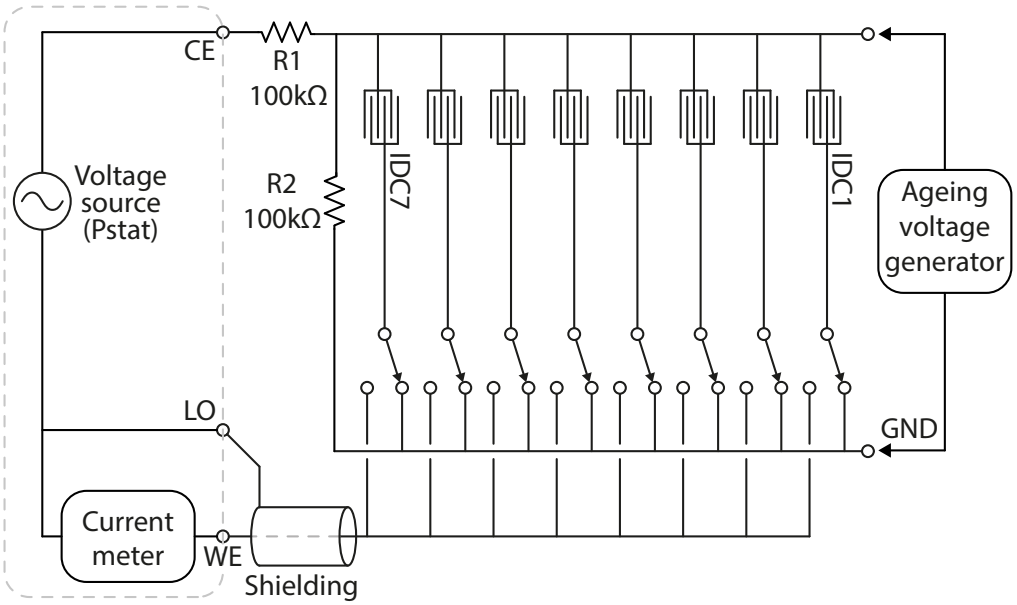


Figure 4.5.: Simplified schematic of one module of the test platform. Resistor R_1 is for limiting the current from the voltage source in case one of the DUTs fails causing a short circuit while resistor R_2 limits the voltage across the IDCs that are not currently under measurement (adapted from [16]).

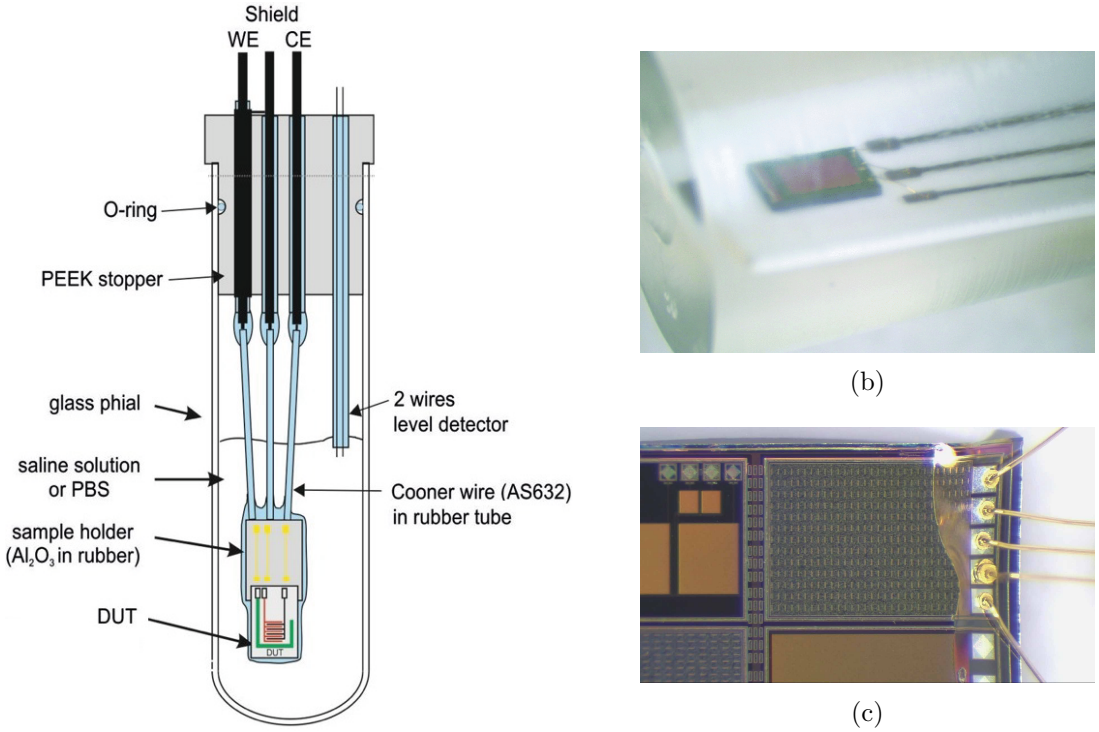


Figure 4.6.: Set up of and connection of individual samples within the platform for accelerated life testing: (a) Diagram of the PBS-filled test tube for ageing tests (image courtesy of Prof Nick Donaldson); (b) IDC sample bonded to alumina substrate and encapsulated in silicone [2]; (c) Screened IDC sample prepared for test without polymer encapsulation (image courtesy of Mr Kambiz Nanbakhsh).

When a measurement has to be performed, the reed relay associated to the desired DUT is activated, to connect the test IDC to the instrumentation. The counter electrode (CE) side is driven by the voltage source that performs a frequency sweep from 10^{-2} to 10^{5} Hz. The resulting current at working electrode (WE) is then measured by the femtoammeter. The WE is also shielded along its full length (including on the silicon die by the *guard* metal track) to collect leakage currents.

4.2.3. Results

Different batches of silicone encapsulated IDCs have been aged at 47 °C, 67 °C, and 87 °C. If a failure occurs in an IDC that causes leakage through the two comb electrodes, we expect to observe a change in phase from $-90°$ to $-45°$ at low frequency (around 10 mHz) caused by a resistive effect. Moreover, an increase in the overall capacitance of the IDC can be an indicator of moisture penetration inside the dielectric layers, in a mechanism similar to the one exploited for the humidity sensor.

A summary of the ageing test results from the ongoing experiments is reported in

Table 4.1.: Results of accelerated life tests on IDC structures under constant DC bias and at different ageing temperatures.

Temperature (°C)	Voltage	Days	Samples	Failures
47	5 V DC	360	12	0
67	5 V DC	393	12	2
87	5 V DC	365	12	2

Table 4.1. The samples aged at 47 °C have shown no failure, while the ones at 67 °C and 87 °C have reported two failures each. One of these failures has occurred at the wirebond location on the silica adapter, where silicone has delaminated from the substrate (see Figure 4.7a), while the other three resulted as sudden open circuits in the output characteristic, caused by failure of soldered connections within the bung. So far no failure related to the CMOS samples has been reported, and their measured characteristic shows no anomalies in either the magnitude or the phase measurement (see Figure 4.8).

Tests conducted on unencapsulated IDC samples (from Mr Kambiz Nanbakhsh) have also shown good reliability. Unshielded IDC samples show good performance and can withstand continuous DC bias for a month in 67 °C PBS before showing visible damage. The presence of the Metal 4 screen layer extends the lifetime considerably (latest measurements available at 298 days) and offer similar results as samples with silicone encapsulation, justifying the use of such protective layer.

The interconnections from the DUTs and the test equipment are currently the main source of failure, in particular because of the known poor adhesion between silicone and PtAu. Nevertheless, the absence of CMOS failures is very promising, and suggests that active CMOS based implants might have the capability to reach decades of lifetime even when protected by a single polymer encapsulation layer.

This ongoing work has proven to be beneficial to the research community by providing



(a) (b)

Figure 4.7.: Degradation of the silicone encapsulation during accelerated life tests: (a) Delamination of silicone over PtAu tracks on alumina substrate; (b) Void formation inside the bulk of silicone. The similar alignment of the voids might suggest a relation with mechanical stresses inside the silicone (images courtesy of Prof. Nick Donaldson).

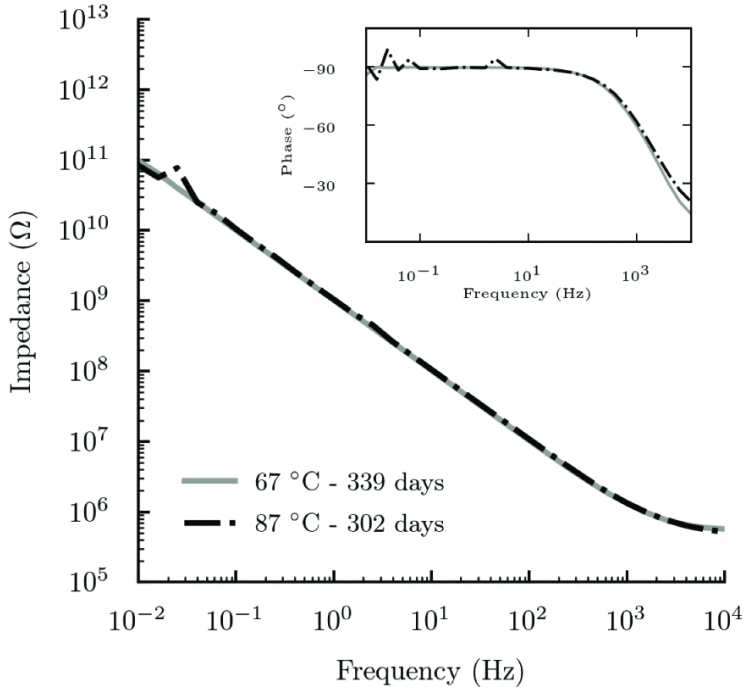


Figure 4.8.: Magnitude and phase plots of impedance measurement of samples aged at different temperatures. The constant magnitude at high frequencies is a consequence of the current limiting resistor in series with the DUTs [2].

meaningful results regarding the long-term reliability of generic active implantable devices [19]. The use of a reliable polymer encapsulation would be very beneficial, as it can help scaling down the size of the implants, while at the same time providing a soft interface with the surrounding tissue.

4.3. Integrated Devices for Micro-Package Integrity Monitoring

In section 4.2 we have presented the use of structures specifically designed for encapsulation monitoring during accelerated life testing. Here we propose two novel active circuits that tackle the issue of moisture penetration inside a CMOS package, and allow a chronic monitoring of the phenomenon instead of being a lab tool for bench-top testing. These circuits can be considered as *in situ* instrumentation, for moisture ingress monitoring and real time failure detection. Differently from the RH sensor proposed in chapter 3, that senses the presence of humidity inside a micro-cavity, these circuits aim at sensing infiltration of moisture within the layers that compose the silicon die. This type of infiltration arises from diffusion of water molecules within the oxide layers or thanks to the presence of micro cracks, and although it may not cause any build up of moisture inside a cavity, it can nevertheless lead to the corrosion of metal traces and might compromise the operation of the device.

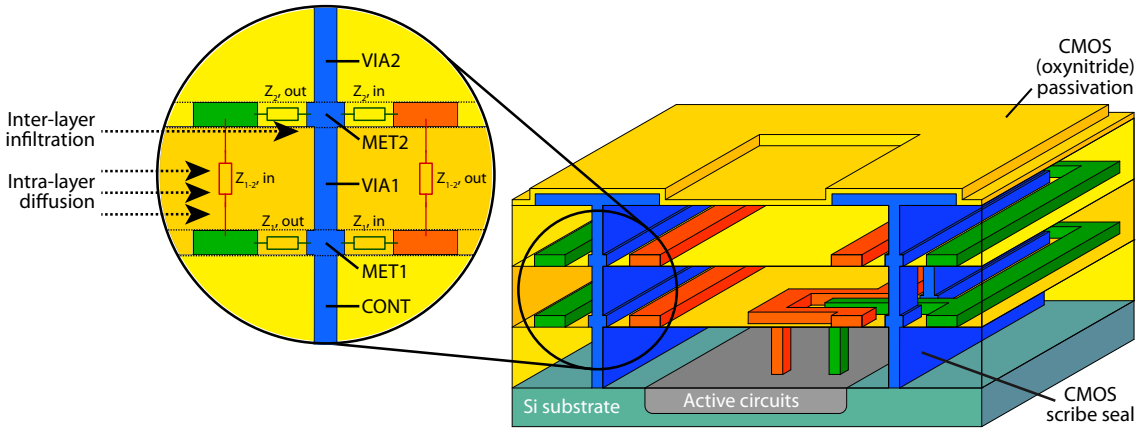


Figure 4.9.: Cross-section of a CMOS die showing the proposed structure to measure moisture penetration within the oxyde layers. The red and green metal tracks run around the perimeter, parallel to the die seal ring (dimensions of the metal traces not to scale).

The proposed circuits target this issue by detecting impedance changes in the ILDs stack. Both architectures take advantage from the presence of the die seal ring, that is usually present in CMOS circuits to protect the active devices placed within its boundaries. The die seal ring is formed by continuous parallel metal tracks on all available metal layers, all shorted together through vias, and it also connects to the silicon substrate by means of substrate contacts. It usually runs about 100 µm from the scribe line, i.e. the edge where the dicing saw will cut the silicon wafer to separate the individual dies. Both circuits deal with the issue of moisture infiltration from the side of the silicon die by performing an impedance measurement, however each circuit has been designed to assess specific features. The concept is illustrated in Figure 4.9. Along all the metal layers available in the CMOS process, a set of parallel metal tracks (drawn in orange in the figure) run around the die inside the the seal ring (drawn in blue), at a set distance from it. Similarly, another set of metal tracks (pictured in green) run at the same distance on the outside of the die seal ring. This allows for a differential measurement between the external tracks, which are the first ones affected by any ingress of moisture, and the internal ones, that are protected by the presence of the die seal ring. Both sets of metal tracks have contacts with the active part of the substrate. For the outer set, minimal apertures are made in the die seal ring to allow for electrical connection.

The two proposed architecture have been designed with the opportunity to be implemented together on the same die, by having the possibility to either connect or not the metal tracks together using programmable switches, so that the instrumentation can alternate between one configuration or the other whenever needed. This gives also the possibility to either use all of the metal traces as sensing terminals to enhance sensitivity, or to select a specific layer, for example Metal 2, to localise at which depth the failure has occurred.

4.3.1. Inter-layer infiltration

In this scenario we expect moisture penetration at the interface between the different silicon dioxide ILDs. This may be caused by defects during the fabrication phase, or by cracks induced by mechanical or thermal stress. Moisture continues to infiltrate deeper along the interface of ILDs, eventually leading to the formation of a conductive path between the outer metal tracks and the die seal ring. In this case a differential measurement along the horizontal direction is necessary to determine if the infiltration has reached the die seal ring. With reference to Figure 4.9, this corresponds to a comparison between the current leaking from $Z_{1,out}$, $Z_{2,out}$ to the seal ring, and the one leaking from $Z_{1,in}$, $Z_{2,in}$ to the seal ring.

In order to proceed with the design of the sensing circuit, it is necessary to estimate the order of magnitude of the leakage currents to be sensed. Given the wide range of failures that can be caused by water ingress and corrosion, it is difficult to accurately predict the value of such currents, however it is possible to use as a starting reference the value of leakage current for MOS devices reported on the datasheet of the proposed technology (AMS 0.35 µm). For devices under normal operational conditions, the leakage current is of the order of units of fA. If a conductive path was to be formed because of water penetration, we could estimate an increase of 3 to 4 orders of magnitude [20]. For our application we consider the leakage currents to be in the range of units to tens of pA.

The proposed circuit for this differential current measurement is shown in Figure 4.10a. It is composed of two amplification stages, where the inner and outer impedances under test (coloured in orange and green respectively) are connected to the inputs of a first fully differential amplification stage, which is then followed by a discrete time trans-impedance amplifier (TIA).

The purpose of the first stage is to amplify the difference between the leakage currents i_{out} and i_{in} coming from the two impedances under test, while the second stage TIA operates as a charge sensitive amplifier, where the output voltage V_{OUT} has a slope proportional to the charge integrated over time on the feedback capacitor C_F. The use of charge sampling has proven to be one of the best techniques for low-noise current sensing [21], but in order to avoid charge saturation over time, a periodic reset is necessary to discharge the sensing capacitors at every measurement cycle. With reference to the timing diagram shown in Figure 4.10b, this reset is performed by switches in parallel with the capacitors, driven by the periodic signal ϕ_{rst}. At the end of the reset phase, ϕ_{rst} is turned off and the integration phase starts, where C_F integrates the incoming current over the interval T_{int}. The resulting slope of V_{OUT} can then be sampled by using a S&H after the TIA (represented in the schematic as the switch driven by ϕ_S). To allow measurements in either condition $i_{in} < i_{out}$ or $i_{in} > i_{out}$, and therefore to account for positive or negative slopes of V_{OUT}, the TIA is biased with a common mode voltage $V_{DD}/2$ that sits in the middle of the supply voltage.

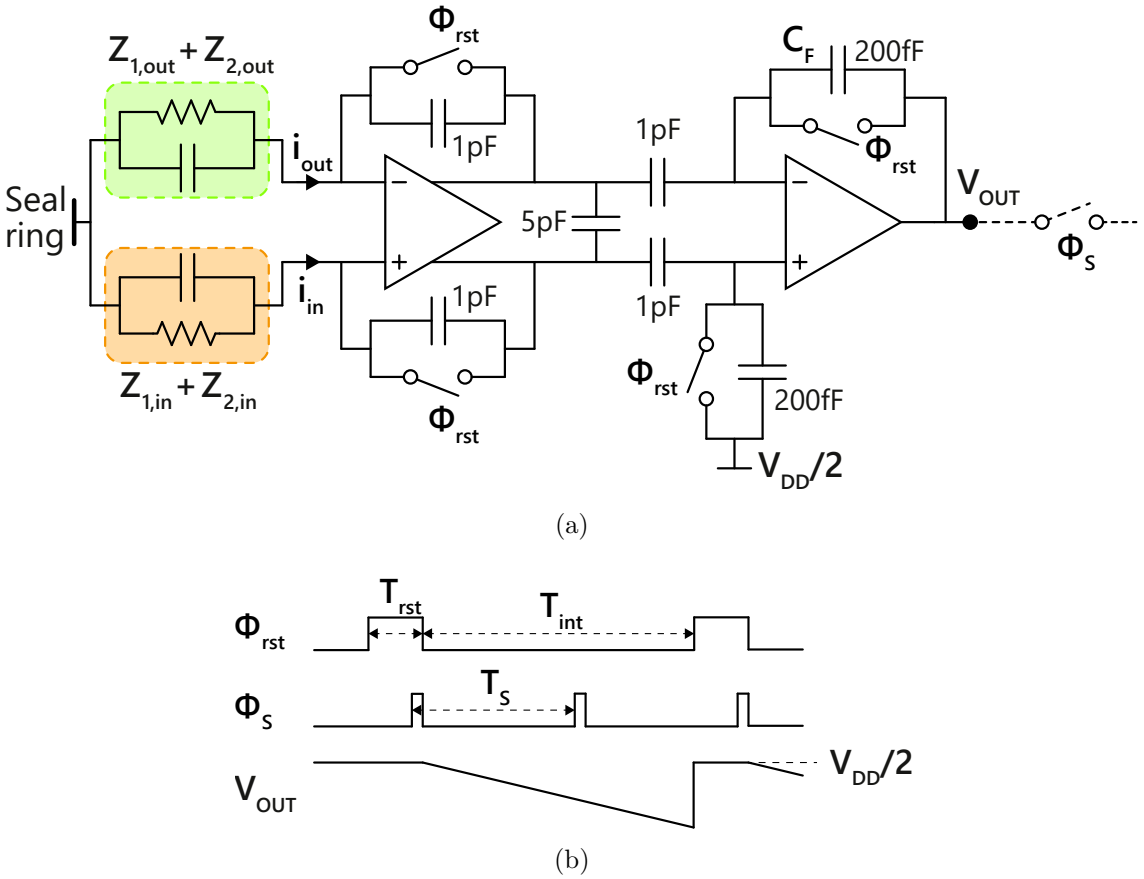


Figure 4.10.: Proposed circuit for sensing moisture ingress along the interface between ILD layers: (a) Schematic of the TIA-based circuit for the measurement of leakage currents between metal tracks and die seal ring; (b) Timing diagram of the TIA-based circuit.

Compared to conventional current sensing circuits, the signal bandwidth in the proposed system is near DC with magnitude in the range of 1 to 100 pA. This justifies the choice of using a discrete time sensing circuit, which is more suitable for low bandwidths than continuous time circuits [21]. A smaller amplification bandwidth is therefore preferred to reduce the overall noise bandwidth and the aliasing of high frequency noise inside the bandwidth due to sampling. A low sampling frequency is also required, lower than the corner frequency of the flicker noise, and it allows a low duty cycle for power saving.

The use of a lower sampling frequency however means that a larger portion of the wide-band noise will be translated down to base-band due to aliasing. Therefore a larger pMOS pair (600 µm/1 µm) is used in the first stage folded cascode amplifier [22], with 1 pF matched capacitors used in the feedback loops to minimise the effect of noise due to input parasitic capacitance.

A further enhancement could be provided by employing CDS after the TIA. By sampling the output voltage when the circuit is in the reset state, it is possible to obtain the value of offset voltage and noise, that can then be subtracted from V_{out} at the next measurement

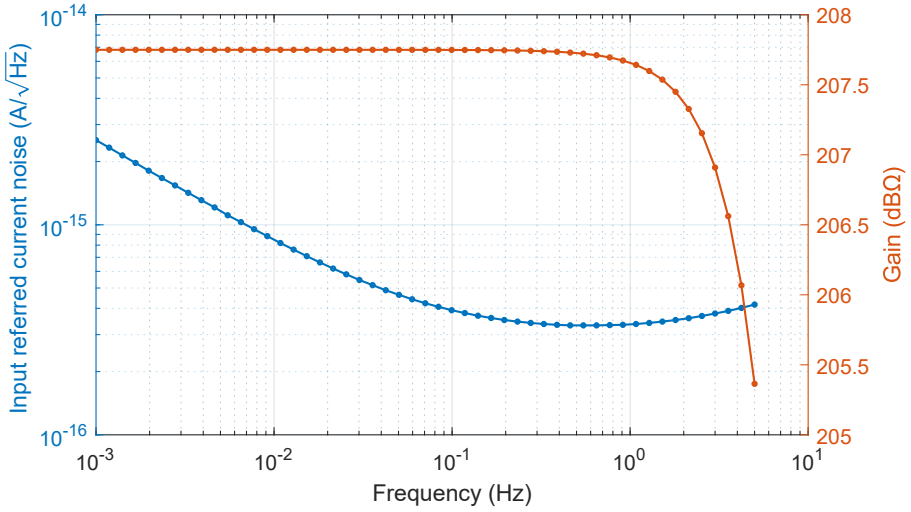


Figure 4.11.: Simulation results for the frequency response and noise profile of the leakage current sensing circuit. For this simulation the input currents under test were set to $i_{out} = 1\,\text{pA}$ and $i_{out} = 0$.

Table 4.2.: Specification table of the two-stage TIA circuit

Input current range	1-100 pA
I to V gain	207.75 dB Ω @ $f_S < 1$ Hz
Resolution	5 fA
Power consumption	4.76 µW @ 3 V supply

cycle [23].

The results from the simulations of the proposed circuit are reported in Figure 4.11, which shows the transfer function and the current noise spectrum. The main parameters of the circuit are summed up in Table 4.2. The integrated current noise in the band 1 mHz - 5 Hz is 4.4 fA, indicating that the circuit can achieve approximately 5 fA input current resolution. This however will need to be verified through testing, since the use of the seal ring as sensing terminal is an experimental technique, and its reliability requires proper evaluation.

4.3.2. Intra-layer diffusion

In this second case the focus is on sensing the moisture that diffuses within the oxide layers. If sustained for a sufficient amount of time, this phenomenon can also lead to SiO_2 dissolution [24]. The diffusion of moisture in the oxide does not guarantee the creation of a conductive channel metal traces, so sensing leakage currents like in the previous section would be very challenging. However, it causes a change in the permittivity of the silicon dioxide, that can be sensed with an impedance measurement, this time along the vertical direction. With reference to Figure 4.9, the objective is to compare the magnitude of the impedances $Z_{1\text{-}2,\text{out}}$ and $Z_{1\text{-}2,\text{in}}$, since we expect the diffusion starting from the edge of the

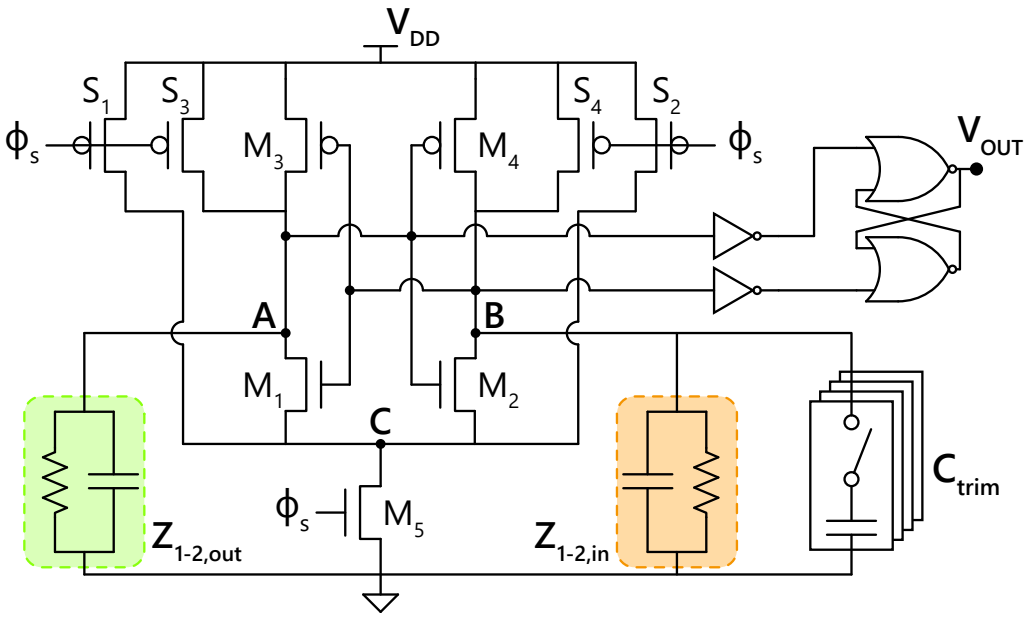


Figure 4.12.: Schematic of the circuit for sensing moisture diffusion in silicon dioxide by evaluating the impedance between metal tracks on different layers. The two highlighted components are the impedances under test.

CMOS die to first affect the impedance between the outer metal tracks before reaching the inner ones.

An estimate of the value of the impedances to be measured and their variation in presence of moisture is necessary prior to the design of the sensing circuit. The AMS 0.35 µm technology datasheet indicates the value of capacitance between tracks on contiguous metal layers to be in the range of 26 to 59 aF/µm^2. If metal tracks with a width of 0.5 µm are used to cover the perimeter of a 4 mm × 4 mm silicon die, this gives a total capacitance ranging from approximately 200 to 480 fF. An estimation of the capacitance variation due to the presence of water molecules is obtained using Looyenga's formula, similarly to the procedure used for polyimide detailed in subsection 3.3.2. The result in case of maximum water absorption shows an increase of approximately 25% in the value of SiO_2 permittivity, and therefore a similar increase in capacitance. This value remains a rough approximation and will need further experimental verification, but serves as an indicator of the required resolution for the sensing circuit, which is in the units of fF.

The proposed sensing circuit is shown in Figure 4.12. The goal of this circuit is not to characterise the impedances under test, but instead to sense the difference the difference in capacitance between the inner and the outer impedance. For this purpose, the proposed topology is a regenerative comparator based on the StrongARM latch described in [25], but instead of sensing a differential voltage, it is modified to sense the difference in the impedances seen on the two branches of the comparator.

The circuit operates in the following way: when signal ϕ_S is low, the four switches S_1 to S_4 charge nodes A, B and C to the supply voltage V_{DD}. Then ϕ_S is triggered to start

Table 4.3.: Specification table of the comparator

Minimum input capacitance	10 fF
Minimum detectable capacitance margin	3 fF
Power consumption	0.8 µW @ $f_{\phi_S} = 1$ kHz

the measurement phase, and node C is pulled to ground by transistor M_5, activating the comparator formed by the cross-coupled inverter pair consisting of transistors M_1, M_3 and M_2, M_4. The voltages at nodes A and B decrease towards $V_{DD} - V_{th,pmos}$, but they do so at different rates, with a pull-down strength that depends on mismatch and on the total capacitance seen at each node. Transistors M_3 and M_4 turn on, and the positive feedback of the comparator drives the node with the highest voltage, either A or B), to V_{DD} while the other is pulled to ground. At the end of the measurement phase, the node which has been pulled to V_{DD} is the one with the highest capacitance, indicating if $Z_{1\text{-}2,out} > Z_{1\text{-}2,in}$ or vice versa. To store the result of the evaluation while the comparator is reset and to get rid of commutation spikes, the outputs A and B are connected to a XOR based SR-latch.

In the ideal case where the impedances seen at node A and node B are the same, the output of the circuit would randomly switch at every measurement cycle between the states $V_A > V_B$ and $V_A < V_B$. In reality, the comparator noise and the mismatch in both drive strength and parasitics will cause one side to prevail, even in the case where $Z_{1\text{-}2,out} = {}_{1\text{-}2,in}$. To compensate for this, an array of switchable small value (< 10 fF) trimming capacitors is added on the reference side [26].

The main circuit specifications are reported in Table 4.3. High speed operation is not required for the desired application, and the circuit can be effectively run at very low frequency for power saving purposes, since power dissipation only occurs during the commutations of ϕ_S, while there is no static power consumption. The results from circuit simulations indicate that a stable output is obtained for a difference in capacitance seen at nodes A and B of $|C_A - C_B| > 3$ fF. This is the minimum difference between $Z_{1\text{-}2,out}$ and $Z_{1\text{-}2,in}$ that can be reliably detected by the comparator. This value corresponds approximately to a 1% variation in the capacitance of either of $Z_{1\text{-}2,out}$ or $Z_{1\text{-}2,in}$, and therefore the proposed circuit seems suitable to detect moisture diffusion in the SiO_2 layers, but *in vitro* experimental results are needed for a full validation.

The two circuits presented here could act not only as useful on-board diagnostic devices for commercial devices, but also as a novel research tool to better understand the mechanism of water ingress in active silicon-based packages. They have been designed for a reduced power consumption and allow for an integration into low-power implants. This work has created interest in the research community, as demonstrated by the published results that build upon the concepts proposed here [27].

4.4. Conclusions

In this chapter we have presented two approaches to study the issue of moisture penetration in silicon based implantable devices: one based on the use of test structures for accelerated life testing, the other using on chip instrumentation for a real time monitoring of encapsulation failure due to moisture ingress. Based on the presented devices and test results, we draw the following conclusions:

- Ageing tests of CMOS dies encapsulated in silicone have shown promising results for long-term applications, with no failures sensed by the IDC structures.
- When conducting such kind of experiments, the test setup is of prime importance, as its parasitic contributions can mask the desired results. It is also necessary to try to minimize the failures due to the test platform.
- The use of dedicated instrumentation circuits to monitor encapsulation can prove beneficial both in bench top applications and for on chip chronic testing.
- The results obtained in the long term tests and the use of on chip circuits to evaluate the integrity of silicon devices have proven to be relevant in the scientific community, which has been building upon them and expanding the results for a wider range of applications (not limited to neural implants) and a broader selection of materials, such as ALD coatings or platinum electrodes [28, 29].

Bibliography

[1] F. Mazza, Y. Liu, N. Donaldson, and T. G. Constandinou, "Integrated devices for micro-package integrity monitoring in mm-scale neural implants," in *2018 IEEE Biomedical Circuits and Systems Conference (BioCAS)*, pp. 1–4, IEEE, 2018.

[2] C. Lamont, F. Mazza, and N. Donaldson, "A bayesian demonstration of reliability for encapsulated implanted electronics," in *2019 9th International IEEE/EMBS Conference on Neural Engineering (NER)*, pp. 730–733, IEEE, 2019.

[3] X. Meng, Y.-C. Byun, H. S. Kim, J. S. Lee, A. T. Lucero, L. Cheng, and J. Kim, "Atomic layer deposition of silicon nitride thin films: a review of recent progress, challenges, and outlooks," *Materials*, vol. 9, no. 12, p. 1007, 2016.

[4] R. S. Bonilla, B. Hoex, P. Hamer, and P. R. Wilshaw, "Dielectric surface passivation for silicon solar cells: A review," *physica status solidi (a)*, vol. 214, no. 7, p. 1700293, 2017.

[5] A. Zonenberg, "Process overview: UMC 180nm eNVM," 2014 (accessed November 26, 2019). Available at `http://siliconexposed.blogspot.com/2014/02/process-overview-umc-180nm-envm.html`.

[6] F. Schindler-Saefkow, F. Rost, A. Otto, R. Pantou, R. Mroßko, B. Wunderle, B. Michel, S. Rzepka, and J. Keller, "Stress impact of moisture diffusion measured with the stress chip," *Microelectronics Reliability*, vol. 54, no. 6-7, pp. 1243–1252, 2014.

[7] D. Liu, J. Wang, R. Liu, and S. Park, "An examination on the direct concentration approach to simulating moisture diffusion in a multi-material system," *Microelectronics Reliability*, vol. 60, pp. 109–115, 2016.

[8] P. Mou, D. Xiang, and G. Duan, "Mathematical and simulation modelling of moisture diffusion mechanism during plastic IC packages disassembly," *Advances in Mechanical Engineering*, vol. 5, p. 928671, 2013.

[9] J. Troyk, R. Francovik, and J. Anderson, "Experimental techniques for electrical testing of microelectronics coatings," *IEEE transactions on components, hybrids, and manufacturing technology*, vol. 14, no. 2, pp. 428–435, 1991.

[10] J. Park and R. S. Lakes, *Biomaterials: an introduction*. Springer Science & Business Media, 2007.

[11] J. M. Wasikiewicz, D. Paul, N. Roohpour, J. Vaghela, M. F. Grahn, and P. Vadgama, "Isopropyl myristate modified silicone as a potential new encapsulating material for implantable devices," *Journal of Applied Polymer Science*, vol. 119, no. 5, pp. 2917–2924, 2011.

[12] X. Fan and J.-H. Zhao, "Moisture diffusion and integrated stress analysis in encapsulated microelectronics devices," in *2011 12th Intl. Conf. on Thermal, Mechanical & Multi-Physics Simulation and Experiments in Microelectronics and Microsystems*, pp. 1–8, IEEE, 2011.

[13] A. Inmann and D. Hodgins, *Implantable sensor systems for medical applications*. Elsevier, 2013.

[14] X. Zhong, L. Chen, B. Medgyes, Z. Zhang, S. Gao, and L. Jakab, "Electrochemical migration of sn and sn solder alloys: a review," *RSC advances*, vol. 7, no. 45, pp. 28186–28206, 2017.

[15] S. Bruck, "Leachable components in polymeric medical implants and disposables: a brief critical review.," *Medical progress through technology*, vol. 16, no. 3, pp. 131–143, 1990.

[16] N. Donaldson, C. Lamont, A. S. Idil, M. Mentink, and T. Perkins, "Apparatus to investigate the insulation impedance and accelerated life-testing of neural interfaces," *Journal of neural engineering*, vol. 15, no. 6, p. 066034, 2018.

[17] P. Yeon, M.-g. Kim, M. S. Bakir, O. Brand, and M. Ghovanloo, "Automated high-throughput hermetic failure monitoring system for millimeter-sized wireless implantable medical devices," in *2019 20th International Conference on Solid-State Sensors, Actuators and Microsystems & Eurosensors XXXIII (TRANSDUCERS & EUROSENSORS XXXIII)*, pp. 2235–2238, IEEE, 2019.

[18] Y. Gong, W. Liu, R. Wang, M. H. Brauer, K. Zheng, and W. Li, "Stability performance analysis of various packaging materials and coating strategies for chronic neural implants under accelerated, reactive aging tests," *Micromachines*, vol. 11, no. 9, p. 810, 2020.

[19] K. Nanbakhsh, M. Kluba, B. Pahl, F. Bourgeois, R. Dekker, W. Serdijn, and V. Giagka, "Effect of signals on the encapsulation performance of parylene coated platinum tracks for active medical implants," in *2019 41st Annual International Conference of the IEEE Engineering in Medicine and Biology Society (EMBC)*, pp. 3840–3844, IEEE, 2019.

[20] K. Roy, S. Mukhopadhyay, and H. Mahmoodi-Meimand, "Leakage current mechanisms and leakage reduction techniques in deep-submicrometer cmos circuits," *Proceedings of the IEEE*, vol. 91, no. 2, pp. 305–327, 2003.

[21] M. Crescentini, M. Bennati, M. Carminati, and M. Tartagni, "Noise limits of cmos current interfaces for biosensors: A review," *IEEE transactions on biomedical circuits and systems*, vol. 8, no. 2, pp. 278–292, 2013.

[22] M. Akbari, S. Biabanifard, and S. Asadi, "Input referred noise reduction technique for trans-conductance amplifiers," *Electrical and Computer Engineering: An International Journal (ECIJ)*, vol. 4, no. 4, pp. 11–22, 2015.

[23] D. Kim, B. Goldstein, W. Tang, F. J. Sigworth, and E. Culurciello, "Noise analysis and performance comparison of low current measurement systems for biomedical applications," *IEEE transactions on biomedical circuits and systems*, vol. 7, no. 1, pp. 52–62, 2012.

[24] M. Schuettler and T. Stieglitz, "Microassembly and micropackaging of implantable systems," in *Implantable Sensor Systems for Medical Applications*, pp. 108–149, Elsevier, 2013.

[25] B. Razavi, "The StrongARM latch - a circuit for all seasons," *IEEE Solid-State Circuits Magazine*, vol. 7, no. 2, pp. 12–17, 2015.

[26] A. Abidi and H. Xu, "Understanding the regenerative comparator circuit," in *Proceedings of the IEEE 2014 Custom Integrated Circuits Conference*, pp. 1–8, IEEE, 2014.

[27] O. C. Akgun, K. Nanbakhsh, V. Giagka, and W. A. Serdijn, "A chip integrity monitor for evaluating long-term encapsulation performance within active flexible implants," in *2019 IEEE Biomedical Circuits and Systems Conference (BioCAS)*, pp. 1–4, IEEE, 2019.

[28] K. Nanbakhsh, R. Ritasalo, W. A. Serdijn, and V. Giagka, "Long-term encapsulation of platinum metallization using a hfo 2 ald-pdms bilayer for non-hermetic active implants," in *2020 IEEE 70th Electronic Components and Technology Conference (ECTC)*, pp. 467–472, IEEE, 2020.

[29] O. C. Akgun, K. Nanbakhsh, V. Giagka, and W. A. Serdijn, "A chip integrity monitor for evaluating moisture/ion ingress in mm-sized single-chip implants," *IEEE Transactions on Biomedical Circuits and Systems*, vol. 14, no. 4, pp. 658–670, 2020.

5. Design of a Microwire-based Mm-scale Cortical Recording Implant

The previous two chapters of this thesis have focused on devices and instrumentation circuits dedicated to the assessment of long term integrity of implantable devices. Building upon that, we propose a fabrication strategy for a chronic millimetre-sized cortical implant, developed within the scope of the ENGINI project first described in chapter 2.

The design choices presented here tackle the fabrication, encapsulation, feedthroughs, and assembly method of a full subdural probe, while the work towards the realization of the dedicated neural recording circuitry as well as the power and data transmission strategy has been the subject of investigation of other doctoral research [3, 4].

This chapter first provides a few considerations regarding the materials used for the encapsulation of implantable devices and the strategies currently used to fabricate microwire-based implants. Based on such considerations, it presents the design of two generations of probes for cortical recording based on the ENGINI architecture, pictured in Figure 5.1.

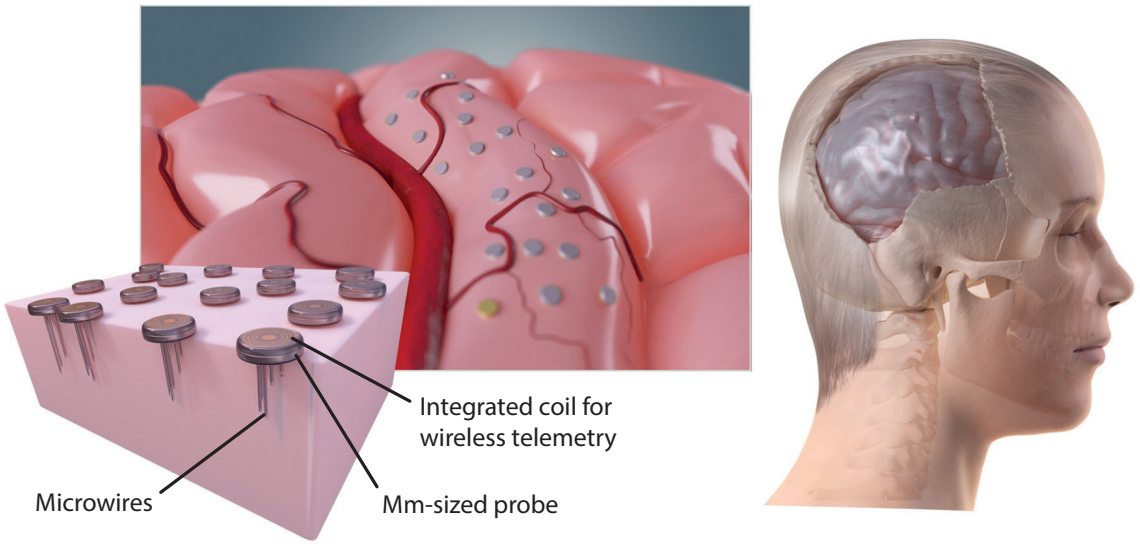


Figure 5.1.: Illustration of the mm-sized ENGINI probes implanted in the motor cortex.

A portion of the material presented in this chapter has been published in [1, 2]. The work presented in section 5.2 has been part of a collaborative research with Ms Katarzyna Szostak, who developed the initial concept and carried out most of the fabrication steps for the first version of the ENGINI neural probe.

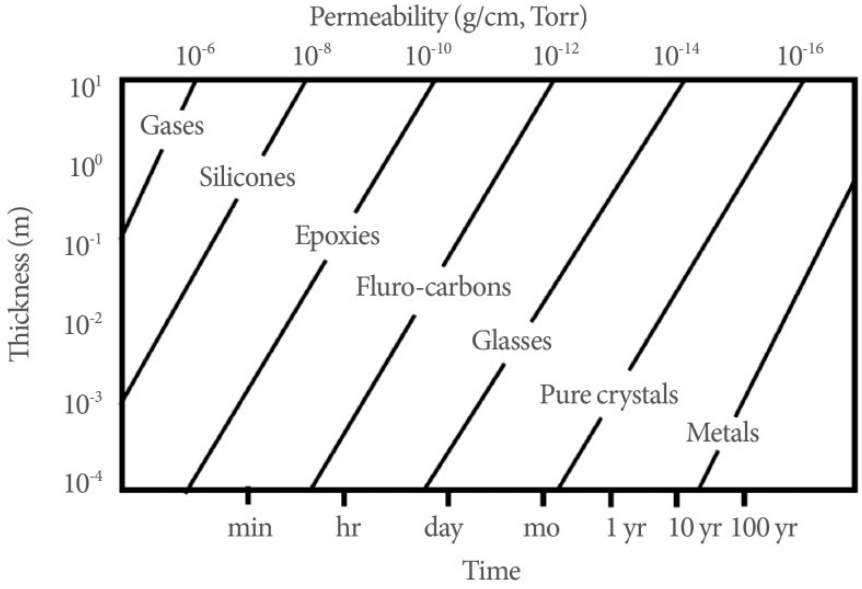


Figure 5.2.: Permeability to helium gas of different materials used for medical devices, as a function of thickness and time [5].

5.1. Materials for implantable devices

The process of designing an implantable device must strike the right balance between being effective in its desired interaction with the surrounding tissue, while at the same time cause minimal disruption to the body's environment. As mentioned in chapter 2, the degree of invasiveness of an implanted device has to be kept to a minimum, to reduce as much as possible the effects of the inevitable onset of FBR, which causes the affected tissue to encapsulate the implant with layers of scar tissue, thus progressively impairing its efficacy.

One of the major features that influences bio-compatibility and overall long term bio-stability is the choice of materials used for the packaging of the implant. These materials are in charge of protecting the electronics inside the device, as well as reducing tissue damage. This can be achieved for example by using external coatings that are mechanically compliant with the tissue and that can help in reducing mismatch and minimising the damages caused by relative motion [6].

The importance of package hermeticity, highlighted in previous chapters, also has crucial impact on material choice. As reported in Figure 5.2, each class of materials has an associated gas permeability which has an impact on their capabilities to survive for long periods of time in an environment like the human body. The best chronic performances belong to metals, which are the most common choice of packaging for IMDs. Metal enclosures provide a very high level of protection to the electronics and are chemically inert. However, they present some limitations for the specific use we are targeting: they do not allow for inductive or optical wireless power transfer and telemetry, and they usually

require welding or brazing techniques to create hermetic packages, which are technologies that do not scale easily to the sub-millimetre scale.

Bio-grade ceramics and glasses are also common in medical implants. Like metals, they still provide good hermeticity, but at the same time they are electrically insulating. This makes them the class of materials of choice for feedthrough connectors, as they allow metal conductors to run through them. They also do not shield from inductive wireless communication and, if the material is transparent to the desired range of frequencies, also optical communication can be achieved [7].

Polymer encapsulation is largely used with implants for acute applications. As discussed in chapter 4, polymer coatings are easy to apply and can be conveniently moulded [8], however they have the highest permeability when compared to the previously mentioned materials, they suffer from water diffusion and do not provide an hermetic barrier against moisture, due to their intrinsic porous nature.

The choice of packaging materials and fabrication method plays a significant role in device reliability, even more so in the case of miniaturized distributed interfaces, where there is the need to produce many identical implants with a high yield.

5.1.1. Microwire-based feedthrough connections

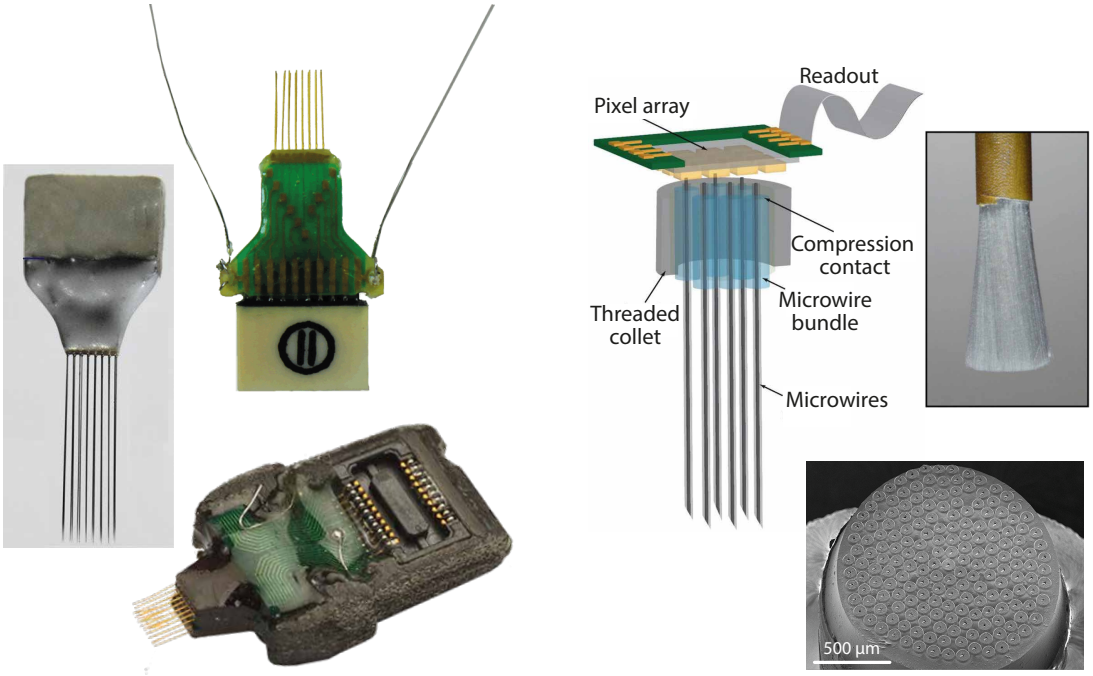
Neural implants for cortical recording based on microwires have shown the best chronic performances regarding signal quality over time [9]. However, the connection of microwires with CMOS electronics on an integrated platform has proven challenging.

Feedthrough connections have the key task of transporting signals recorded from the tissue to the electronics in charge of processing (or vice versa in case of stimulating devices). In order to achieve this, they need to cross the hermetic barrier of the implant without impairing its efficacy. This makes the fabrication of feedthroughs in implantable devices a complex design challenge.

In most commercial IMDs, such as the ones presented in section 2.1, feedthrough connectors are realized using insulating materials with embedded electrical contacts. To ensure a stable connection, spring contacts are used. However, this configuration does not scale easily to millimetre-sized devices, and new solutions are required when connecting to microwires that are a few tens of microns in diameter.

Most microwire based solutions rely on attaching the wires to a passive connector, either via soldering or wire bonding, and then securing them in place with epoxy resin or other glues (see Figure 5.3a). The connectors used are extremely bulky, and usually do not host any active elements, but are simply wired to external recording electronics. Also the assembly process is still very laborious, and the time required for fabrication scales linearly with the desired number of channels, and therefore of microwires.

To overcome this limitations new architectures have been proposed, like the example reported in Figure 5.3b. Here thousands of microwires are bundled together, and then one of the extremities of such bundle is pushed towards a two-dimensional array of sensing



(a) (b)

Figure 5.3.: Examples of microwire-based implants for neural recording: (a) Three commercial devices for research applications (from Tucker-Davis Technologies and Clunbury Scientific LLC). Note the the size of the connectors and the epoxy encapsulation; (b) Microwire array design proposed by Paradromics [10], based on a camera sensor array coupled with a bundle of microwires.

pixels [10]. By doing so, most of the microwires will make contact with one of the pixels, and be able to operate correctly. The contact is formed only by compression of the wires against the IC, and is then secured with the use of epoxy. This approach however is practical only for very large bundles of microwires, which in turn neutralize the benefits of using thin wires to minimize tissue damage.

Microwire arrays also require a dedicated insertion method, in order to avoid bending the thin wires and minimize tissue dimpling. The material of the microwires plays an important role in this, with metals such as tungsten being more stiff than other solutions using platinum or niobium. The difficulty of insertion of softer wires however is compensated by their better tissue integration [11].

It is important to note that the design requirements of a neural implant can vary depending on its function, in particular if it is a recording or a stimulating device. The insulation requirements for the interconnections of recording implants can generally be less stringent that the ones for stimulating devices. This is due to the fact that a deterioration in the insulation of the recording electrodes would cause signal degradation but without harmful consequences for the tissue. On the contrary, in a stimulating device this might cause current leakage, with an excessive, and potentially dangerous amount charge being delivered to the tissue.

5.2. First generation ENGINI probe design

Given the considerations made in the previous section, we approached the design of the first practical iteration of the microwire-based implantable probe, developed as a *proof of concept* for the ENGINI project. Summarizing the requirements, the design should feature: (i) minimum overall size of the implant; (ii) hermeticity of the section hosting the electronics, for chronic operation; (iii) use of microwires for cortical recording; (iv) compatibility with inductive power and data transfer [2]. A further objective is to utilize a fabrication process that can be easily scaled for the simultaneous production of multiple probes, reducing the possibilities of failures during manufacturing and assembly.

The design of the first version of the probe is reported in Figure 5.4. It is composed of three main parts: the CMOS die containing the active electronic circuits; a passive silicon interposer with metal connections acting as a redistribution layer (RDL) to interface the CMOS with the microwires; a glass module to mechanically secure the microwires in place and reinforce the overall probe.

The silicon interposer has four holes patterned with deep reactive-ion etching (DRIE), one in every corner. The use of DRIE allows for the creation of high aspect ratio structures, achieving a hole diameter of approximately 50 µm through a 350 µm thick silicon substrate. The inside of these holes is then metallized with Au/Cu, and a metal trace is patterned on the top surface of the silicon to connect each hole to a corresponding bond pad in the centre of the interposer, where the CMOS IC will be attached using eutectic bonding to provide a hermetic seal around the active electronics. The connection with the microwires is performed as follows (see Figure 5.5): the wires are inserted in the holes of the interposer,

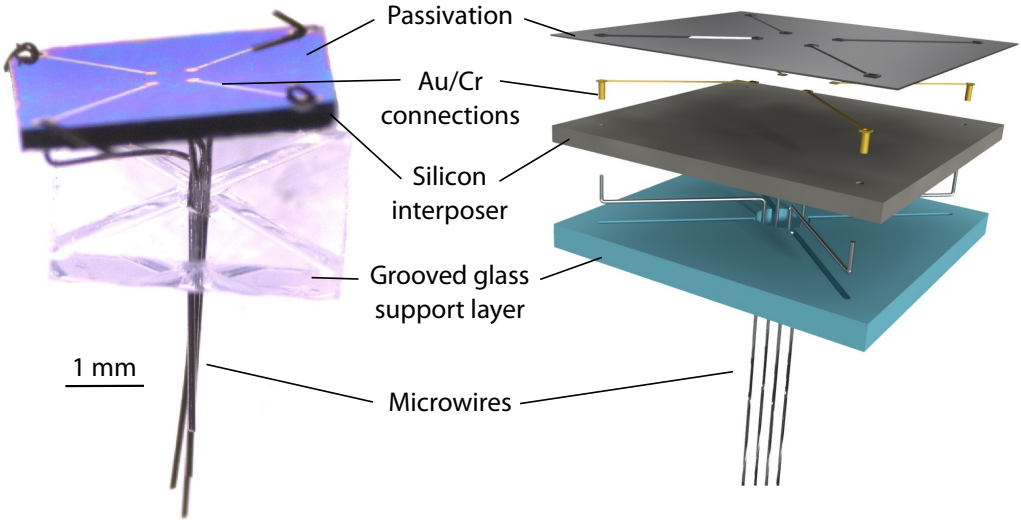


Figure 5.4.: Concept and prototype of the passive section of the first version of ENGINI neural probe. The CMOS IC, not depicted here, is bonded in the middle of the silicon interposer to make contact with the metal tracks that connect to the microwires.

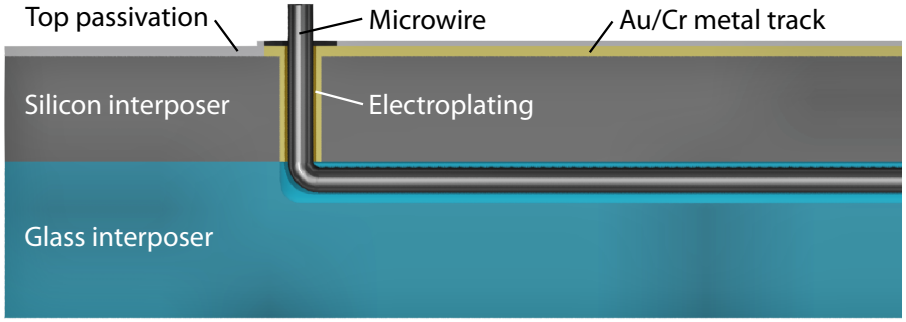


Figure 5.5.: Detail of the microwire attachment to the silicon interposer using electroplating, and glass module to support the wire.

and kept in place by slightly bending their top end. Electroplating is then used to deposit gold in order to fill the space between the surface of the plated holes and the microwire. This forms an electrical and mechanical contact between the wires and the metal traces. To provide more support to the wires, the glass layer is added. It has the same area of the silicon interposer, and contains four grooves to host the microwires. These grooves are made using a dicing saw without cutting all the way through the glass. The glass layer is finally attached to the interposer using anodic bonding.

Overall, the probe head measures $4 \times 4\,\mathrm{mm}^2$. The dimensions have been kept to a minimum, while still providing the necessary space for the electronics and the coil necessary for the inductive link. Smaller probes have been proposed [12, 13], but with very reduced data processing capabilities. Moreover, in our design the head of the probe sits on top of the brain cortex, while only the microwires are penetrating, thus causing minimum tissue displacement.

Being a first prototype of the probe, a few issues were encountered during the fabrication process. The initial operations on the silicon interposer, such as patterning the metal traces and shaping the holes with DRIE, proved to be successful with a high yield, which was expected since these processes rely on the use of well established semiconductor manufacturing techniques and equipment. However, the subsequent electroplating step to fix the microwires in place inside the DRIE holes proved to be particularly challenging. In order to attain manageable plating times and good uniformity, the diameter of the hole in the silicon interposer had to match as much as possible the one of the microwire to be inserted, making the manual threading process of the wires extremely laborious. Moreover, the gold contained in the plating solution infiltrated and lifted off the passivation layer protecting the metal traces on the interposer (see Figure 5.6). Handling the microwires before and after insertion was not practical, and it proved beneficial to pre-bend them in shape, to avoid excessive manipulation once they were in place. The realization of the glass interposer also presented some issues. While the use of glass for micropackages is well established, it usually requires specific equipment when realizing features below the millimetre scale, such as laser micro-manufacturing. The use of a wafer dicing saw to cut

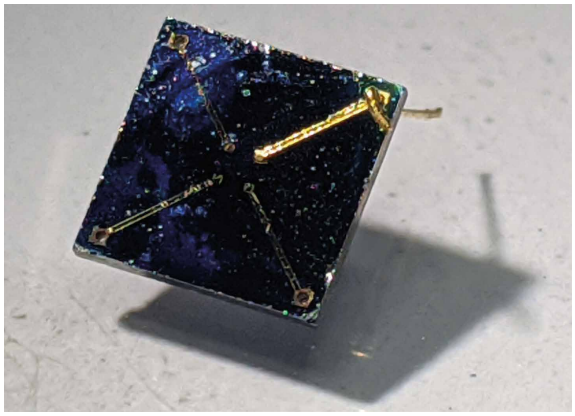


Figure 5.6.: Passivation lift-off and excessive trace metallization during the electroplating process to attach the microwire to the silicon interposer in the first version of the neural probe.

grooves in the glass, although useful for prototyping, wasn't fully suitable for the brittle glass, and accuracy in groove width and placement was hard to achieve consistently. Assembling the two interposers together with the microwires in between resulted in further complications. The uneven surface of the glass after the grooves were manufactured did not provide good adhesion with the silicon interposer. Moreover, the resistance to deformation of the microwires tended to act as a spring when joining the glass and the silicon interposers, worsening the contact between the two and finally jeopardizing the success of the anodic bonding.

The prototype fabrication has shown the advantages and limitations of this first iteration of the design. We were not able to produce a fully testable probe using this architecture, but its construction provided very useful insight to be considered for future iterations.

Pros

- The overall size can be kept to the desired specifications of $4 \times 4\,\mathrm{mm}^2$, which is a *state of the art* result for a neural probe with such processing capabilities.
- The microwires are mechanically secure thanks to the combination of silicon interposer and glass module, together with their double bend.
- The whole fabrication process can be performed *in house* in the cleanroom of the Centre for Bio-Inspired Technology, providing a cost effective solution.

Cons

- The hermeticity of the active circuits is entirely given by the eutectic seal around the CMOS die. The realization of this seal has proven challenging, with low repeatability.
- The assembly of the microwires (bending and threading through the interposer holes) is completely manual and particularly time consuming.

- The microwire attachment to the interposer by electroplating has proven problematic and unreliable.
- All of the assembly process is carried out at die level, giving a lower repeatability and proving difficult to automate.

5.3. Second generation ENGINI probe design

Building upon the lessons learned from the fabrication of the first design iteration, we propose a new concept for the second version of the ENGINI neural recording probe. Apart from the geometrical differences, also the materials used for encapsulation have been revised, to allow for a higher level of hermeticity and therefore chronic reliability.

The main idea of the proposed design is to separate the whole probe into two components: one is a hermetic micro-package that houses the active electronics and the transmission coil, while the other is a module to support the connection to the microwire electrodes. The new proposed round shape avoids sharp edges in contact with the tissue. The full glass architecture takes advantage of glass micro-manufacturing techniques, including glass 3D structuring and glass-to-glass laser welding, which have demonstrated excellent capabilities and high repeatability [14, 15]. Figure 5.7 is used as a reference for the following description of the individual parts.

5.3.1. Hermetic micro-package

The top portion of the implant is a micro-package that hosts the CMOS die and the gold antenna for power and data telemetry. It is composed of a flat interposer and a cap. These two parts are fabricated out of glass, which is bio-compatible, has a higher quality surface compared to silicon and allows for the use of glass-to-glass femto-second laser welding. This is a sealing process that can produce highly hermetic packages, while keeping a seal width of few tens of micrometers. Also the use of extremely short laser pulses to locally weld the two glass parts together causes minimal thermal stress to the surrounding components, and can be performed in the vicinity of CMOS dies [16]. The interposer has metallised through-glass-vias (TGVs) to allow for the electrical connection between the IC and the microwires. The metal deposition process for the creation of the bonding pads on the interposer can be used to simultaneously deposit the coil for the wireless transmission. This allows the deposition of a thicker coil compared to the on-chip one used in the first design concept, enhancing inductive coupling and efficiency. The enhancement is incremented by the use of a glass substrate, since it has lower dielectric losses compared to silicon. The IC is then flip-chip bonded to the interposer to establish connections with both the TGVs and the coil. Finally, the glass cap is bonded to the interposer with the previously mentioned laser welding technique to form the hermetic cavity protecting the electronics.

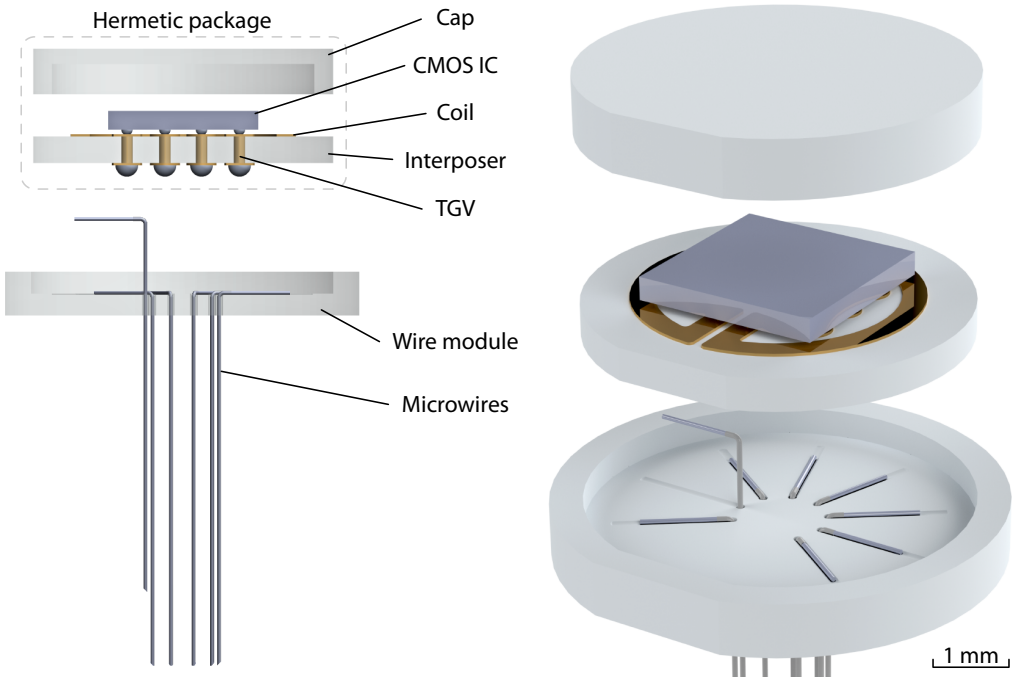


Figure 5.7.: Cross-section and exploded view rendering of the proposed neural implant design. Note the funcitonal separation between the hermetic package and the wire module.

5.3.2. Wire module

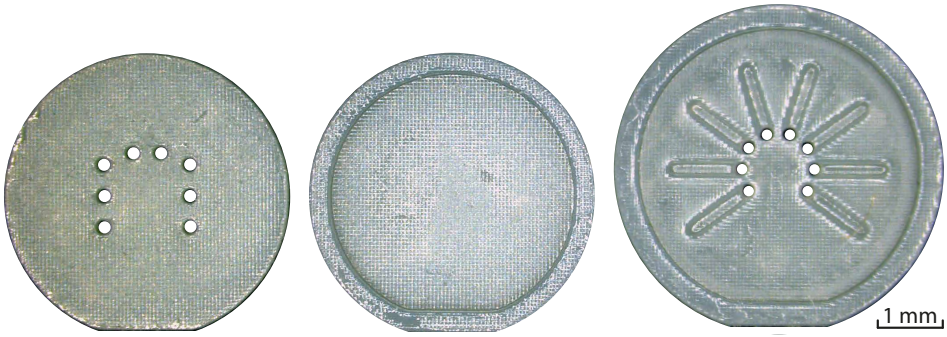
The proposed design builds upon the previous concept of using a glass layer to mechanically support the microwires. The module consists of a single piece of micro-structured glass. The total diameter of the part is slightly larger than the one of the hermetic module, to accommodate it with precise alignment, thanks to the presence of alignment flats on the side of all three glass components. The wire module has eight central holes (one for each microwire) and from every one of this holes, a horizontal micro-channel, shallower than the microwire diameter, spreads radially from the centre, and acts as a guide for the wire. During the assembly process, the microwires are threaded through the holes and then bent into these channels. The creation of this L-shaped bend provides additional mechanical resistance to the wires being pulled out, while at the same time keeping the wire in place before the final assembly steps. The insulation of the microwires has to be removed in the bent section, to allow for the electrical contact with the hermetic package's bond pads.

5.3.3. Prototype fabrication

The fabrication of the glass parts was tested using a Rofin LFS laser cutting system on a borosilicate glass substrate. Although we were able to produce some samples of the glass interposer (see Figure 5.8), the resolution of the laser workstation was unfortunately not sufficient to produce 3D structured parts with sharp edges, like the cap and the wire



Figure 5.8.: Borosilicate glass sample of the interposer with TGVs, fabricated using a Rofin LFS laser workstation.



(a) (b) (c)

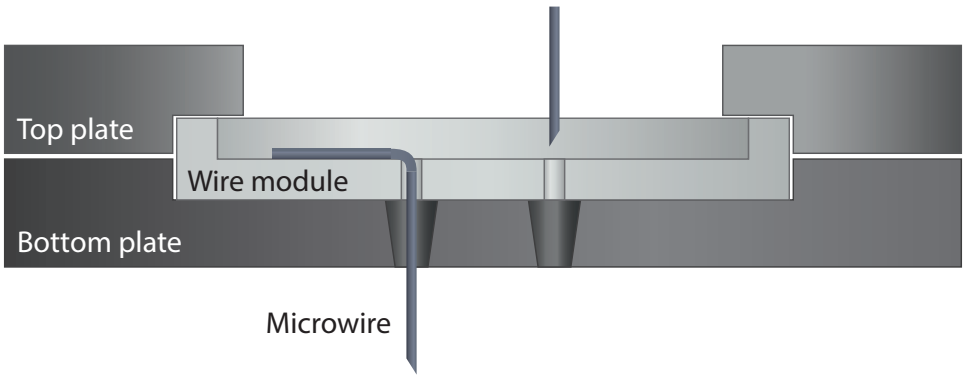
Figure 5.9.: Prototypes of the three implant components manufactured form plastic resin using 3D printing: (a) interposer, (b) cap, (c) wire module. Comparing the interposer (a) with the similar part fabricated in glass shown in Figure 5.8, it is possible to notice the higher feature resolution obtained with the 3D printing process, which is able to produce smaller and closer via holes.

module. A laser micromachining system with a smaller laser spot size should be able to achieve higher aspect ratio structures, with better defined edges.

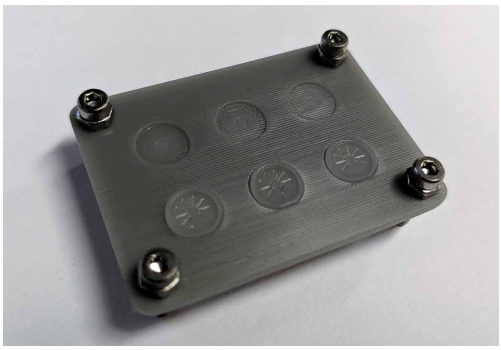
Nevertheless, to validate the design of the probe the parts have been fabricated to scale using 3D printing on the Figure 4 printer by 3D Systems. This gives us the opportunity to evaluate handling of the parts and the assembly method, even though the materials are not the same as the initial design. The printed parts are presented in Figure 5.9.

5.3.4. Prototype assembly

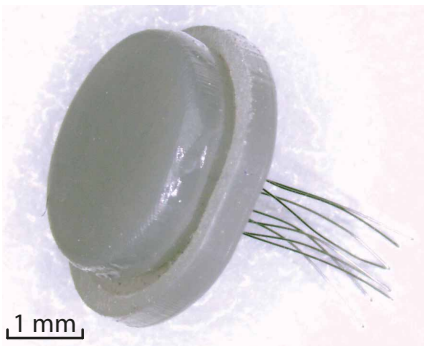
Once the various parts have been fabricated, the assembly consist of inserting the microwires in the corresponding holes and bringing the two parts of the probe together. As noticed during the assembly of version 1 of the ENGINI probe, threading the microwires is usually the most laborious task when assembling such devices. To help facilitate this process, a dedicated support has been designed (see Figure 5.10a) and fabricated using the same high resolution 3D printing process already employed for the implant prototype. It consists of a bottom mounting plate with a recess in the same shape of the wire module, and with similarly aligned through holes. The microwire module is then placed in its



(a)



(b)



(c)

Figure 5.10.: Assembly platform of the 3D printed probe prototype: (a) Diagram of the platform for microwire insertion. Only one microwire module is depicted, but the top and bottom plates are designed to hold several modules at the same time, as shown in the next figure; (b) Platform for microwire insertion. Note the three microwire modules inserted into their respective slots, and the M2 screws for height adjustment (the top plate is absent to make the microwire modules visible); (c) Fully assembled plastic prototype of the probe.

housing, and a top mounting plate holds it firmly in place by clasping its sides. This is necessary since the individual wire modules are extremely light and can move around very easily during the assembly. The threading of the microwires can now be carried out with a very stable support. The microwires are inserted in the wire module from the top, and threaded all the way through the bottom plate. This operation was initially accomplished by hand, but it might be improved and sped up in the future with the use of a fine placer for automatically feeding the microwires with very high positional accuracy. After the wires are inserted in their respective vias, they are cut and bent into their corresponding micro-channel, as explained in the previous section. As a guide to simplify the process, the thickness of the top mounting plate is chosen to correspond to the height at which the microwire is cut. A further adjustment is provided by four screws at the corners of the mounting plates. Aside from firmly securing the top and bottom plate together, they set the height of the whole assembly jig from the support surface, thus adjusting the length

of the microwires exposed under the implant to the desired measure.

At this point, the last step is to align and insert the hermetic package in the wire module, so that the solder bumps of the former make contact with the bent portion of each microwire. A drop of glue or epoxy resin in the middle of the wire module can help in securing the assembly (see Figure 5.10c). Once finished, the probe can be dip-coated in a bio-compatible polymer, such as PDMS or Parylene-C, as an extra layer of encapsulation. This will also make the outside of the probe softer and more compliant with the tissue.

5.3.5. Design outcomes

The design concept presented here improves on the previous iteration by separating the two main modules that compose the probe. This is a unique feature that introduces the following benefits:

- it allows to have two separate fabrication processes, specifically tailored to each part's requirements. The head part has strict hermeticity constraints, but since its fabrication is conceptually similar to a generic glass-packaged MEMS, it can therefore profit from a more streamlined, high yield production method. For example, this part can be fully fabricated at wafer level, from TGVs creation to pads and coil metallization, IC bonding and final cap glass laser welding. The same laser micromachining workstation that performs the welding can be used to then dice the wafer into individual devices. On the other hand, the wire module does not demand the same level of exactitude, and can be more easily produced *in house*.

- it makes the probe more versatile. It is in fact possible to use the same top part and fit it to different wire modules. This gives the possibility of experimenting with various microwire arrangements, materials, diameters, and coatings. Also, by eliminating the requirement on the matching between via holes and microwire diameter, it greatly simplifies the threading process.

- it increases the production yield, by splitting the fabrication process into two parallel procedures. In case of failure of one of the two parts during one of the production steps, the whole probe does not have to be discarded. Also, the hermetic package is fully testable as a standalone device by probing the contacts under it, to allow for the validation of the electronics before the complete assembly.

Moreover, the design of the probe has been carried out keeping in mind the ease of implantation, and it is compatible with the syringe-like insertion device specifically developed by Mr Matthew Cavuto [17]. This device allows for a smooth insertion of the microwires in the cortex while preventing their buckling, which would otherwise occur because of the pressure excerpted during insertion and the elasticity of the brain tissue.

While the mentioned advantages show the promising potential of the device, it is worth noting that the design of this prototype is not definitive and would require validation through both *in vitro* accelerated life tests and *in vivo* experiments.

Also, the fabrication process of the probe takes advantage of glass micro-manufacturing, which can produce very high quality devices, but it is not a widespread manufacturing method and requires expensive equipment, requiring high initial costs even at the prototyping phase. Even though the price per unit would scale down with the growing amount of implants produced, this type of manufacturing currently cannot compete with the highly parallel processes of semiconductor production.

A further point of optimization is in the assembly process of the probes. Although a significant improvement in the time required for the assembly has been achieved compared to version 1 of the implant, it is still based on a manual operation. The transition to a fully automatic assembly will therefore require some modifications in the platforms and tools described in subsection 5.3.4.

It is important to underline that the ENGINI project is an ongoing endeavor, and multiple solutions for the realization of the implantable probe are being considered. Aside from the glass concept proposed here, another modular approach using a cofired ceramic base plate with embedded metal tracks is in development. This approach also takes advantage over other techniques currently under investigation, like the gold to gold thermocompression bonding between gold stud contacts on different substrate materials, such as silicon and ceramic.

All of the above considerations underline the final objective of delivering an effective next generation neural recording interface which might in the future be translated into an approved medical device.

5.4. Conclusions

In this chapter we have described the design process of a millimetre-scale cortical neural implant. The choices of materials and device form-factor have been justified in regards to the desired application of the implant within the scope of the ENGINI project.

A first version of the implant was realized to act as proof of concept, and it allowed us to understand the most critical phases of the implant fabrication and assembly. In particular the handling of the microwires and their integration within a silicon die has proven particularly challenging, as well as bonding together the various parts that form the implant in a reliable and time efficient process.

The second version of the probe's design was built upon the experience of the previous iteration. Although still in its early prototype stage, this second design provided significant improvements, and brought us to the following considerations:

- It has proven beneficial to divide, whenever possible, the fabrication process in independent, parallel tasks. This can be achieved with a modular design, and it allows

for a quicker fabrication time and a reduced chance of damaging the limited CMOS dies. It also allows for experimenting with different microwire lengths, diameters, and materials, thus proving to be a useful research tool.

- The design of the device must go together with the design of the required tools for a streamlined device assembly. Only by doing this it is possible to optimize otherwise laborious tasks like manual microwire threading. The overall fabrication yield greatly benefits from the use of dedicated assembly jigs and tools.

While providing us with the mentioned insights, the second version of the probe is not a final design. Here are the main points of improvement that have been identified with the benefit of hindsight:

- The construction and assembly of the probe still require a considerable amount of operations performed by hand, mostly concerning the handling of the microwires. A possible strategy to investigate would be to partially embed the eight microwires of each probe into a flexible substrate, to keep them together during assembly. Such substrate could be engineered to be soluble once the fabrication is complete, or could even be exploited to deliver medications at the implantation site.

- The assembly platform proposed here, although partially scalable, is suitable for small numbers of devices to be produced at the same time. The need for a higher number of units would require a rethinking of such platform, which should also consider the use of automated processes. A first step in this direction that could have been implemented in the current platform would have been the use of self aligning features and marks in the two plates of Figure 5.10a.

- The suggested use of advanced glass micro-manufacturing techniques, while allowing for highly hermetic devices, could not be performed *in house* while at the same time outsourcing the fabrication of the glass parts was difficult because of the high tooling costs. A technology like 3D laser micro-structuring of glass requires dedicated equipment, and its use can become more affordable when producing a high number of samples, but not for initial prototyping.

Bibliography

[1] K. M. Szostak, F. Mazza, M. Maslik, L. B. Leene, P. Feng, and T. G. Constandinou, "Microwire-cmos integration of mm-scale neural probes for chronic local field potential recording," in *2017 IEEE Biomedical Circuits and Systems Conference (BioCAS)*, pp. 1–4, IEEE, 2017.

[2] N. Ahmadi, M. L. Cavuto, P. Feng, L. B. Leene, M. Maslik, F. Mazza, O. Savolainen, K. M. Szostak, C.-S. Bouganis, J. Ekanayake, *et al.*, "Towards a distributed, chronically-implantable neural interface," in *2019 9th International IEEE/EMBS Conference on Neural Engineering (NER)*, pp. 719–724, IEEE, 2019.

[3] L. B. Leene, M. Maslik, P. Feng, K. M. Szostak, F. Mazza, and T. G. Constandinou, "Autonomous soc for neural local field potential recording in mm-scale wireless implants," in *2018 IEEE International Symposium on Circuits and Systems (ISCAS)*, pp. 1–5, IEEE, 2018.

[4] P. Feng, M. Maslik, and T. G. Constandinou, "Em-lens enhanced power transfer and multi-node data transmission for implantable medical devices," in *2019 IEEE Biomedical Circuits and Systems Conference (BioCAS)*, pp. 1–4, IEEE, 2019.

[5] Y.-H. Joung, "Development of implantable medical devices: from an engineering perspective," *International neurourology journal*, vol. 17, no. 3, p. 98, 2013.

[6] J. H. Lee, H. Kim, J. H. Kim, and S.-H. Lee, "Soft implantable microelectrodes for future medicine: prosthetics, neural signal recording and neuromodulation," *Lab on a Chip*, vol. 16, no. 6, pp. 959–976, 2016. [Online].

[7] G. Jiang and D. D. Zhou, "Technology advances and challenges in hermetic packaging for implantable medical devices," in *Implantable Neural Prostheses 2*, pp. 27–61, Springer, 2009.

[8] K. M. Szostak, L. Grand, and T. G. Constandinou, "Neural interfaces for intracortical recording: Requirements, fabrication methods, and characteristics," *Frontiers in Neuroscience*, vol. 11, p. 665, 2017.

[9] A. Jackson and J. B. Zimmermann, "Neural interfaces for the brain and spinal cord—restoring motor function," *Nature Reviews Neurology*, vol. 8, no. 12, p. 690, 2012.

[10] A. M. Obaid, M.-E. S. Hanna, Y.-W. Wu, M. Kollo, R. R. Racz, M. R. Angle, J. Muller, N. Brackbill, W. Wray, F. Franke, *et al.*, "Massively parallel microwire arrays integrated with cmos chips for neural recording," *bioRxiv*, p. 573295, 2019.

[11] Z. J. Du, C. L. Kolarcik, T. D. Kozai, S. D. Luebben, S. A. Sapp, X. S. Zheng, J. A. Nabity, and X. T. Cui, "Ultrasoft microwire neural electrodes improve chronic tissue integration," *Acta biomaterialia*, vol. 53, pp. 46–58, 2017.

[12] D. Seo, J. M. Carmena, J. M. Rabaey, E. Alon, and M. M. Maharbiz, "Neural dust: An ultrasonic, low power solution for chronic brain-machine interfaces," *arXiv preprint arXiv:1307.2196*, 2013.

[13] P. Yeon, S. A. Mirbozorgi, B. Ash, H. Eckhardt, and M. Ghovanloo, "Fabrication and microassembly of a mm-sized floating probe for a distributed wireless neural interface," *Micromachines*, vol. 7, no. 9, p. 154, 2016.

[14] M. Masuda, K. Sugioka, Y. Cheng, N. Aoki, M. Kawachi, K. Shihoyama, K. Toyoda, H. Helvajian, and K. Midorikawa, "3-d microstructuring inside photosensitive glass by femtosecond laser excitation," *Applied Physics A*, vol. 76, no. 5, pp. 857–860, 2003.

[15] I. Miyamoto, A. Horn, J. Gottmann, D. Wortmann, and F. Yoshino, "Fusion welding of glass using femtosecond laser pulses with high-repetition rates," *J. Laser Micro/Nanoeng*, vol. 2, no. 1, pp. 57–63, 2007.

[16] S. Richter, S. Nolte, and A. Tünnermann, "Ultrashort pulse laser welding-a new approach for high-stability bonding of different glasses," *Physics Procedia*, vol. 39, pp. 556–562, 2012.

[17] M. L. Cavuto and T. G. Constandinou, "Investigation of insertion method to achieve chronic recording stability of a semi-rigid implantable neural probe," in *2019 9th International IEEE/EMBS Conference on Neural Engineering (NER)*, pp. 665–669, IEEE, 2019.

6. Conclusion

Understanding the human brain and unravelling its mechanisms is one of the greatest unsolved challenges of our time. Despite the vast amount of research dedicated to the endeavor, the mysterious nature of our brain still eludes us. The technological revolution we are witnessing seems to finally provide the instruments necessary to unlock the profound secrets of the brain.

The challenges are many and distributed across multiple domains: from medicine and biology for the study of tissue and cell behaviour, to hardware design to build the required system for interfacing the neurons with the electronics, to software and signal processing to decode and interpret efficiently the acquired signals.

However, the issue that seem to mostly stand in the way of the research efforts on their transition to become established medical devices, is given by the chronic degradation of the performances of implants. Even worse, the higher the required resolution is, for example to decode complex motor tasks, the more such degradation manifests itself early on.

This work tackles the aspect of cronicity, both from an investigative point of view, providing instruments and test structures to evaluate the causes of performance degradation, as well as suggesting solutions for the realization of neural implants that can work reliably and effectively over long periods of time.

6.1. Summary and original contributions

This section provides a summary of the chapters of this thesis, focusing on the results achieved and original contributions of the research work. The related scientific publications can be found in Appendix A.

Chapter 2

A review of the main available tools for sensing brain activity is presented, with particular focus on invasive neural interfaces and the challenges associated with these technologies. The case for reducing the size of the implanted devices is made, and the current design trends for miniaturized neural interfaces are presented. Within these solutions, the main features of the ENGINI system are introduced to set the framework of the research work.

Chapter 3

This chapter introduces the issue of hermeticity in implantable electronic micro-packages. The ability to resist water damage is an essential feature to ensure reliable and safe device operation. The proposed solution is to equip the implant with an *on board* humidity sensor that can sense the presence of water inside the micro-package, thus providing insight on seal quality and implant life span. In particular, the following outcomes are achieved:

- A novel integrated humidity sensor is designed, based on a interdigitated capacitive structure. The miniaturized sensing area, down to $300 \times 300\,\mu m^2$, allows for the use of the sensor in sub-millimetre devices. The geometry of the sensor also requires minimal post processing, with strong integration within the active CMOS circuitry of the implantable device.

- In order to set the geometrical parameters of the humidity sensor for optimizing its performance, a custom application is built using Matlab. The results of the application are validated using multiphysics modelling in COMSOL. Given its features, the use of the Matlab script can be extended to the design of IDC structures for a larger variety of applications.

- The use of an *off the shelf* humidity sensor is investigated for operation in millimetre-sized packages that employ eutectic bonding to achieve hermeticity. The calibration curve of the commercial sensor is tested through the high temperature cycle typical of the AuSn eutectic process, to verify if it would withstand the bonding process. This procedure, conducted with the use of a custom solderless PCB platform, validates the use of the sensor in applications that require this type of bonding process to create a hermetic package.

- The same commercial sensor is used in the context of a bench top testing platform of package hermeticity using optical telemetry. This can prove to be a useful tool to evaluate the quality of the seal of fabricated hermetic packages.

Chapter 4

This chapter presents the problem of moisture penetration within silicon substrates and their subsequent degradation due to corrosion. This phenomenon is of general interest for the lifetime of silicon-based devices, but becomes a primary concern when dealing with implantable devices. To better understand this process, two paths are followed: one is the use of test structures for accelerated life tests, the other is the design of *on board* circuits to detect water infiltration within the silicon layers. The outcomes of this work are the following:

- Four different types of structures are specifically designed using commercial CMOS technology for accelerated life testing. They include three different types of inter-

digitated capacitors, and various single MOSFETs topologies. These devices, coated in silicone, are used in an experimental setup, where they are constantly monitored for failure while immersed in PBS solution. The results of these experiments have provided useful insights regarding the devices' capabilities to withstand degradation caused by moisture penetration inside the porous polymer layer, and its effect on the passivation surface and on the silicon dioxide layers.

- Two novel impedance sensing circuits are proposed. They are designed to be integrated on the active die of an implantable device, and their aim is to sense the presence of moisture diffusing within the oxide layers of a CMOS stack. To perform the sensing, these instrumentation circuits take the innovative approach of using the metal traces of the scribe line within the silicon chip.

Chapter 5

In this chapter, the challenges related to the fabrication of microwire-based neural implants are highlighted, together with the importance of material choice for long lasting implantable devices. Building upon these considerations, two design iterations for a miniaturized cortical neural implant are developed, in compliance with the architecture proposed in the ENGINI project. The specific contributions are the following:

- A first *proof of concept* version of the implantable probe is designed and fabricated. It is based on the use of two interposer layers, a silicon one and a glass one, that provide mechanical rigidity to the implant and protect the microwires' attachment to the electronics. However, the overall assembly of this probe proved to be problematic, with adhesion problems between different components, finally compromising its functionality.

- The second version of the probe is designed, targeting the critical issues faced in version one. In particular the proposed design employs highly hermetic glass as packaging material, and it adopts a parallel fabrication strategy, splitting the probe architecture into two subsystems, in order to increase the production yield. This second design is prototyped using 3D printed plastic materials to validate the probe dimensions. A dedicated assembly jig is also proposed and demonstrated, to reduce the complexity of manual operations required when attaching the microwires.

6.2. Future work

The research presented in this thesis has targeted the topic of long-term reliability of implantable neural microsystems, envisioning a new form factor for cortical recording devices, as well as proposing *ad hoc* circuits to monitor and diagnose device failure. The obtained results are part of the continuing effort towards the realization of next generation

of neural interfaces and the work introduced in this dissertation would greatly benefit from further developments in each of its research areas.

Humidity sensing in micro-packages

A full characterization of the capacitive humidity sensor should be performed. This unfortunately could not be performed in time due to severe delays in materials delivery. Consequently, the sensor could be further optimized for an even smaller footprint, and its operation further integrated with the rest of the neural probe subsystems, for example by adding a digital reading for the output. In addition, it would be worth investigating a possible integration between the IDC electrodes and the antenna used for data telemetry, since both devices benefit from larger metallization volume on the CMOS die.

The work on the humidity sensor integrated with an optical link across the encapsulation of a micro-package could be expanded to obtain a reliable experimental platform to characterize the efficacy of different packaging materials and bonding processes.

Moisture ingress and corrosion in implantable silicon devices

The accelerated life experiments using the proposed test structures are still undergoing, and continue to provide insightful results on the lifetime of electronic implantable devices. It would be useful to further exploit the experimental setup, which is suitable for testing a larger variety of samples and different CMOS technologies.

The two circuit topologies for impedance measuring should be validated *in silica*. In particular it is necessary to verify that the novel use of the scribe line's metal layers as sensing electrodes does not produce undesired effects on the lifespan of the CMOS die.

Design of miniaturized microwire-based cortical implants

The prototype of the ENGINI probe described in this thesis demonstrates a new form factor for microwire-based wireless neural implants. However the design requires proper validation with the use of glass as hermetic encapsulation. It is also worth to explore the use of other hermetic materials, like cofired ceramics, and the overall optimization of the assembly process for larger production.

A further aspect to consider is the integration of the probe with the surgical tools, and its possible use as delivery vessel for targeted therapy. An example is the promising research towards the use of bio-active coatings that stimulate cell regrowth and prevent tissue scarring.

These three research domains are part of the larger scientific effort to deliver a new generation of BCIs, based on very high node count and wireless telemetry. This is the paradigm pursued by a large portion of the current academic and industry research, and might be

the future of treatment for a variety of neural diseases that impact the lives of millions of people worldwide.

6.3. Final thoughts

I would like to conclude this thesis with a personal reflection on my PhD journey and the future of brain interfaces.

At the start of the doctorate my research was mainly focused on electronics and sensor design. During the years of the PhD, through a series of unpredicted circumstances, I was more and more exposed to working on the form factor of a miniaturized cortical implant, dealing with materials and fabrication processes. This allowed me to gain a broader perspective of the field of neural interfaces, which I found extremely stimulating. At the same time, the subject of BCIs was suddenly brought to the attention of the general public and press, thanks to a few resounding announcements made by giant tech companies and entrepreneurs. This created a lot of legitimate interest, but it also brought along some inevitable misinformation and sensationalism. In light of these events, I am grateful that the PhD research provided me with the tools to critically discern reliable information from dubious statements, and to navigate this exceptionally broad field of study, whose complexity spans from interactions at the molecular level up to the meaning of consciousness itself.

It is also my hope that the modest contribution of this research work could be a reminder for future researchers about the importance of practical aspects that are too often overshadowed by more captivating topics. Keeping in mind that the well-being of people is the ultimate goal, the issues of reliability, safety, and security cannot be considered of secondary relevance. The realization of an implantable BCI that can seamlessly interface with the central nervous system while retaining its functionalities for years of operation, is an endeavor that requires a multidisciplinary and holistic approach, with a close synergy between all disciplines, from medicine to biology, from engineering to computer science, with the health of people as preeminent aim.

A. Publications

The following parts of this thesis include work previously published as research papers.

Chapter 2 includes content from:

- K. M. Szostak, P. Feng, F. Mazza, and T. G. Constandinou. "Distributed neural interfaces: challlenges and trends in scaling implantable technology". *Springer Handbook of Neuroengineering*. Currently under review

Chapter 4 includes content from:

- F. Mazza, Y. Liu, N. Donaldson, and T. G. Constandinou. "Integrated devices for micro-package integrity monitoring in mm-scale neural implants". *2018 IEEE Biomedical Circuits and Systems Conference (BioCAS)*

- C. Lamont, F. Mazza, and N. Donaldson. "A Bayesian Demonstration of Reliability for Encapsulated Implanted Electronics". *2019 9th International IEEE/EMBS Conference on Neural Engineering (NER)*, p. 730-733

Chapter 5 includes content from:

- K. M. Szostak, F. Mazza, M. Maslik, L. B. Leene, P. Feng, and T. G. Constandinou. "Microwire-CMOS integration of mm-scale neural probes for chronic local field potential recording". *2017 IEEE Biomedical Circuits and Systems Conference (BioCAS)*

- N. Ahmadi, M. L. Cavuto, P. Feng, L. B. Leene, M. Maslik, F. Mazza, O. Savolainen, K. M. Szostak, and others. "Towards a distributed, chronically-implantable neural interface". *2019 9th International IEEE/EMBS Conference on Neural Engineering (NER)*, p. 719-724